CRANFIELD UNIVERSITY

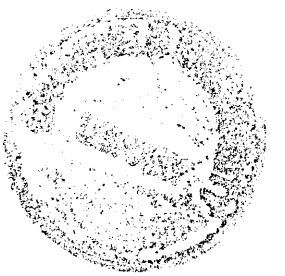

DAVID J. TAYLOR

The distribution of solids in a mechanically stirred liquid

SCHOOL OF MECHANICAL ENGINEERING

Ph.D. Thesis

CRANFIELD UNIVERSITY

SCHOOL OF MECHANICAL ENGINEERING
DEPARTMENT OF PROCESS AND SYSTEMS ENGINEERING

Ph.D. THESIS

Academic Year 1999-2000

DAVID J. TAYLOR

The distribution of solids in a mechanically stirred liquid

Supervisor: Professor D E Brown

September 2000

This thesis is submitted in partial fulfilment of the requirements for the Degree of Doctor of Philosophy

TO MY LATE FATHER

ABSTRACT

The literature available on the effect of vessel geometry, particle properties and liquid properties on the distribution of solids in a mechanically stirred vessel has been examined. This has shown that there are wide discrepancies between different authors on each of these areas.

Solids concentrations have been measured using an electrical conductivity probe at various positions in two stirred vessels 0.61m and 1.83m in diameter. Different impeller designs were examined using A310s and Pitched Blade Turbines to distribute the solids in the vessel. Pitched Blade Turbines with different diameter ratios of D=T/3 and D=T/2 were used. The sand particles used had diameters from 150 μm – 1050 μm.

It has been shown that constant power per unit volume is a reliable design rule for:

1. The effect of vessel scale
2. The effect of impeller diameter
3. The effect of impeller design

on the distribution of solids in a mechanically agitated stirred standard vessel. It has also been shown that the solids concentration data presented here can be correlated on the basis of $N_{\mathrm{mod}} = N(C)d^{a}\left(VPo^{-1}D^{-5}\right)^{b}$ and the vessel operating conditions can be characterised by a design methodology based on its use.

Two methods of modelling the data are presented which describe the system in terms of:

1. An array of oscillating spheres and
2. The 1-d sedimentation dispersion model.

These methods were found to model the data with different degrees of success and were generally disappointing.

The data was used by a CFD expert to optimise the empirical constants in a CFD model at two vessel scales with a particle size of 590 μm.

ACKNOWLEDGEMENTS

I wish to express my sincere thanks to the members of my support panel:
Professor D. E. Brown at Cranfield University;
Dr. N.G. Özcan-Taşkin and Dr. A. Al-Khayat at BHR Group Limited;
Dr. A.W. Etchells III and Dr. R.K. Grenville at DuPont Engineering;
for their invaluable contributions throughout the course of this work.

Thanks are also due to the FMP members and the FMP academic consultants Professor A.W. Nienow and Professor C.D. Rielly, for their enthusiasm and many helpful comments and suggestions.

I am very grateful to my friends and colleagues at BHR Group Limited for their support and encouragement. Special thanks go to Mr. B. Burnapp for his assistance during the experimental phase.

Last, but not least, I wish to acknowledge EPSRC and BHR Group Limited for their financial support, which enabled me to carry out this work.

CONTENTS

NOMENCLATURE

SYMBOL		UNITS
a	Linear distance	[m]
a	Coefficient (Eq. 7.5)	[-]
b	Coefficient (Eq. 7.5)	[-]
b	Coefficient (Eq. **A3.1**)	[-]
C	Particle concentration	[vol/vol]
C	Impeller clearance to impeller centre line	[m]
C′	Impeller clearance to base of impeller	[m]
C_1	Constant of proportionality	[-]
C_2	Constant of proportionality	[-]
C_i	Particle concentration at point i	[vol/vol]
C_n	Particle concentration at the n^{th} position	[vol%]
C_{max}	The maximum particle concentration in a slurry	[vol/vol]
C_0	Tank averaged particle concentration	[vol/vol]
C_D	Particle drag coefficient (Eq. 7.46)	[-]
d	Particle diameter	[m]
d_{32}	Sauter mean diameter (Eq. 5.1)	[m]
D	Impeller swept diameter	[m]
D_S	Particle diffusivity	[$m^2\ s^{-1}$]
$\overline{E}_z$	Vertical component of particle kinetic energy	[$kg\ m^2\ s^{-2}$]
F	Linear dimension	[m]
Fr	Modified Froude number (Eq. **3.13**)	[-]
Fr'	Modified Froude number (Eq. **3.39**)	[-]
Fr''	Modified Froude number (Eq. **3.18**)	[-]
g	Gravitational constant	[$m\ s^{-2}$]
G	Linear dimension	[m]
Ga	Galileo number (Eq. **3.36**)	[-]
h	Vertical height from vessel base	[m]
h	Slurry height above impeller mid-plane	[m]

H	Fill level	[m]
H_h	Hub height	[m]
H_h	Hub outside diameter	[m]
k	Friction factor	[kg s^{-1}]
k_E	Einstein constant (Eq. **3.65**)	[-]
k_H	Huggin's constant (Eq. **3.65**)	[-]
K	Dimensionless group (Eq. **3.8**)	[-]
K	Dimensionless group (Eq. **A3.2**)	[-]
L	Linear concentration (Eq. **A2.7**)	[m m^{-1}]
m	Mass of a single particle	[kg]
M	Mass of slurry in vessel	[kg]
n	Number of blades	[-]
n_{pt}	Number of measurement points	[-]
n_{imp}	Number of impellers	[-]
n_{McC}	Exponent in McCabe expression (Eq. A3.1)	[-]
N	Impeller speed	[rev s^{-1}]
$N(C)$	Impeller speed for to obtain concentration, C	[rev s^{-1}]
N	Number of bins (Eq. 5.1)	[-]
N_{homo}	Impeller speed for homogeneous suspension	[rev s^{-1}]
N_{JS}	Impeller speed for just suspension	[rev s^{-1}]
N_{mod}	Modified impeller speed (Eq. 7.5)	[rev s^{-1} $m^{(a-2b)}$]
N_{RSD}	Impeller speed for a given RSD	[rev s^{-1}]
p	Power input to particle at surface	[W]
p_{avg}	Difference between single and multiphase power	[W]
P	Shaft power	[W]
Pe	Péclet number (Eq. **3.6**)	[-]
Po	Impeller power number (Eq. **3.9**)	[-]
Po'	Modified impeller power number (Eq. **3.11**)	[-]
Pr_T	Turbulent Prandtl number	[-]
r	Radial distance from shaft centre line	[m]
R	Linear dimension	[m]
R	Tank radius	[m]

Re	Impeller Reynolds number (Eq. **3.36**)	[-]
Re'	Modified Reynolds number (Eq. **3.12**)	[-]
Re_P	Particle Reynolds number (Eq. **3.64**)	[-]
S_i	Suspension index (Equation 1.4)	[-]
t	Time	[s]
T	Tank diameter	[m]
u	Liquid velocity	[m s^{-1}]
u_m	Maximum velocity at the wall	[m s^{-1}]
u_t	Terminal particle settling velocity	[m s^{-1}]
U_{core}	Velocity in the core of a jet (Eq. **3.24**)	[m s^{-1}]
V	Volume of slurry in vessel	[m^3]
V_L	Volume of liquid	[m^3]
V_P	Volume of one Particle	[m^3]
V_S	Total volume of solids	[m^3]
V_T	Total volume	[m^3]
V_{tip}	Impeller tip velocity	[m s^{-1}]
$V_{tip,Njs}$	Impeller tip velocity at N_{js}	[m s^{-1}]
V_r	Impeller tip velocity	[m s^{-1}]
V_θ	Impeller tip velocity	[m s^{-1}]
w_{SS}	Settling velocity of a swarm of particles	[m s^{-1}]
W	Linear distance	[m]
W	Blade width	[m]
W_P	Projected blade width	[m]
x	Linear distance	[m]
x_s	Distance between particle surfaces	[m]
X	Force due to collisions	[kg ms^{-2}]
z	Vertical height	[m]

GREEK

α	Exponent in Eq. **3.55**	[-]
α	Jet discharge angle	[rads]
α	Pitched angle to the horizontal	[m]

α	Empirical constant in Equation A2.3	[m]
β	Exponent in Eq. **3.55**	[-]
β	Empirical constant in Equation 7.26	[-]
$\bar{\varepsilon}$	Tank averaged power input	[W kg^{-1}]
$\dot{\gamma}$	Rate of strain	[s^{-1}]
μ	Dynamic viscosity	[Pa s]
μ_S	Apparent slurry dynamic viscosity (Eq. **3.15**)	[Pa s]
μ_T	Eddy viscosity	[Pa s]
ν	Kinematic viscosity	[m^2 s^{-1}]
ρ_{avg}	Slurry density	[kg m^{-3}]
ρ_L	Liquid density	[kg m^{-3}]
ρ_S	Solid density	[kg m^{-3}]
$\Delta\rho$	Density difference	[kg m^{-3}]
χ	Blade thickness	[m]
σ	Standard deviation (Equation 1.5)	[vol%]
θ	Angle between baffle and measurement position	[rads]
φ	Jet discharge angle	[rads]
τ	Relaxation time	[s]
Λ	Torque	[m]

ABBREVIATIONS

4PBT45	45 degree 4 bladed pitched blade turbine
A310	Lightnin A310 hydrofoil impeller
CFD	Computational fluid dynamics
DNS	Diect numerical simulation
LES	Large eddy simulation
PBT	Pitched blade turbine
RDT	Rushton disk turbine
RSD	Relative standard deviation

LIST OF TABLES

LIST OF FIGURES

CHAPTER 1.Introduction

The suspension of solids in liquids using a mechanically agitated vessel is used extensively. Example applications are: the use of solid catalyst particles to improve the kinetics of a liquid phase reaction; the homogenisation of a strawberry-syrup mixture before canning of the fruit; crystallisation of a product from solution and; dissolution of the solid phase prior to further processing.

Some work has been performed in the literature to examine the effect of vessel geometry and particle properties on the distribution of solids in a mechanically stirred vessel. Most of these experiments were performed at scales much smaller than those used industrially and so, reliable application of these data to real processes will be difficult.

To address this issue the solids concentration profiles for a variety of sand sizes in water have been measured using a solids concentration probe. The scales used were significantly larger than many of those used in the literature. A variety of empirical and semi-empirical methods to model the data to gain further physical insight have been used. In association with a CFD expert this data has been used to optimise and validate a numerical model of solid liquid mixing in a mechanically stirred vessel.

At the moment, there is a need for reliable design tools for mechanically stirred vessels which have been developed using data obtained over a range of conditions and most importantly at scales where design engineers can confidently extrapolate from. This work has gone some way in addressing this need but further data is required on physical properties other than particle size and vessel geometry.

CHAPTER 2. Literature review on the effect of scale, impeller design, impeller and diameter on the distribution of solids in a mechanically stirred vessel

Shamlou (1993) gives an insight into the problems associated with the lack of sufficient information on the multiphase area by quoting figures that show that 60% of solid-handling plants achieve their desired rates compared with 90% for a *fluid only* plant. Experience also show that a *fluids only* plant was able to start up in three months while those handling solids varied between nine and eighteen months. Better understanding of solids processing would alleviate these problems.

In industrial applications that require solid-liquid contacting, reaching the *just suspension* state is often sufficient to achieve good mass transfer. *Just suspension* and *complete off bottom suspension* refer to the conditions where particles do not remain stationary for more than 1 to 2 seconds on the vessel base (Zwietering, 1958). Above the impeller speed for *just suspension* (N_{JS}), the mass transfer coefficient changes very slightly even though the power consumption can change significantly (Harnby *et al.*, 1997). Therefore, industry often chooses this condition to minimise the energy requirement for the process.

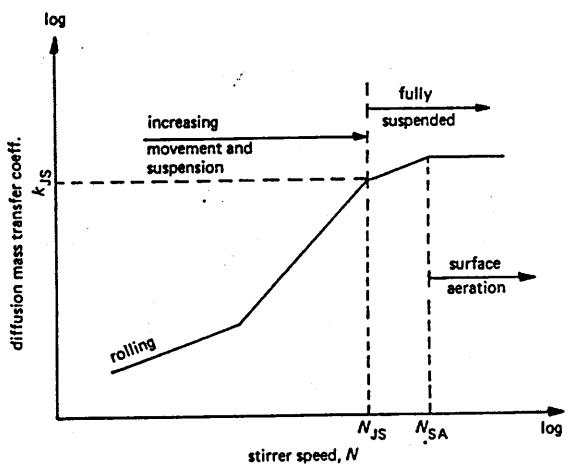

Figure 2.1. The variation of mass transfer coefficient in a mechanically stirred liquid with impeller speed.

(After Harnby *et al.* (1997))

Although operating at or slightly above N_{JS} can achieve a good rate of mass transfer, it does not necessarily provide a good distribution of solids in the vessel. This can be very important in situations such as a continuous process where slurry is withdrawn from the tank. Inappropriate positioning of the outlet may cause too many solids (washout) or too few solids being removed. The latter may cause the impeller to become buried and consequently damaged. The factors that would affect the operation of a continuous process are numerous. This research project has investigated the distribution of solids in batch systems.

Process engineers that wish to design mixing equipment require an understanding of how to scale laboratory apparatus to the full size plants that will produce the desired material. An excellent summary of the different strategies for scale-up can be found in McDonough (1992). For example, scaling-up on the basis of constant power per unit volume in liquid blending operations results in longer blend times. Since the cost of running a plant is proportional to the power supplied to it there is a business driver here to keep the power as low as possible whilst maintaining the desired process result. Unfortunately, different researchers have presented different criteria for the scale-up of solids distribution which range from keeping power per unit volume constant to reducing it. For the purposes of scale-up the larger the largest scale of experimentation the better since the design engineer will not be required to extrapolate the conclusions of a piece of research as far. This is something that has been lacking in the literature. Many researchers only operate at scales up to 0.6m in diameter. Extension of these results to a 4m vessel is clearly risky and engineers will typically design conservatively which could result in higher capital and running costs.

There are a variety of impeller designs that can be provided by the many equipment vendors from all around the world. For a fully baffled vessel, these can be classed into three common types:

Radial flow

Mixed flow

Axial flow

Radial flow impellers generate the flow pattern shown in Figure 2.2(a). Since the point of solids suspension in the upward flowing liquid at the vessel centre is a region of low energy dissipation, these impellers are generally unsuitable for solids suspension operations especially those involving fast settling solids. Axial flow impellers generate the flow pattern shown in Figure 2.2(c). Since there is a high energy dissipation zone in the discharge flow, this impeller is highly suited to solids suspension operations. This impeller generates flow efficiently, which means that the Power Number, Po is low. In between these two type of impellers are those which have a discharge angle between that of the radial and axial flow impellers (Figure 2.2(b)). PBTs belong to this class of impellers. Mixed flow impellers are also generally suitable for solid suspension applications.

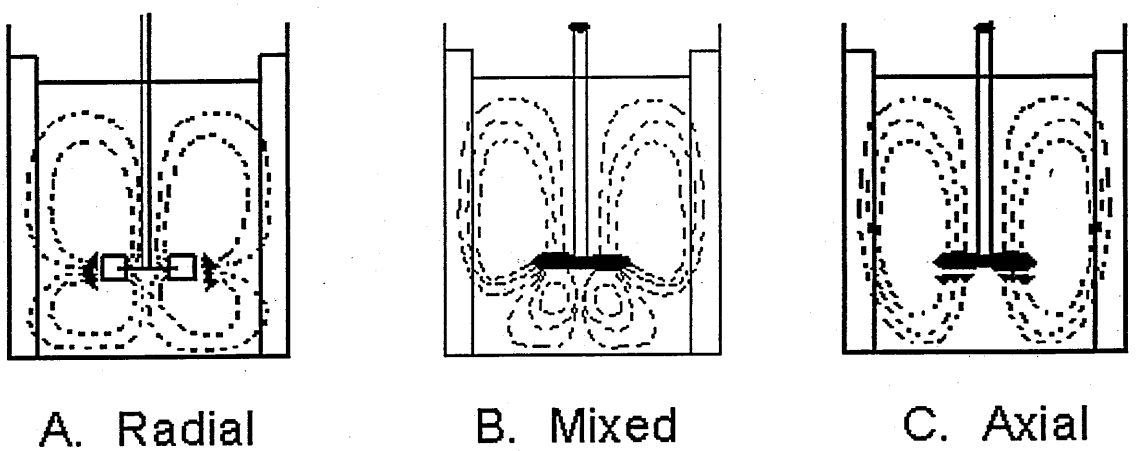

Figure 2.2. The flow patterns generated by three common impeller designs.

There has been a limited amount of data published where the effect of impeller design has been investigated and the conclusions reached vary somewhat. Some small scale tests have suggested that different impeller designs produce similar concentration profiles when compared on the basis of power per unit volume.

Should a process be upgraded for it is often necessary to increase the power supplied to the mixer so that it can handle more throughput or suspend more solids. Within industry most mixers are manufactured as fixed speed devices. Since increasing the speed for these systems requires that either a new gearbox or motor be purchased the option of increasing the speed to increase power can be uneconomic. An alternative method of increasing the power draw is to increase the diameter of the impeller. Provided that the gearbox can tolerate the increase in torque and the motor can tolerate the increase in power, this can be a good way of avoiding new capital equipment. The literature suggests that this has another beneficial effect since larger impellers can convey solids higher within the vessel volume making the vessel more homogeneous.

A summary of the information available in the open literature can be found in Table A1.1. The Table illustrates the variety of conditions that have been used but it is difficult to draw out useful information from such an eclectic source.

2.1 Effect of scale

Mak and Ruszkowski (1992) measured the particle concentration of 180 μm diameter sand suspended with a 4PBT45 ($D=T/2$) in T=0.61 m, 1.83 m and 2.67 m diameter mixing vessels. They analysed their results in terms of how the relative standard deviation (*RSD*) as shown in Equation 2.1, varied as a function $ND^{-0.78}$, which was the result of Buurman *et al.* (1985), and with N, ND, N^3D^2, PoN^3D^2 and N^2D.

$$RSD = \sqrt{\frac{1}{i-1}\sum_{1}^{i}\left(\frac{C}{C_0}-1\right)^2} \tag{2.1}$$

Of these comparisons, equal power per unit volume ($N \propto D^{-0.67}$) was recommended for the scale-up of constant RSD of a particle concentration distribution.

By using RSD, a single value related to suspension homogeneity can be obtained but it reveals no information about the actual particle concentration at different positions. Data analysis is further discussed in Section 3.1.

Buurman *et al.* (1985) carried out experiments using 157 μm diameter sand in standard vessels 0.12 m, 0.24 m, 0.48 m and 4.3 m in diameter using a 4PBT45 (D=0.4T, C=0.37T). Their three measurement points were at 0.40T, 0.61T and 0.82T from the vessel base and 0.15T from the vessel wall in the 4.3 m diameter vessel. In all the conditions that were examined in the 4.3 m diameter vessel, the suspension layer was at the liquid surface so there was little variation in concentration between the measurement points. Concentration measurements were taken above N_{js}. In the smaller scale vessels they found that there was a homogeneous zone above which the concentration fell rapidly. The mass balance for this geometry was poor with only 85% of the total mass of particles accounted for. Nasr-el-din (1987) suggested that this might have been due to the difficulties that occur in trying to achieve isokinetic sampling. Buurman *et al* (1985), analysed their data on the basis of a modified Froude number given by Equation 2.2:

$$Fr_{\mathrm{mod}} = \frac{\rho_L \, N^2 \, D^2}{g \, \Delta\rho \, d} \left(\frac{d}{D}\right)^{0.45} \tag{2.2}$$

This dimensionless group suggests that for geometrically similar systems, scaling-up will be on the basis of $N \propto D^{-0.78}$.

Magelli *et al.* (1990) found that $ND^{0.9}$ was to be kept constant for scale-up. This result was based on a comparison between single and multi-impeller work and no systematic study of either the effect of D/T or T was performed. As is often the case, the data was analysed by looking at the relative homogeneity rather than the absolute solids concentration.

A similar result to that of Magelli *et al.* (1990) was predicted by the modelling work of Barresi and Baldi (1987). Their one dimensional sedimentation-dispersion model predicted that scale-up of particle concentration profiles should be based on constant impeller tip speed, V_{tip}, (Equation 2.3) (i.e. $N \propto D^{-1}$).

$$V_{tip} = \pi N D \tag{2.3}$$

The model was only checked experimentally at a scale of 0.39m and the standard deviation of the solids concentration was used for the basis of the analysis. The one dimensional sedimentation-dispersion model assumed that the radial concentration profiles were negligible. Radial homogeneity does not always occur and the results from the 0.61m diameter vessel presented in Section 7.5 clearly show radial inhomogeneities.

Rieger *et al.* (1988) performed experiments in vessels from 0.2-0.4m in diameter. Their results indicated that specific power is an appropriate scale-up rule over a range of operating conditions.

2.1.1 Summary of findings

A summary of the different scale-up criteria that have been found in the literature are listed in Table 2.1. Detailed experimental conditions can be found in Table A1.1 at the end of this report.

Table 2.1. Alternative scale-up criteria for solids distribution

Author	Scaling criteria	
	Impeller speed	Power/Volume
Mak and Ruszkowski (1992) Rieger *et al.* (1988)	$N \propto T^{-0.67}$	$P/V \propto T^{0}$
Buurman *et al.* (1985)	$N \propto T^{-0.78}$	$P/V \propto T^{-0.34}$
Magelli *et al.* (1990)	$N \propto T^{-0.9}$	$P/V \propto T^{-0.70}$
Barresi and Baldi (1987)	$N \propto T^{-1}$	$P/V \propto T^{-1}$
For comparison: Zwietering (1957)	$N_{js} \propto T^{-0.85}$	$P/V \propto T^{-0.55}$
For comparison: Tip speed	$N \propto T^{-1}$	$P/V \propto T^{-1}$
For comparison: Specific power	$N \propto T^{-0.67}$	$P/V \propto T^{0}$

Figure 2.3 illustrates what value of specific power each of these scale-up criteria would require upon scale-up.

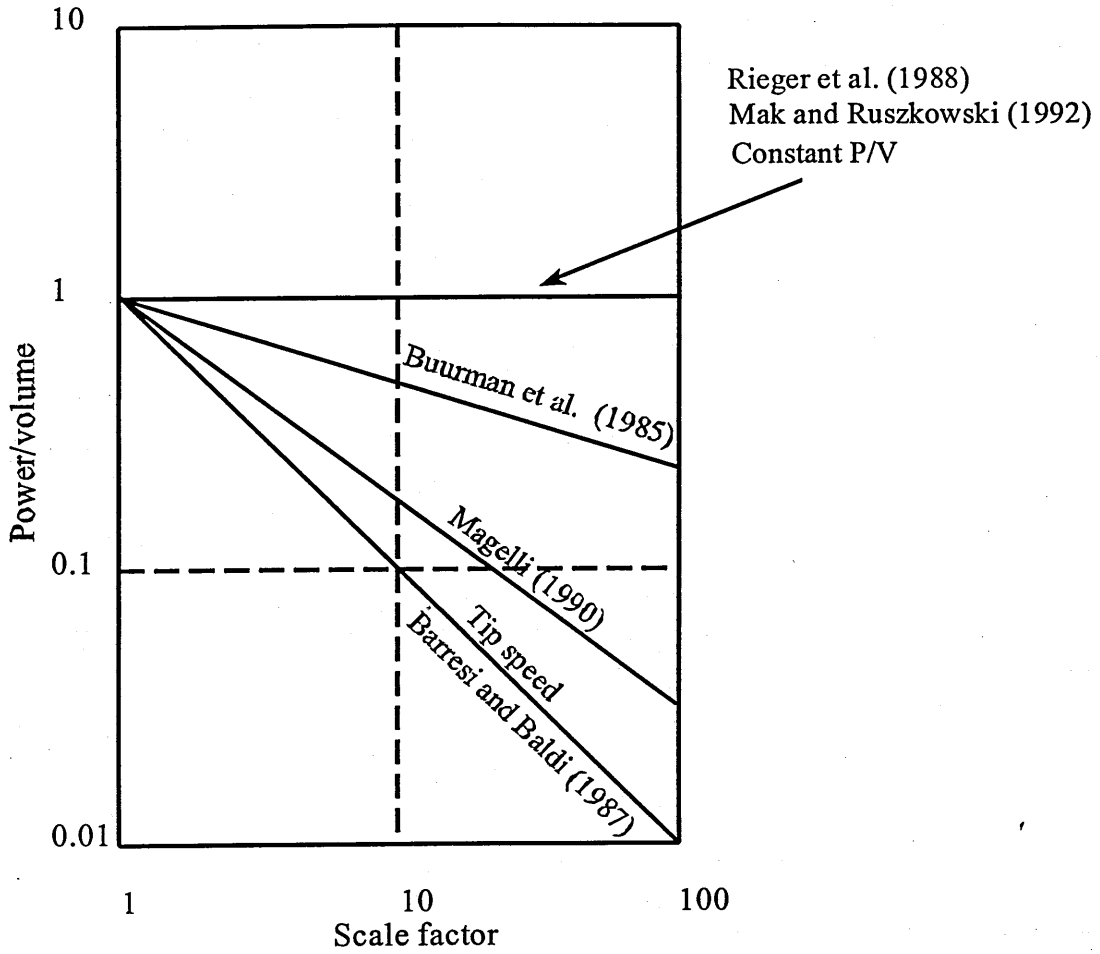

Figure 2.3. Prediction of specific power required for scale-up, depending on different criteria proposed by previous researchers.

It can be seen that there is a wide spread of results depending on which criterion is chosen for use. Much of the work in this area has been with small sized vessels, about 0.3 m in diameter. Mak and Ruszkowski (1992) and Buurman *et al.* (1985) performed limited work in larger tanks. Buurman *et al.* (1985) performed experiments in the 4.26 m vessel at speeds where the suspension reached the liquid surface. Hence, their data is limited to scales up to 0.48 m. Their slurry draw-off technique has also been shown to be inappropriate by Nasr-el-din (1987). The data set of Mak and Ruszkowski (1992) is therefore the only reliable large-scale work that has been performed. Their data were analysed on the basis of RSD, which only gives an indication of the homogeneity rather than the solids concentration. The results are specific to a $T/2$ PBT and d=180 μm sand. Other impellers or particle sizes were not investigated. Further work in this area was therefore required which has been one of the objectives of this study.

2.2 Effect of impeller design

Heywood *et al.* (1991) examined the concentration profiles produced by 5 different designs of impeller: a) D=0.38T 4 blade PBT; b) a pair of D=0.67T EKATO Intermig's; c) a D=0.33T and 0.44T marine propeller; d) a D=0.42T Scaba 'SHP' and; e) a pair of Denver 'MIL' propellers. It is difficult to obtain clear conclusions from their study, as the impeller diameter they quote is not well defined. From the diagrams that give the dimensions of the impellers they do not seem to have used the swept diameter. Although the authors mention that they only used one marine impeller, they quote two impeller diameters. The clearances chosen varied for each impeller according to the recommendations by the impeller manufactures and varied between 0.17 and 0.33T. These factors made the comparisons difficult. The particle concentration was measured by γ-ray backscatter.

Using this technique it is possible to obtain information on the axial variation in concentration but more difficult for the radial variation. Only the axial variation of the concentration was considered. The radial variation was considered to be insignificant.

The authors used the suspension index (Equation 2.4), S_i and the standard deviation, σ (Equation 2.5) to analyse how their experimental data varied with power. S_i is the ratio of the mass of solids in the upper half of the tank to that in the lower half:

$$S_i = \frac{\sum_{H=0.5}^{H=1} C_n h}{\sum_{H=0}^{H=0.5} C_n h} x\,100\ \% \tag{2.4}$$

Here C_n is the particle concentration in wt% at position n and h is the vertical distance between the measurement points. The standard deviation is defined by Equation 2.5.

$$\sigma = \sqrt{\frac{1}{n} \sum_{n=1}^{n=21} \left(\frac{C_n}{C_0} - 1 \right)^2} \tag{2.5}$$

Here, C_0 is the average particle concentration and σ is the standard deviation of the concentration measurements.

For a slurry containing sand particles of diameter 380μm at concentrations in the range 50-65%wt, a comparison was made of the performance of the PBT, EKATO Intermig and the Denver MIL propeller. This showed that at a given power input the PBT gave a poorer suspension index and standard deviation than the Denver 'MIL' and the Intermigs. The MIL and Intermigs showed similar suspension indices. This could be because these two impellers were used in pairs and so the circulation pattern for these two impellers was different, allowing the solid particles to be conveyed higher in the tank than with a PBT.

The authors found that the Intermigs and the Denver MIL's were unable to give the high suspension indices that were found with the marine propeller and the Scaba SHP at power inputs greater than about 3.5kW m^{-3}. With smaller particles (100 μm) the effect of the impeller design on S_i and σ at a given power input was less pronounced than that for the coarse (380μm) sand.

Magelli *et al.* (1991) found that, for their system of a tall tank with multiple axial impellers which are defined in Table 2.2, the actual configuration of the impellers was of little importance where comparisons were made on the basis of power per unit mass. This may be due to the uniform flow field, generated by the multiple axial impellers. Magelli *et al.* (1990) found that an arrangement of Rushton impellers required an order of magnitude higher power input than multiple axial impellers to achieve a similar homogeneity. Particles in the range 140 μm to 980 μm were used in liquids of viscosity 0.9 to 18 mPa s.

Table 2.2. Vessel geometry covered by Magelli *et al.* (1991)

System characteristics	Geometry number		
	1	2	3
Vessel diameter, T (m)	0.236	0.236	0.236
Vessel height, H (m)	0.545	0.545	0.944
Vessel volume, V (l)	23.8	23.8	40.1

Table 2.3. Impeller geometries covered by Magelli *et al.* (1991)

Number of impellers, per type, in each geometry:	Geometry number		
	1	2	3
Variable-pitch 2 blade turbine	4	4	0
Back-swept 4-blade turbine	1	0	0
Variable pitch 4-blade turbine	0	1	0
Lightnin A310	0	0	4
Impeller diameter, D (m)	0.124	0.124	0.096
Power number, Po	2.3	2.1	1.2

Mak (1988) conducted a review of tests using 7 types of impellers in a 0.61 m diameter vessel using 180 μm diameter sand at a concentration of 30%wt. His findings were that for a given degree of homogeneity, A310s (*D=T/2)* required higher impeller speeds than PBTs (*D=T/2)*. However, due to the low power number of the A310 they were actually found to be more energy efficient. For these impellers, the solids suspension layer reached the liquid surface before N_{js} was achieved. Therefore, the comparisons were made at speeds where the suspension was almost homogeneous with both impellers. The differences were only marginal in terms of RSD. This feature was seen at all speeds and was probably related to the flow field generated by the impellers. With the A310, the flow field is predominantly axial whereas with a PBT of *D=T/2* it is known that the radial component of the discharge flow is quite strong (Musgrove and Ruszkowski, 1993).

2.3 Effect of impeller diameter

Bohnet and Niesmak (1980) found that in a 0.290 m diameter vessel, a *T/2* pitched blade turbine produced a more homogeneous suspension than the *T/3* diameter impeller when operated at the same impeller speed and impeller clearance. When they used a marine propeller, they found that the *T/2* impeller generally gave the best distribution, the *T/3* impeller gave the worse performance at low speeds but the best at the highest speeds.

Mak (1988) performed particle concentration measurements using 180 μm diameter sand at a concentration of 30%wt in a 0.61 m diameter vessel. They found that a larger diameter A310 gave better distribution at low power inputs although at high speeds the homogeneity began to get worse, possibly due to air entrainment. Air entrainment would result in an increase in the apparent particle concentration at the measurement points especially near to the liquid surface. Increasing particle concentration at the highest speeds can be seen from the figures presented in that report, thus suggesting air entrainment.

Mak (1992) performed experiments with PBTs with a diameter of *T/3, T/2* and *T*/1.7. He found that as *D/T* was increased, lower impeller speeds and power inputs were required for a similar degree of homogeneity. This confirmed the findings of Mak (1988). The comparisons were made at impeller speeds above N_{homo}, the impeller speed at which particles are convected to the top layers of the vessel. The results reflected the better top to bottom mixing of the larger diameter impellers, which resulted in better convection of the particles to the highest points in the liquid. He also showed that with the smaller impellers the maximum degree of homogeneity achievable was better but at higher power input. This could have been a result of the larger impeller drawing more air in and so lowering the apparent degree of homogeneity.

Yung (1995) showed that the speed required to produce complete homogeneity with a PBT (D=T/3) was 50-65% higher than N_{js} while for a PBT (D=T/2) only 20-25% higher was required. This is hardly an assessment of the performance of impellers of different D/T since the values of N_{js} for the two impellers are not equal. She also showed that the radial profiles for both a *D=T/2* and *D=T/3* PBT were fairly uniform even with 900 μm sand. The positions examined were at r/R=(0.50,0.67 and 0.90) and h/H=0.5 and midway between the two baffles.

Corpstein *et al.* (1994) recommended $N/N_{js} = 1.4$ in order for the solids suspension layer to fill 95% of the tank volume using an HE-3 of $D/T = 0.35$ and $N/N_{js} = 1.25$ when using an HE-3 of $D/T = 0.5$. Overall these trends are in agreement with the observations of Yung (1995).

Shamlou and Koutsakos (1989) also obtained similar results. They showed that increasing the impeller diameter for a given impeller speed increases the energy supplied to the liquid which increased the turbulence intensity of the suspension which would increased the particle's apparent diffusivity. This resulted in a better uniformity of the suspension within the vessel.

2.4 Conclusions

2.4.1 Effect of scale

From the limited work performed in industrial scale vessels examining the effect of scale on the distribution of solids in stirred tanks, the work of Mak and Ruszkowski (1992) states that a good way of scaling up distribution quality is on the basis of power per unit volume. Buurman *et al.* (1985) correlated their data to suggest that scaling up the particle distribution should be on the basis of $ND^{-0.78}$. Barresi and Baldi (1987) predicted that scale-up should be performed on the basis of impeller tip speed. Each of these predictions gives a different value for the power required on scale-up as illustrated in Figure 2.3.

There is a clear industrial need for more research to be performed with large-scale vessels focusing on the spatial variation of concentration. Experiments in industrially relevant sized vessels would provide industry with extensively validated data on how scale effects the performance of solid-liquid contacters. This data is very limited at present.

2.4.2 Effect of impeller design

Magelli *et al.* (1991) showed that there was little difference between the standard deviations when different impeller designs were compared on the basis of power per unit volume.

A good variety of impellers were used in the work of Heywood *et al.* (1991) but with significant differences in vessel geometry so the differences in the performance of the impellers is expected. The differences were most pronounced when the experiments were performed with coarse sand.

2.4.3 Effect of impeller diameter

The literature generally showed that increasing the diameter of the impeller reduced both the speed and power per unit volume that are required for a given homogeneity. This implies that large impellers are advantageous for the distribution of solids since they convey solids higher at a given power per unit volume.

CHAPTER 3. Literature review on the effect of liquid and particle properties on the distribution of solids in a mechanically stirred tank

A summary of the information available in the open literature can be found in Table A1.2. The Table illustrates the variety of conditions that have been used and it can be difficult to draw out useful information from such an eclectic source.

The particle and liquid properties influence the solids concentration profile in a stirred tank in many ways: small particles absorb the turbulent energy, which changes the turbulent energy spectrum; small particles also have a low settling velocity, which requires less energy to keep them in suspension; a low density difference between the solid and liquid phases results in a low settling velocity, which also requires less energy to keep the particles in suspension; at high concentrations particle-particle interactions become significant; a high liquid viscosity results in a low particle settling velocity and lower impeller speeds are required to maintain solids suspension.

3.1 Methods of data analysis and modelling used in the literature

The ability to successfully model what is happening in a stirred vessel is required in order to allow a deeper understanding of how the physics affect the solids concentration profile inside a stirred vessel. The physics of multiphase flow have been manipulated in several ways to develop the following models. It has been necessary to include approximations and assumptions, which limit the validity of each model.

3.1.1 1-d Sedimentation dispersion model

The 1-d sedimentation dispersion model is a vertical balance between the particle settling velocity and the particle diffusion. The convective-diffusive equation for this model is of the form:

$$\frac{\partial C}{\partial t} = D_S \frac{\partial^2 C}{\partial z^2} + (u_t - u)\frac{\partial C}{\partial z} \tag{3.1}$$

Here, C is the solid phase concentration, z is the vertical distance, u_t is the particle settling velocity, u is the velocity of the upward flowing liquid, D_S is the particle diffusivity and t is the time. At steady state Equation 3.1 reduces to:

$$D_S \frac{\partial^2 C}{\partial z^2} + (u_t - u)\frac{\partial C}{\partial z} = 0 \tag{3.2}$$

Inclusion of the boundary condition for no flow of solids through the vessel base (Eq. 3.3) and the condition for the total mass of solids in the vessel (Eq. 3.4):

$$(u - u_t)C(0) - D_S \left.\frac{dC}{dz}\right|_{z=0} = 0 \tag{3.3}$$

$$C_0 = \int_{z=0}^{H} C(z)H^{-1}dz \tag{3.4}$$

in the solution of Equation 3.2 gives:

$$\frac{C(z)}{C_0} = \frac{(u_t - u)H/D_S \; e^{\left((u-u_t)z/D_S\right)}}{1 - e^{\left((u-u_t)H/D_S\right)}} \tag{3.5}$$

Introduction of the Péclet number:

$$Pe(z) = (u_t - u)z/D_S \tag{3.6}$$

in Equation 3.5 results in Equation 3.7:

$$\frac{C(z)}{C_0} = \frac{Pe(H)e^{-Pe(z)}}{1 - e^{-Pe(H)}} \tag{3.7}$$

In this analysis it is often assumed that D_S is position independent. In reality, the local energy dissipation rate and so turbulence level will vary throughout the vessel. Some of the turbulent eddies will interact with the particles which will result in a variation in D_S throughout the vessel. Fajner *et al.* (1985) performed experiments in a tall vessel agitated by multiple impellers. This arrangement will give a more uniform turbulence distribution than a single impeller in a standard vessel. As a result, the theoretical predictions and their experimental results matched quite well. The only discrepancy was at the midpoint between impellers where the ring baffles were located. There, the measured concentration profiles were about 30% higher than the positions just above or below. This effect might be due to the sudden change in flow direction at that point from vertical to horizontal. Since the particle has inertia it will carry on and deviate from the streamlines and move into the corner region where a higher concentration has been found.

Tojo and Miyanami (1982) also used this model to describe the particle distribution in a standard stirred vessel. Here the liquid was added and slurry drawn off continuously. The results from these experiments showed that the characteristic particle settling velocity had to be considered to be a model parameter that depended on the experimental conditions. This problem might be because the standard vessel arrangement does not have a homogeneous turbulence distribution, which makes the application of this model awkward since the spatial variation of the particle diffusivity needed to be considered.

Barresi and Baldi (1987a) also used the 1d sedimentation model to produce the dimensionless group given in Equation 3.8:

$$K = \frac{Po^{1/3} ND}{u_t} \tag{3.8}$$

where the power number, Po is defined as:

$$Po = \frac{P}{\rho_L N^3 D^5} \tag{3.9}$$

The authors correlated the data of Bohnet and Niesmak (1980) using this parameter modified by a factor of $C^{-0.13}$ to include the effect of average particle concentration on the standard deviation. There is some deviation between the experimental results and the theoretical results although the two are generally in good agreement.

Yamazaki *et al.* (1991) used the 1d sedimentation dispersion model to set a condition for homogeneity that the ratio of the concentration at the top of the vessel, C_t to the concentration at the base, C_b is given in Equation 3.10:

$$\frac{C_t}{C_b} = 0.8 \tag{3.10}$$

This condition led to the conclusion that the modified power number (Equation 3.11), modified Reynolds number (Equation 3.12) and modified Froude number (Equation 3.13) are related as shown in Equation 3.16:

$$Po' = \frac{P}{\rho_{avg} N^3 D^5} \tag{3.11}$$

$$\mathrm{Re}' = \frac{\rho_{avg} N D^2}{\mu_S} \tag{3.12}$$

$$Fr = \frac{\rho_L u_t^2}{dg\Delta\rho} \tag{3.13}$$

where

$$\rho_{avg} = C\rho_S + (1-C)\rho_L \tag{3.14}$$

and

$$\mu_S = \mu\left(1 + 2.5C + 10.05C^2 + 0.00275e^{(16.6C)}\right) \tag{3.15}$$

$$Po' \propto \mathrm{Re}' Fr^{-0.3} \tag{3.16}$$

For a RDT to satisfy the condition in Equation 3.10, it was found that $\mathrm{Re}' Fr^{-0.3} > 1.5\times10^5$ where $4.4 < Po' < 4.8$. For a marine propeller this required $\mathrm{Re}' Fr^{-0.3} > 2.3\times10^5$ where $0.54 < Po' < 0.61$. The disadvantage of this method is that it is sensitive to the geometry employed. A set of conditions for each impeller and potentially scale would be prohibitively experimentally intensive.

Sessiecq *et al.* (1999) used this model but allowed D_S to vary with axial position. This method produced good agreement between the experimental data and the model. Since the model required significant experimental input so that the variation of D_S with height could be determined, this method is not likely to be generally applicable. For each geometric configuration experimental data to determine D_S would be required.

3.1.2 Energy balance

Einenkel (1980) stated that the energy to suspend all of particles in the vessel is related to the energy supplied by the impeller as shown in Equation 3.17:

$$C_1 w_{ss} \Delta\rho g V C_0 = Po\rho_L N^3 D^5 \tag{3.17}$$

Introduction of the modified Froude number (Equation 3.18), to eliminate ρ_L, resulted in Equation 3.19:

$$Fr'' = \frac{N^2 D}{g}\frac{\rho_L}{\Delta\rho} \tag{3.18}$$

$$Fr'' \frac{\pi ND}{w_{SS}} \frac{1}{C_0} = C_2 \frac{\pi}{Po} \frac{V}{D^3} \tag{3.19}$$

The author found the relationship in Equation 3.20:

$$Fr'' \frac{\pi ND}{w_{SS}} \frac{1}{C_0} \propto \mathrm{Re}^{-0.27} \tag{3.20}$$

The author presented data for different levels of homogeneity. He found that the model fitted the data well when the condition:

$$\sigma^2 = 0.95 \tag{3.21}$$

was used where σ^2 is defined in Equation 3.23. When the suspension was more homogeneous with the condition:

$$\sigma^2 = 0.25 \tag{3.22}$$

the data did not fit the model as well especially at $Re>10^4$.

$$\sigma^2 = \frac{1}{n} \sum_{i=1}^{n} \left(\frac{C}{C_0} - 1 \right)^2 \tag{3.23}$$

Bohnet and Niesmak (1980) plotted the left-hand side of Equation 3.19 against Re for their data and found a very poor agreement. These authors suggested that this meant that Einenkel's method does not represent the processes inside a stirred vessel very well.

3.1.3 Use of impeller discharge characteristics

Bittorf and Kresta (1999) presented a model based on the discharge characteristics of an impeller and used it to predict the suspension height. The velocity in the core of a jet, U_{core} leaving an impeller was found to be given by:

$$U_{core} = 0.054 V_{tip} \left(\frac{G}{T} \right)^{-1.4} \tag{3.24}$$

where G is the total distance that a jet has to travel before it impinges on the wall. G is calculated using Equation 3.25, where the dimensions C', W, x, R, F and φ are defined in Figure 3.1.

$$G = R + F \tag{3.25}$$

The lengths R and F can be calculated using Equations 3.26-3.29:

$$W = C' \tan(90 - \phi) \tag{3.26}$$

$$R = \sqrt{C'^2 + W^2} \tag{3.27}$$

$$\alpha = \tan^{-1}\left(\frac{V_\theta}{V_r}\right) \tag{3.28}$$

$$F = \frac{T}{2} - \left[\frac{(2W + 2x\cos\alpha)^2 - (2x\cos\alpha)^2}{4} + x^2\right]^{1/2} \tag{3.29}$$

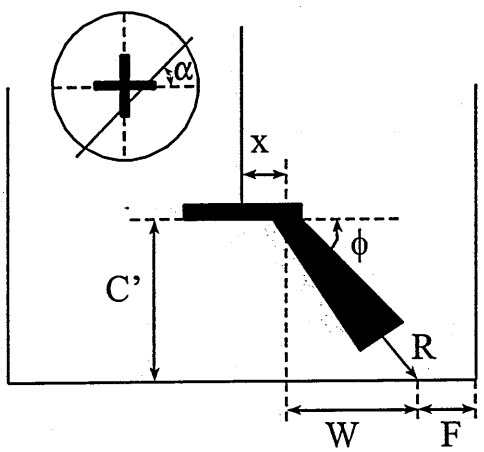

Figure 3.1. The variation of inter-particle distance with concentration (After Bittorf and Kresta, 1999).

V_r and V_θ are the radial and tangential velocity components respectively of the impeller discharge. The distance x is chosen to be the point in the impeller discharge where the maximum velocity occurs.

The maximum velocity at the wall, u_m, was then calculated using Equation 3.30:

$$u_m = 0.27 V_{tip,N_{js}} + u_t \tag{3.30}$$

where $V_{tip, Njs}$ is the tip speed at N_{js} and u_t is the particle settling velocity.

The cloud height, h, was then calculated using Equation 3.31:

$$h = \left(0.28 \frac{U_{core}}{u_m}\right)^{0.87} \tag{3.31}$$

Bittorf (2000) claims that when the above equations are used to calculate the impeller speed for a given cloud height, an accuracy of 25% in the impeller speed is attainable. The variation in concentration between 0.75N and 1.25N would be very great. This is a limitation on this method if it were to be used to calculate the cloud height.

3.1.4 Empirical correlations

Kolář (1961) produced empirical correlations (Equations 3.32, 3.33, 3.34 and 3.35) for the suspension of particles to within $D/4$ of the liquid surface. This condition was termed homogeneous.

Marine propeller ($C=T/9$)

$$\left(\frac{ND}{u_t}\right)=0.357\left(\frac{u_t^{\,2}}{gD}\right)^{-0.316}\left(\frac{C_0}{1-C_0}\right)^{0.153}\left(\frac{\rho_S-\rho_L}{\rho_L}\right)^{0.113}\left(\frac{D}{T}\right)^{-2.570} \tag{3.32}$$

Marine propeller ($C=T/3$)

$$\left(\frac{ND}{u_t}\right)=1.77\left(\frac{u_t^{\,2}}{gD}\right)^{-0.266}\left(\frac{C_0}{1-C_0}\right)^{0.093}\left(\frac{\rho_S-\rho_L}{\rho_L}\right)^{0.112}\left(\frac{D}{T}\right)^{-1.559} \tag{3.33}$$

Pitched blade turbine ($C=T/9$)

$$\left(\frac{ND}{u_t}\right)=0.800\left(\frac{u_t^{\,2}}{gD}\right)^{-0.331}\left(\frac{C_0}{1-C_0}\right)^{0.0748}\left(\frac{\rho_S-\rho_L}{\rho_L}\right)^{0.082}\left(\frac{D}{T}\right)^{-1.514} \tag{3.34}$$

Pitched blade turbine ($C=T/3$)

$$\left(\frac{ND}{u_t}\right)=1.214\left(\frac{u_t^{\,2}}{gD}\right)^{-0.286}\left(\frac{C_0}{1-C_0}\right)^{0.0559}\left(\frac{\rho_S-\rho_L}{\rho_L}\right)^{0.049}\left(\frac{D}{T}\right)^{-1.561} \tag{3.35}$$

Pavlushenko *et al.* (1957) correlated their data for the impeller speed required for the concentration in the upper layer of liquid to reach the bulk concentration using the dimensionless analysis shown in Equation 3.36:

$$\mathrm{Re}=\frac{N\rho_L D^2}{\mu}=0.105\left(\frac{D^3\rho_L^2 g}{\mu^2}\right)^{0.6}\left(\frac{\rho_S}{\rho_L}\right)^{0.8}\left(\frac{d}{D}\right)^{0.4}\left(\frac{T}{D}\right)^{1.9} \tag{3.36}$$

In shorthand form this reduces to

$$\mathrm{Re}=0.105Ga^{0.6}\left(\frac{\rho_S}{\rho_L}\right)^{0.8}\left(\frac{d}{D}\right)^{0.4}\left(\frac{T}{D}\right)^{1.9} \tag{3.37}$$

Where Ga is the Galileo number:

$$Ga = \frac{D^3 \rho_L^2 g}{\mu^2} \tag{3.38}$$

Buurman *et al.* (1986) correlated their data for the suspension height in vessels ranging from 0.24-4.26m in diameter using the modified Froude number (Equation 3.39):

$$Fr' = \frac{\rho_L N^2 D^2}{g \Delta \rho d} \left(\frac{d}{D} \right)^{0.45} \tag{3.39}$$

Although the data used was produced in vessels ranging from 0.24-4.26 m, the data obtained in the 4.26 m diameter tank was limited to a condition where the suspension level was at the liquid surface. Since there are no data in the region where the suspension height is increasing, the authors were unable to test their correlation in this region. The range of applicability of this correlation should therefore be restricted to vessels that are 0.24-0.48m in diameter.

3.1.5 Analysis of the behaviour of a slurry interface

Weisman and Efferding (1960) have described how the interface between the clear layer and the slurry layer behaves. At the interface, the partial differential equation describing the motion of a single particle in the vertical direction can be written as:

$$m\left(\frac{\partial^2 z}{\partial t^2} \right) = -k\left(\frac{\partial z}{\partial t} \right) + X \tag{3.40}$$

where m is the mass of an individual particle, k is the friction factor and X is the force due to collisions. The authors then rearranged Equation 3.40 so that z^2 was the dependent variable rather than z:

$$\frac{m}{2}\left(\frac{\partial^2 (z^2)}{\partial t^2} \right) - \frac{m}{2}\left(\frac{\partial z}{\partial t} \right)^2 = -\frac{k}{2}\left(\frac{\partial (z^2)}{\partial t} \right) + Xz \tag{3.41}$$

The term, Xz, in Equation 3.41 was taken to be zero since collisions were considered to be random. Substituting $\frac{m}{2}\left(\frac{\partial z}{\partial t} \right)^2$ by $2\overline{E}_z$, the vertical component of the kinetic energy and then integrating, the authors found that:

$$\overline{\Delta z}^2 = \frac{2\overline{E}_z}{k/2} t \tag{3.42}$$

where $\overline{\Delta y}$ is the average vertical displacement in the interval t. The authors then replaced the friction factor by the Stokes's free settling velocity to get:

$$\left(\overline{\Delta z}\right)^2 = \frac{4\overline{E}_z u_t}{g V_P \Delta\rho} t \tag{3.43}$$

Rearranging and substituting the vertical component of the kinetic energy by $p/3$, where p is the average power input to a particle at the surface, gave:

$$\frac{\left(\overline{\Delta z}\right)^2}{t^2} = \frac{4 p u_t}{3 g V_P \Delta\rho} \tag{3.44}$$

The left-hand side of Equation 3.44 is the square of the average particle velocity, which is the settling velocity. Hence:

$$p = \frac{3 g V_P \Delta\rho u_t}{4} \tag{3.45}$$

The authors then assumed that this power input is proportional to the difference in power draw between single phase and a solid-liquid mixture at a given N.

$$p_{avg} = \frac{V_P P \Delta\rho}{V \rho_{avg}} \tag{3.46}$$

Rearranging and noting that the ratio of p to p_{avg} will be a function of the geometry, Re and the slurry height above the impeller mid plane gave:

$$p = \left(\frac{V_P P \Delta\rho}{V \rho_{avg}}\right) f_1(C) f_2\left(\frac{h}{T}\right) \tag{3.47}$$

The final functional form of Equation 3.47 is shown below in Equation 3.48:

$$\left(\frac{h}{T}\right) = C_1 \ln\left[\left(\frac{P}{n_{imp} g \rho_{avg} V u_t}\right) C^{-2/3} \left(\frac{D}{T}\right)^{1/2}\right] + C_2 \tag{3.48}$$

The constants C_1 and C_2 were found to be 0.23 and 0.1. ρ_{avg} is the slurry density in the suspension layer and n_{imp} is the number of impellers in the vessel. C is the particle concentration in the slurry layer.

3.1.6 Effect of particle-particle shear on particle concentration

Bagnold (1954) measured the effect of shearing particles on the static liquid pressure on the inner of 2 rotating concentric cylinders. The particle concentration used varied between 13%v/v and 62%v/v. The system was chosen so that their was no difference in particle density between the solid and liquid phases which meant that there were no forces due to radial acceleration. By comparing the torque on the inner cylinder with the static pressure of the liquid that was generated by the shearing particles, a relationship (Equation 3.49) between the dispersive force on a particle due to its interaction with its neighbours was found.

$$F_D = 0.0128 L^{-2} d^2 \dot{\gamma}^2 A \rho_S \tag{3.49}$$

Here, L is the linear distance between particles in a plane, $\dot{\gamma}$ is the rate of shear of the plane of particles and A is the area occupied by a particle in a plane. This concept is used in Section 7.7.

3.2 Effect of particle properties on solids distribution

3.2.1 Effect of particle size

A summary of the studies that have been performed that have examined the effect of particle size on the distribution of solids in a stirred tank are shown in Table 3.1. The information available in the literature has shown that there has been a wide range of predictions on the exponent on particle diameter.

Table 3.1. Prediction of the effect of particle size from the literature

Reference	Range of particle size (μm)	Exponent on d
Barresi and Baldi (1987a)	139-459	1.14
Bohnet and Niesmak (1980)	125-1125	0.38
Bujalski *et al.* (1999)	115-678	>0
Buurman *et al.* (1985)	157-2200	0.27
Einenkel (1980)	90-1500	0.16 (Turbulent) 0.62 (Laminar)
Heywood *et al.* (1991)	100-380	>0
Kolář *et al.* (1961)	131-1641	0.38-0.53
Kudrna *et al.* (1986)	450-925	>0
Magelli *et al.* (1990)	140-980	0.82
Magelli *et al.* (1991)	330-980	0.61
Nasr-el-din *et al.* (1996)	82-410	>0
Nienow (1968)	324-2230	>0
Oldshue (1969)	[-]	>0
Pavlushenko *et al.* (1957)	35-825	0.4
Rieger *et al.* (1988)	185-1360	>0
Shamlou and Koutsakos (1989)	175-1100	>0
Sýsová (1984)	450-925	>0
Weisman and Efferding (1960)	45-140	0.38
White and Sumerford (1933)	137-416	>0
Yamazaki *et al.* (1991)	87-264	1.3
Yung (1995)	140-980	0.40 or 0.73

Increasing the particle diameter increases the settling velocity of the particle. Consequently, the mean and turbulent velocities of the liquid must be higher to keep the solids in suspension. Therefore, one would expect that an increase in diameter would result in a reduction in the suspension homogeneity at a given operating condition. This was confirmed by the findings from several researchers (Bujalski *et al.*, 1999, Heywood *et al.*, 1991, Nasr-el-din *et al.*, 1996, Nienow, 1968, Rieger *et al.*, 1988, Shamlou and Koutsakos, 1989 and Yung, 1995).

Nasr-el-din *et al.* (1996) stated that increasing the particle diameter at a given operating condition resulted in a reduction in both radial and axial homogeneities. The authors assigned this observation to the propensity of the larger particles to deviate from the streamlines at the vessel wall. This resulted in a higher concentration at the same vertical position as the impeller plane of the RDT.

Near the liquid surface, the time averaged liquid flow field must be parallel to the surface due to the boundary condition of no vertical flow through this plane. Since there is little vertical drag force, particles will spend little time in this region of the vessel. Oldshue (1969) found that it was difficult to get fast settling ($u_t > 0.03$ ms^{-1}) particles to distribute into the top 2% of the vessel due to the lack of forces acting on the particles. Yung (1995) also found that the maximum homogeneity that was achievable decreased with increasing particle diameter.

The differences in settling velocities between particles of different sizes means that in a mixture, faster settling particles will concentrate in areas of low velocity since it is less likely that they will convected away from these areas. Aeschbach and Bourne (1972) performed experiments in a continuous system with a spread of particle sizes and found that there was some classification of the small particles in the vessel. This resulted in the small particles being preferentially carried over at the surface exit.

Results from an unbaffled vessel from the work of White and Sumerford (1933) suggested that a mixture of particles will tend to segregate. The authors found that the large particles settled beneath the impeller and the small particles moved towards the vessel wall. White and Sumerford (1933) also showed that increasing the particle size resulted in an increase in the impeller speed to achieve a given concentration.

Much of the analysis in the literature has been based on the settling velocity of particles rather than investigating the effect of different particle properties separately. This is a logical choice of physical property since in steady flow the particle motion is the liquid flow field superimposed on the particle settling velocity such as in a horizontal sedimentation tank. In unsteady flow, however, particles will experience forces to which they will take a finite length of time to respond. The characteristic relaxation time for a particle in Stokes flow is given by Equation 3.50:

$$\tau = \frac{\rho_S d^2}{18\mu} \tag{3.50}$$

If this time is short compared to the timescale for the disturbances then the particle will move with the flow, otherwise it will deviate from the flow field.

Yung (1995) correlated her data as in Equation 3.51:

$$N_{RSD} \propto d^{0.4} \tag{3.51}$$

Here, N_{RSD} is the impeller speed for given relative standard deviation (RSD), as defined in Equation 3.52:

$$RSD = \frac{1}{C_0}\left[\frac{1}{(n-1)}\sum_{i=1}^{n}(C_i - C_0)^2\right]^{\frac{1}{2}} \tag{3.52}$$

Yung (1995) also correlated her data as a function of particle settling velocity (Equation 3.53):

$$N_{RSD} \propto u_t^{0.64} \tag{3.53}$$

By using Equation A3.1 in Appendix A3 to eliminate u_t, a different exponent on d is predicted (Equation 3.54):

$$N_{RSD} \propto d^{0.73} \tag{3.54}$$

Since the exponents from the two regressions are different, the effect of particle size on the distribution of solids must be more than just the effect that it has on the particle settling velocity. Since the simple 1-d sedimentation dispersion model where the parameter Pe is just a function of u_t, this model is expected to fail.

Kolář (1961) performed measurements of the suspension height that included varying the particle diameter. The results of the regression analysis are shown in Equations 3.32 to 3.35. In the same manner as Yung (1995) the published equations have been modified using Equation A3.1 and the results shown in Table 3.2.

Table 3.2. Effect of particle size from Kolář (1961)

Impeller	Effect of d
Propeller (C=T/9)	$N \propto d^{0.42}$
Propeller (C=T/3)	$N \propto d^{0.53}$
45PBT-4 (C=T/9)	$N \propto d^{0.38}$
45PBT-4 (C=T/3)	$N \propto d^{0.48}$

Experimental results performed in a tall vessel with multiple axial impellers by Magelli *et al.* (1991) were correlated in the form of a Péclet number (Equation 3.55).

$$Pe \propto \left(\frac{u_t}{ND}\right)^{\alpha}\left(\frac{\nu^3}{\bar{\varepsilon}d^4}\right)^{\beta} \tag{3.55}$$

Most of the results presented are in the intermediate settling regime ($u_t \propto d^{1.14}$) with some results in the Stokes regime ($u_t \propto d^2$). Eliminating u_t from Equation 3.55 results in the predictions shown in Table 3.3 for the effect of particle size on the impeller speed for a given degree of homogeneity. The results obtained by Magelli *et al.* (1990) for a system of multiple Rushton impellers are also presented, with the predictions for each of the geometries examined, in Table 3.3.

Table 3.3. Prediction of the effect of particle size from Magelli (1991)

Geometry	α	β	Stokes regime	Intermediate regime
1	1.40	0.20	$N \propto d^{1.43}$	$N \propto d^{0.57}$
2	1.89	0.24	$N \propto d^{1.49}$	$N \propto d^{0.63}$
3	1.58	0.22	$N \propto d^{1.44}$	$N \propto d^{0.58}$
Ave. (1-3)	1.68	0.22	$N \propto d^{1.47}$	$N \propto d^{0.61}$
Rushton	1.17	0.095	$N \propto d^{1.68}$	$N \propto d^{0.82}$

Most of the results obtained were in the intermediate regime. The range of predictions for the exponent on d from Table 3.3 for the intermediate regime is 0.57 to 0.63 for the axial configuration of impellers and 0.82 for the system of Rushton impellers.

Barresi and Baldi (1987a) analysed their data in the form of the dimensionless group in Equation 3.8. They also found that the data from Bohnet and Niesmak (1980) were well correlated by the dimensionless group. The dimensionless group predicts that the impeller speed for a given concentration, $N \propto u_t$. The particles are mainly in the intermediate regime where $u_t \propto d^{1.14}$, thus $N \propto d^{1.14}$. One particle size used is in the fully turbulent region where $N \propto d^{0.5}$ but since the other points are well inside the intermediate regime the model predicts that $N \propto d^{1.14}$ in the range of particle sizes that the model tested.

It was shown by Einenkel (1980) (Section 3.1.2) that the energy balance between the settling velocity of a swarm, w_{ss} and energy dissipation in the vessel predicts that the impeller speed to keep particles in suspension, N is proportional to $w_{SS}^{1/3}$. Small particles, which are in the Stokes settling regime were found to vary as $N \propto d^{0.67}$.

Particles that are in the turbulent settling regime were found to require a smaller increase with $N \propto d^{0.16}$. The author argues that this is because the settling velocity, $w_{ss} \propto d^2$ in the laminar regime and $w_{ss} \propto d^{0.5}$ in the turbulent regime. The correlation that he proposed (Equation 3.20) predicted that $N \propto d^{0.67}$ and $N \propto d^{0.17}$ in the turbulent and laminar regimes respectively which is in agreement with what was observed experimentally. Bohnet and Niesmak (1980) found that this analysis was insufficient to analyse their data (Section 3.1.2).

The design correlation (Eq. 3.16) of Yamazaki *et al.* (1991) predicts that $N \propto d^{1.3}$ in the intermediate particle settling regime for a given degree of homogeneity. The correlation of Pavlushenko *et al.* (1957) for the impeller speed at which the solids distribution becomes almost uniform predicts that $N \propto d^{0.4}$. These experiments mainly covered the Stokes particle-settling regime, although some particles were in the intermediate regime.

Buurman *et al.* (1986) correlated their experimental data in the form of a modified Froude number (Equation 3.39). This method of data analysis predicted the relationship in Equation 3.56 for the impeller speed for a given suspension height.

$$N \propto d^{0.27} \tag{3.56}$$

A summary of the predictions for the exponent on particle size is presented in Table 3.1. There is clearly some spread in the effect of particle size in the literature. The basis of the analysis varied from suspension height to degree of homogeneity and this may be a source of the discrepancy. An evaluation of the different analysis methods is performed in Section 3.1. Another source of the differences will be due to the effect of particle size on the settling velocity. This effect will vary between the different settling regimes. The difference found by Yung (1995) between a regression based on particle settling velocity and one on particle size is of interest.

3.2.2 Effect of density difference

A summary of the studies that have been performed that have examined the effect of particle density on the distribution of solids in a stirred tank are shown in Table 3.4. The information available in the literature has shown that there has been a wide range of predictions on the exponent on particle density.

Table 3.4. Prediction of the effect of density difference from the literature

Paper	Range of density differences	Exponent on $\Delta\rho$
Barresi and Baldi (1987b)	1600-3280	0.71
Buurman *et al.* (1985, 1986)	250-1600	0.5
Einenkel (1980)	2870	0.62 (Laminar) 0.47 (Turbulent)
Hicks *et al.* (1997)	19-1590	0.45
Kolář (1961)	163-2172	0.24-0.35
Magelli *et al.* (1990)	150-7410	0.71
Magelli *et al.* (1991)	1450	0.71
Pavlushenko *et al.* (1957)	1630-3750	0.8
Raghavendra Rao, and Mukherji (1953)	1620-4500	0.51
Weisman and Efferding (1960)	1250-3480	0.24
Yamazaki *et al.* (1991)	1370-1620	0.41
Yung (1995)	50-4550	0.53 or 0.46

Increasing the difference in density between the liquid and solid phases has been shown to reduce the maximum homogeneity that is achievable in a given system (Bohnet and Niesmak, 1980).

Magelli *et al.* (1990 and 1991) and Barresi and Baldi (1987b) all based their analysis on particle settling velocity. By using Equation A3.1, the effect of density difference can be studied. The results obtained by Barresi and Baldi (1987b) were all in the transitional regime so their analysis predicts the relationship in Equation 3.57. Magelli *et al.* (1990 and 1991) used particles in both the Stokes and transitional regimes so Equations 3.57 and 3.58 apply. Most of the results obtained are in the transitional regime and so the results should be predicted by Equation 3.57. The concentration of solids in these experiments was low (0-1.9%v/v). The consequence of this is shown in Section 3.2.3.

$$N_{RSD} \propto (\Delta\rho)^{0.71} \tag{3.57}$$

$$N_{RSD} \propto \Delta\rho \tag{3.58}$$

The use of the modified Froude number (Equation 3.39) by Buurman *et al.* (1985 and 1986) produces a different prediction for the effect of density difference as illustrated in Equation 3.59:

$$N \propto (\Delta\rho)^{0.5} \tag{3.59}$$

Yung (1995) directly calculated the effect of density difference and produced the relationship shown in Equation 3.60. Basing the analysis on a regression analysis on the particle settling velocity, produces a slightly different exponent as shown in Equation 3.61.

$$N_{RSD} \propto (\Delta\rho)^{0.53} \tag{3.60}$$

$$N_{RSD} \propto (\Delta\rho)^{0.46} \tag{3.61}$$

The design correlation (Eq. 3.16) of Yamazaki *et al.* (1991) predicts that $N \propto \Delta\rho^{0.43}$. This result is based on a very narrow range of particle densities (Table A1.2) and should be used with caution despite the observation that it fits in well with the other results.

Einenkel (1980) produced a correlation that included the effect of density difference although the experimental data was limited to glass particles with a density of 2870 kg m^{-3}. This correlation predicts that the impeller speed for a given suspension height is $N \propto \Delta\rho^{0.62}$ in the laminar regime and $N \propto \Delta\rho^{0.47}$ in the turbulent regime.

The correlation of Pavlushenko *et al.* (1957) for the impeller speed for the concentration in the upper portion of the vessel to reach the average concentration predicts that $N \propto \Delta\rho^{0.8}$.

Raghavendra Rao, and Mukherji (1953) compared the impeller speeds required for a given mass concentration at a point in the vessel. They found that increasing the density of the solid phase resulted in an increase in the impeller speed required to keep the concentration constant.

Kolář (1961) found that the impeller speed for a given suspension height varied with impeller design as well as density difference as summarised in Table 3.5. A correction has been used to include the effect that density difference has on the particle settling velocity using Equation A3.1.

Table 3.5. Effect of density difference from Kolář (1961)

Impeller	Effect of Δρ
Propeller (C=T/9)	$N \propto \Delta\rho^{0.27}$
Propeller (C=T/3)	$N \propto \Delta\rho^{0.35}$
45PBT-4 (C=T/9)	$N \propto \Delta\rho^{0.24}$
45PBT-4 (C=T/3)	$N \propto \Delta\rho^{0.31}$

Hicks *et al.* (1997) found that the suspension height for different particles was the same when comparisons were made on the basis of N/N_{js}. The only discrepancy was found to be when experiments were performed with coarse sand which had the highest settling velocity of all the particles tested. Here it was found that the suspension height was somewhat lower than that for the other materials. Since $N_{js} \propto \Delta\rho^{0.45}$ the relationship below applies:

$$N \propto (\Delta\rho)^{0.45} \tag{3.62}$$

The experiments that were performed in standard mixing vessels (Buurman *et al.*, 1985, Hicks *et al.*, 1997 and Yung, 1995) produced similar results. The results that were obtained in dilute systems (Magelli *et al.*, 1990, Magelli *et al.*, 1991 and Barresi and Baldi, 1987b) produced results that indicate a higher exponent on the effect of density difference.

3.2.3 Effect of particle concentration

Overall, the effects of average particle concentration on the impeller speed for a given homogeneity, suspension height or distribution is very small. The largest effect was reported by Weisman and Efferding (1960) who found that the impeller speed for a given suspension height, N, varied with C_0 as follows:

$$N \propto (C_0)^{0.22} \tag{3.63}$$

This result was based upon data obtained for the cases where the concentration was greater than 4.4 %v/v. Concentrations below this value gave results that were not

reproducible.

The findings from other researchers are shown in Table 3.6:

Table 3.6. Prediction of the effect of particle concentration from the literature

Paper	Range of conc/vol%	Exponent on C_0
Barresi and Baldi (1987a)	0.19-0.56	0
Barresi and Baldi (1987a)	0.56-1.9	>0
Bohnet and Niesmak (1980)	0.2-2.0	>0
Buurman *et al.* (1985, 1986)	3-40	0
Einenkel (1980)	5-25	0.31
Fajner *et al.* (1985)	0.041-0.61	0
Heywood *et al.* (1991)	25.6-39.0	>0
Hicks *et al.* (1997)	0-10	>0
Hicks *et al.* (1997)	10-40	0
Hicks *et al.* (1997)	40-49	<0
Kolář (1961)	0.12-10	0.056-0.153 depending upon system
Magelli *et al.* (1990, 1991)	0.041-0.61	0
Mak (1992)	6.3-14	0.05
Nasr-el-din *et al.* (1996)	10-30	>0
Pavlushenko *et al.* (1957)	1.9-7	>0
	7-16	0
Rieger *et al.* (1988)	2.5-10	>0
Shamlou and Koutsakos (1989)	0.35-2.15	<0
Weisman and Efferding (1960)	4.2-27	0.22
Yamazaki *et al.* (1991)	5-20	>0

The results indicate that for very dilute systems (Fajner *et al.*, 1985, Magelli *et al.*, 1990 and 1991 and Barresi and Baldi, 1987a) when the average particle concentration is less than about 1%vol/vol there is no effect on the impeller speed to give a particular distribution of solids when the analysis is performed as normalised concentration. Above this concentration, there is evidence (Bohnet and Niesmak, 1980, Kolář, 1961, Pavlushenko *et al.*, 1957, Rieger *et al.*, 1988, Mak, 1992, Weisman and Efferding, 1960, Yamazaki *et al.*, 1991, Nasr-el-din *et al.*, 1996 and Heywood *et al.*, 1991) that a higher impeller speed to achieve a given homogeneity which increases slowly with the average concentration.

Pavlushenko *et al.* (1957) found that, there was an effect only at low concentrations. This is in contradiction to other researchers in the area. The difference may stem from the use of an unbaffled vessel, which would have a different flow pattern to a baffled vessel, or it could stem from the use of their sampling technique and errors that are found with this method (Nasr-el-din *et al.*, 1996).

Einenkel (1980) found that the impeller speed for a given level of homogeneity is influenced through the effect of concentration on the settling velocity of a swarm of particles. In the case of dilute suspension there is no effect. At high concentrations (C_0>15%v/v) the effect would be very strong.

The correlations published by Kolář (1961) (Equations 3.32 to 3.35) for the suspension of particles to a particular level show that there is a small positive power on the particle concentration term. This was shown to be a function of the vessel geometry and differences are shown between impeller clearance and impeller design. From this observation, one concludes that the hydrodynamics of a system influence the dependency on concentration.

Yamazaki *et al.* (1991) (Section 3.1.1) included the effect of particle concentration in the slurry density and the apparent slurry viscosity. This results in a significantly non-linear variation of impeller speed with concentration. The chosen impeller speed was that at which the concentration at the top of the vessel was 0.8 times that at the vessel base. Their model predicts an increase in impeller speed required with an increase in particle concentration.

Hicks *et al.* (1997) performed experiments with ion exchange resin between 0 and 49%vol/vol. At low particle concentrations it was found that, at a given impeller speed, increasing the particle concentration lowered the height to which the particles were suspended. Between 10-40%vol/vol there was little effect of the increasing particle concentration on the suspension height. Above 40%vol/vol the suspension height increased as the particle concentration was increased. Since an increase in impeller speed above N_{js} invariably results in an increase in the suspension height there are three

regions. The low concentration region, where the impeller speed has to be reduced with increasing particle concentration in order to maintain the same suspension height. The intermediate position, where the impeller speed is maintained constant with increasing concentration and the high concentration region, where the impeller speed has to be reduced as the concentration is increased in order to maintain the same suspension height. Above C_0=40%vol/vol the particle concentration in the suspended layer remained at approximately 64%. In Section 3.3.1 it is shown that for weak flows the maximum concentration that a slurry can attain is 64%. It seems reasonable that the increase in suspension height at the high particle concentrations is a result of steric interactions between the particles.

At low particle concentrations the individual particles will interact only with the liquid phase. Single particles experience an increase in drag due to the interaction with the turbulent eddies (Fajner *et al.*, 1985, Levins and Glastonbury, 1972 and Schwartzberg and Treybal, 1968). This can result in a much-reduced settling velocity for large particles (Fajner *et al.*, 1985). Superimposed upon the particle settling velocity is the impeller induced time-averaged flow field. The effect of particle concentration would be expected to be negligible since the solids will effect the time-averaged and unsteady flow components to such a small effect.

In Figure 3.2, L has been defined as the ratio of the surface to surface distance, x_s and the particle diameter, d as defined in Equation A2.7. At high particle concentrations, particle-particle interactions need to be considered. For a close-packed structure the centre to centre distances vary as shown in Figure 3.2.

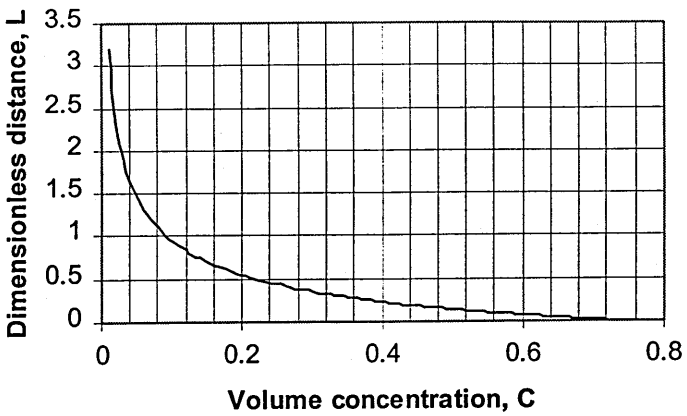

Figure 3.2. The variation of inter-particle distance with concentration.

It can be seen that the average inter-particle distance is one particle diameter when the particle concentration is about 10 %vol/vol. It might be expected that some inter-particle contact will take place at concentrations around 10 %vol/vol and higher. Figure 3.3 shows that the effect of particles on apparent viscosity is small when the concentration is below about 15%vol/vol, which supports the hypothesis that particle-particle interactions only become significant at about 15%vol/vol.

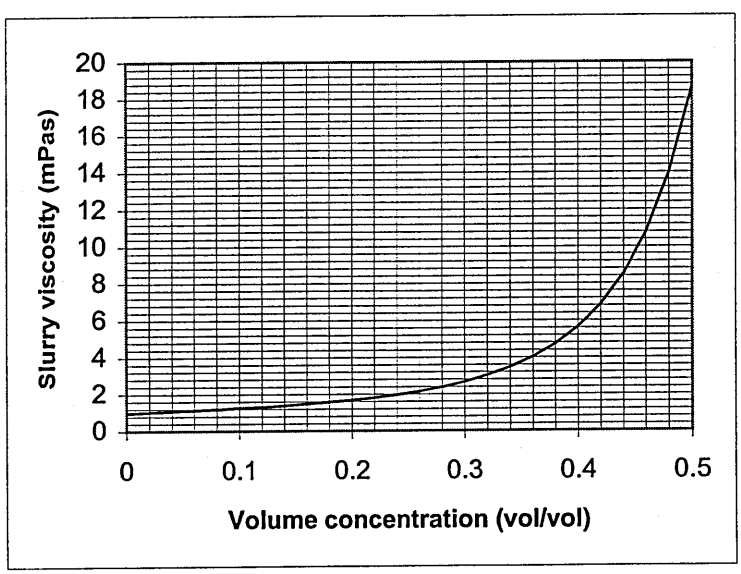

Figure 3.3. The variation of apparent viscosity with concentration.

Hicks *et al.* (1997) showed that at very high particle concentrations, steric interactions have a significant effect on the height to which solids were suspended.

The particle Reynolds number, Re_P is defined as shown in Equation 3.64:

$$Re_P = \frac{\rho_L u_t d}{\mu} \tag{3.64}$$

There will be a strong effect of turbulence damping (Hetsroni, 1989) by small particles (Re_P<110) on the fluid at high concentrations. There is also some evidence of this from the work of Bujalski *et al.* (1999) that found that the mixing times in the clear liquid layer above the suspension and the slurry were significantly different from those where no solids were present. The energy dissipation in the clear layer was found to be low and so the mixing time was found to be long. Large particles (Re_P>400) are turbulence enhancing (Hetsroni, 1989) due to vortex shedding off the particle surface.

At intermediate concentrations the effect of particle concentration would be between the two extremes. Bittorf and Kresta (1999) found that both turbulence and large scale structures were damped out at high solids concentrations.

These observations on the effect of the particles on the fluid flow help to explain the effect that concentration has on the homogeneity. At low concentrations there is little effect on the flow field generated by the impeller as seen in work at concentrations below about 1%vol/vol. As more particles are introduced, the turbulence gets damped and the fluid experiences a drag due to the particles. At very high concentrations there will be some particle-particle interactions and the effect of concentration will become greater as illustrated in Table 3.6.

3.3 Effect of liquid properties on solids distribution

3.3.1 Effect of liquid viscosity

A summary of the studies that have been performed that have examined the effect of liquid viscosity on the distribution of solids in a stirred tank are shown in Table 3.7. The information available in the literature has shown that there has been a wide range of predictions on the exponent on liquid viscosity.

Table 3.7. Prediction of the effect of liquid viscosity from the literature

Reference	Range of liquid viscosity (mPa s)	Exponent on μ
Pavlushenko *et al.* (1957)	1.12-120.6	-0.2
Kolář *et al.* (1961)	1.029-7.01	-0.20-(-0.14)
Hixson and Tenney (1935)	0.89-43.9	>0
Einenkel (1980)	1-96	-0.39 (Laminar) -0.08 (Turbulent)
Buurman *et al.* (1985)	0.54-3.0	0
Weisman and Efferding (1960)	1-25	-0.14
Magelli *et al.* (1990)	0.9-19	-0.15
Magelli *et al.* (1991)	0.7-21	-0.03-0
Yamazaki *et al.* (1991)	1	0.14

A slurry can be characterised using an apparent viscosity as shown in Equation 3.65 (Liu and Masliyah, 1996), which is valid both for dilute and concentrated flows:

$$\mu_S = \mu\left[\left(1-\frac{C}{C_{\max}}\right)^{-2} + \left(k_E - \frac{2}{C_{\max}}\right)C + \left(k_H - \frac{6}{C_{\max}^2}\right)C^2\right] \tag{3.65}$$

where μ_S is the slurry viscosity, μ is the viscosity liquid of the liquid phase, C is the volume fraction of solids and C_{max} is the maximum physically-attainable concentration. For weak flows $C_{max} = 0.64$, for strong flows $C_{max} = 0.71$. The parameter k_E, the Einstein constant, has the value 2.5 and k_H, the Huggin's constant has a value of 6.0 for weak flows ($\dot{\gamma} \to 0$) and 7.1 for strong flows ($\dot{\gamma} \to \infty$). If the conditions of strong flow in water are taken, the function is of the form shown in Figure 3.3.

Figure 3.3 shows that the apparent viscosity of the slurry varies very little with particle concentration in the dilute region (C<0.2vol/vol) and it is in this region where much of the work in the literature has been performed. Since most of the research in the literature has been performed in a region where viscosity effects due to particle concentration are small, this section is limited to the work that is available on the effect of the continuous phase viscosity. Increasing the continuous phase viscosity effects the drag on a single particle, which results in a lower settling velocity. The lower settling velocity results in the solids distribution being more homogeneous. Fajner *et al.* (1985) and Pavlushenko *et al.* (1957) have reported this effect of viscosity.

Increasing the viscosity also decreases the impeller Reynolds number (Equation 3.66).

$$\mathrm{Re} = \frac{\rho_L N D^2}{\mu} \tag{3.66}$$

If *Re* is changed sufficiently, then the hydrodynamic regime may move from the fully turbulent through the transitional into the laminar regime. Moving into the laminar regime results in an increase in power. Considerations on the basis of the same power could indicate that the increase in viscosity would have an increase in the power for a given homogeneity. Weisman and Efferding (1960) noted this.

The analysis of Yamazaki *et al.* (1991) predicts that $N \propto \mu^{0.14}$. The positive exponent is a result of the assumption that *Re* is an important dimensionless group. The data analysis was based only on water and should be used with caution.

Pavlushenko *et al.* (1957) produced the empirical equation shown in Equation 3.36, which predicted the impeller speed for the concentration in the upper part of the tank to reach the average concentration to be $N \propto \mu^{-0.2}$.

The correlation by Einenkel (1980) for the impeller speed for a given homogeneity (Equation 3.20) predicts that in the laminar regime $N \propto \mu^{-0.39}$, and $N \propto \mu^{-0.08}$ in the turbulent regime.

Hixson and Tenney (1935) analysed their data by calculating the ratio of the measured concentration to that at which the system is homogeneous. An average of the ratios from 7 measurement positions was used as a measure of the suspension uniformity. The authors suspended a 2%v/v mixture of 800 μm sand in tap water and sucrose solutions using an upwards-pumping 4PBT45 in an unbaffled vessel. Their results showed that increasing the viscosity at a given impeller speed increased the mixing index. There are two effects here. The first is the initial suspension off the vessel base and second the distribution of the solids in the vessel. This paper lumped the two together, which makes interpretation difficult. What can be seen from their observations is that the clear layer at the top of the vessel was less pronounced at the higher viscosities indicating that the distribution was aided by an increase in liquid viscosity at a given impeller speed.

Kolář (1961) correlated the impeller speed for a given suspension height with settling velocity (Equations 3.32, 3.33, 3.34 and 3.35). These results have been modified using Equations A3.1 and A3.2 to examine the effect of liquid viscosity. The results of this are shown in Table 3.8.

Table 3.8. Effect of particle diameter from Kolář (1961)

Impeller	Effect of μ
Propeller (C=T/9)	$N \propto \mu^{-0.15}$
Propeller (C=T/3)	$N \propto \mu^{-0.20}$
45PBT-4 (C=T/9)	$N \propto \mu^{-0.14}$
45PBT-4 (C=T/3)	$N \propto \mu^{-0.18}$

3.4 Conclusions

The data modelling methods shown in Section 3.1 are quite varied. Simple models based on particles settling against a diffusive force are used extensively, the reason being their simplicity. These types of models have been shown to be useful in vessels where the turbulence distribution is homogeneous such as in tall vessels stirred by multiple impellers. Other methods have been devised based on energy balances and dimensionless analysis, which have also been found to be useful in describing the solids concentration profiles.

Most methods of data analysis in the literature involve the settling velocity and this may be a useful method of looking at the effect of liquid and particle properties. The area where most disagreement lies is with the effect of particle density and diameter. This may be due to the particle settling regime. Ideally, experiments should be performed in either the fully turbulent or fully laminar settling regime or the effect included through the use of the particle drag coefficient.

The data analysis methods used in the literature were usually performed using the settling velocity as the characteristic physical parameter. The results in the literature that were based on the settling velocity were split into individual physical effects by using the correlation for the effect of particle diameter on the particle settling velocity from McCabe *et al.* (1985).

The exponents that were found in the literature for the effect of particle size (Section 3.1) were found to be in the range $N \propto d^{0.27\text{-}1.3}$. The wide range of predictions for the effect of particle diameter is a result of the models chosen to describe the particle size effect. The prediction for $N \propto d^{0.27}$ was obtained in the work of Buurman *et al.* (1986) who examined their results on the basis of a modified impeller Froude number. The prediction of $N \propto d^{1.3}$ was obtained for the work of Yamazaki *et al.* (1991) who based their results on the sedimentation-dispersion model and set the unique condition that the concentration at the liquid surface is 80% of that at the vessel base.

An examination of the information in the literature on the effect of density difference reveals that the predictions are in the range $N \propto \Delta\rho^{0.24\text{-}0.8}$. The largest value was produced from data obtained by Pavlushenko *et al.* (1957) for the condition that the local concentration in the upper part of an unbaffled vessel reached C_0. The smallest value was found by Kolář (1961) who measured the impeller speed for a given suspension height in a fully baffled vessel. The discrepancy in the value of the exponent found is not surprising given the range of vessel geometries employed and conditions used to describe the distribution, as shown in Section 3.2.2.

The literature review on the effect of concentration (Section 3.2.3) indicates that below about C_0=1%vol/vol the amount of solids present has no effect on the impeller speed to attain a given normalised particle concentration. Above 1%vol/vol it would appear that higher impeller speeds are required to obtain the same suspension quality as the particle concentration increases. The largest effect of particle concentration was found by Einenkel (1980) with $N \propto C_0^{0.31}$. Other researchers have found the value to be about $N \propto C_0^{0}$.

Findings from previous researchers on the effect of liquid viscosity (Section **3.3.1**) indicates that $N \propto \mu^{-0.2}$ although there is some spread in the values found. This is not surprising since an increase in viscosity results in a reduction in the particle settling velocity. Slower settling particles require smaller velocity fluctuations and steady flows to be convected upwards.

CHAPTER 4.AIMS OF WORK

The aims of this study were:

1) To investigate the effect of vessel scale on the solids concentration at different points in a stirred vessel for:
   - A 4PBT-45 (D=T/2, C=T/4)
   - A 4PBT-45 (D=T/3, C=T/4)
   - A Lightnin A310 (D=T/3, C=T/4).

2) To examine the effect of impeller design on the solids concentration at different points in a stirred vessel.

3) To examine the effect of particle size on the solids concentration at different points in a stirred vessel.

4) To produce design correlations for the distribution of solids in a standard mechanically stirred vessel.

5) To supply reliable large scale data to the CFD modelling group within BHR Group.

CHAPTER 5.EQUIPMENT, MATERIALS AND METHODS

Experiments were conducted in 0.61 m and 1.83 m diameter vessels. The larger vessel used in this work was approaching the sizes of those used industrially. The larger the scale of operation, the more reliable will be the scale-up rules that are derived from the work become. The conductivity of the suspension was measured which allowed the particle concentration to be calculated. The shaft torque was also measured so that the power supplied to the vessel contents could be calculated.

5.1 Experimental work

5.1.1 Mixing equipment

a) Vessels

Tests were performed in two geometrically similar cylindrical vessels with internal diameters of 0.61 m and 1.83 m (Figure 5.1), to examine the effect of scale-up.

The 0.61 m (T_{61}) diameter vessel was constructed from Perspex® to enable visual observations. The 1.83 m (T_{183}) diameter vessel was constructed from mild steel with four Perspex® windows to allow flow visualisation.

In all cases, the impeller shaft was mounted centrally in the vessel. The slurry height, H, was equal to the vessel diameter T, for all experiments. This gave a total slurry volume of 0.165 and 4.46 m^3 in T_{61} and T_{183} respectively.

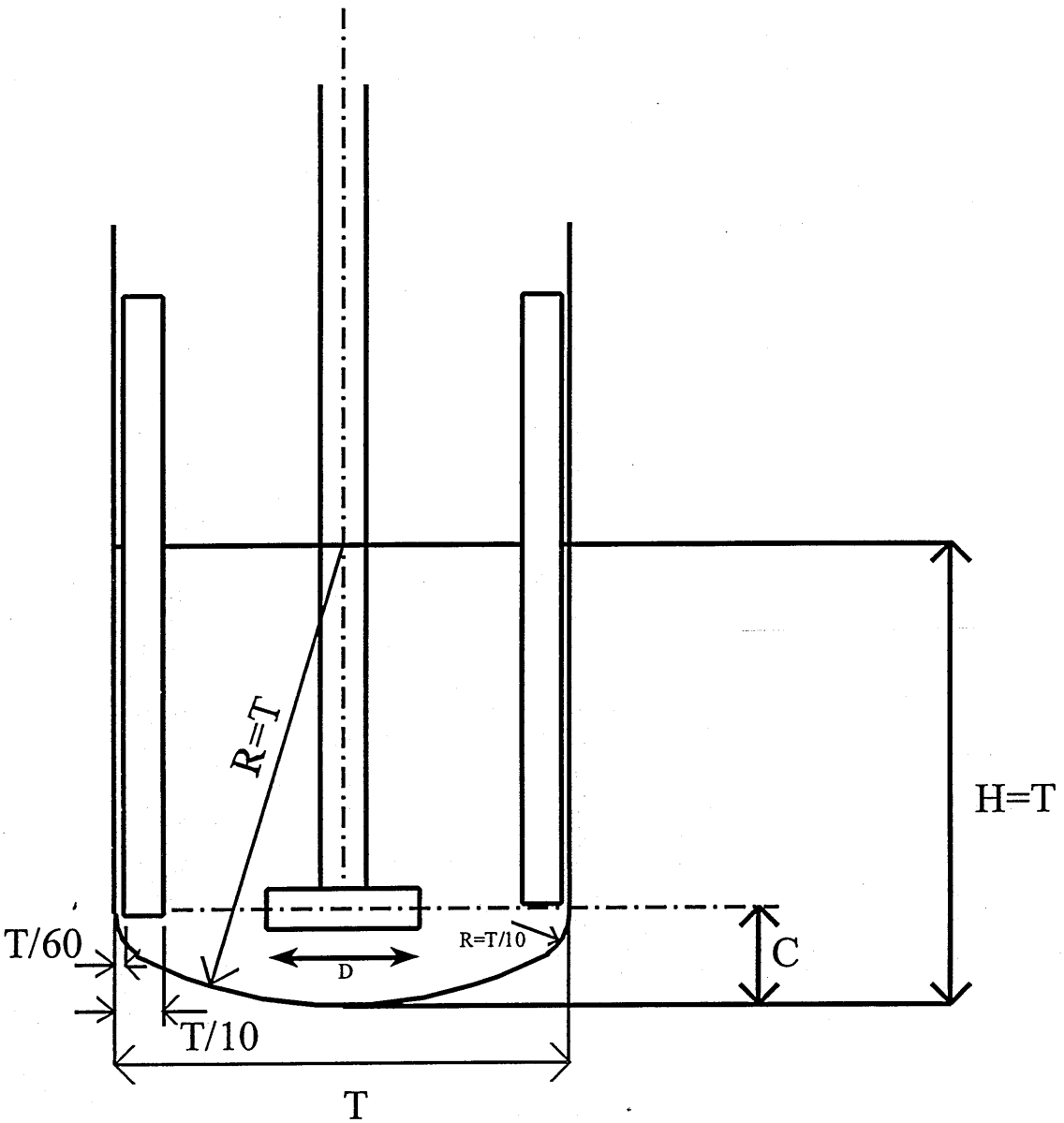

Figure 5.1. Details of the vessel configurations.

The torispherical vessel bases for T_{61} and T_{183} were constructed from Perspex® and mild steel respectively and were manufactured according to Deutsche Norm 28011. This code has bottom and knuckle radii of T and $T/10$ respectively, which results in a depth from the lower tangent line to the bottom of the vessel of $T/5.1$.

Four vertical strip baffles were spaced equally around the circumference of the vessel. Each baffle was $T/12$ wide and spaced $T/60$ from the vessel wall, giving a total distance of $T/10$ from the inner baffle edge to the vessel wall.

b) Impellers

Two sizes of pitched blade turbines (PBTs) and one size of Lighnin' A310 hydrofoil impeller were used in this study. Figure 5.2 shows the nomenclature used for the impeller dimensions. The dimensions of the impellers used in this study are summarised in Table 5.1.

The off- bottom clearance, C between the lowest point in the vessel and the impeller centre was $T/4$ during the experiments.

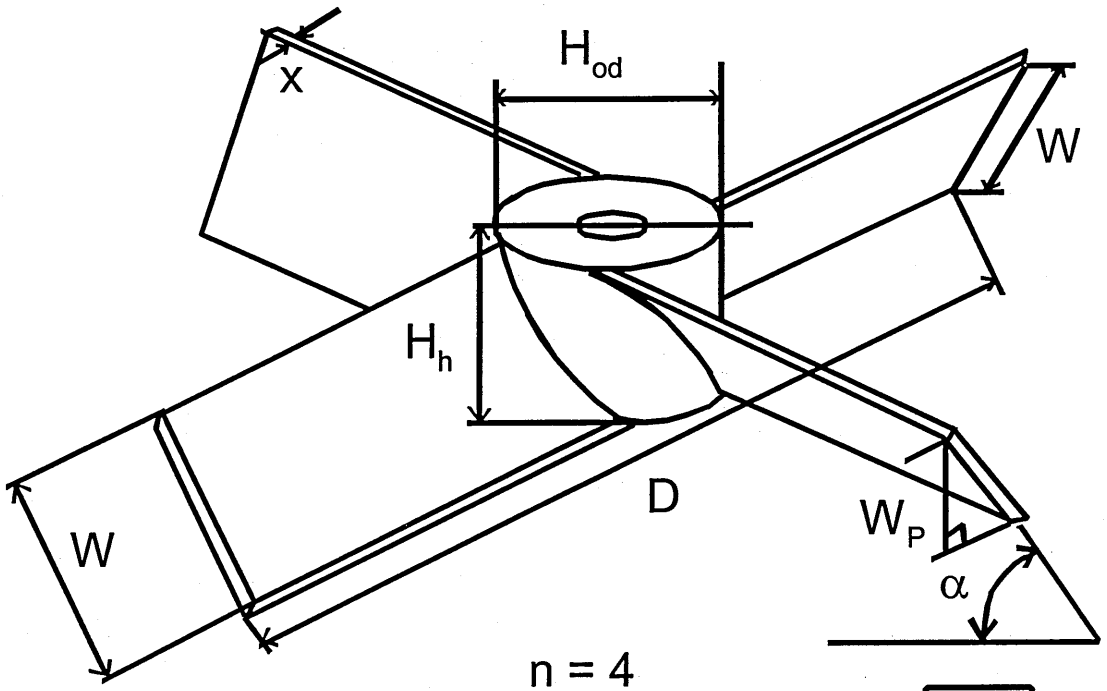

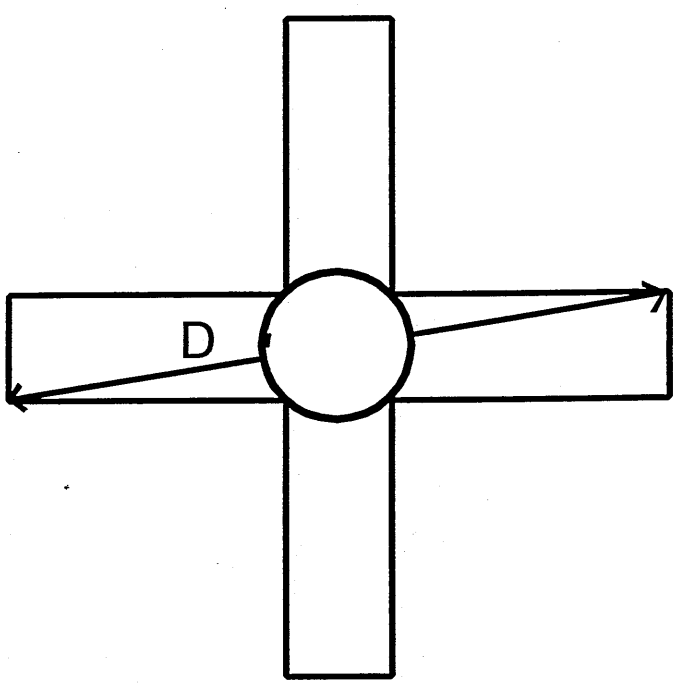

D	-	Impeller Swept Diameter
H_h	-	Hub Height
H_{od}	-	Hub Outside Diameter
n	-	Number of Blades
W	-	Blade Width
W_p	-	Projected Blade Width
α	-	Pitched Angle to Horizontal
x	-	Blade Thickness

Figure 5.2. Pitched blade turbine configuration

Table 5.1. Characteristics of impellers used

Vessel diameter (m)	Impeller	D(m)	H_h(m)	H_{od}(m)	n	W(m)	W_P(m)	α(°)	χ(m)	Po (-)
0.61	T/2 45°PBT4	0.278	0.050	0.050	4	0.055	0.039	45	0.003	1.20
	T/3 45°PBT4	0.205	0.040	0.057	4	0.057	0.040	45	0.003	1.68
	T/3 A310	0.193	-	-	3	-	-	-	-	0.32
1.83	T/2 45°PBT4	0.920	0.120	0.165	4	0.173	0.120	45	0.010	1.38
	T/3 45°PBT4	0.620	0.120	0.165	4	0.174	0.120	45	0.010	1.93
	T/3 A310	0.611	0.085	-	3	-	-	-	0.006	0.30

5.1.2 Test media

The experiments examining the effect of impeller design and impeller diameter were performed with Chelford 30 sand of mean size 590 μm. Additional experiments examining the effect of particle size and vessel scale were performed with particles of sauter mean diameter, d_{32} = 150, 320, 590, and 1050 μm. d_{32} is defined in Equation 5.1:

$$d_{32} = \frac{\sum_{i=1}^{N} n_i d_i^{\,3}}{\sum_{i=1}^{N} n_i d_i^{\,2}} \tag{5.1}$$

Here n is the number of particles of diameter d_i and N is the total number bins upon which the calculation of d_{32} is based.

All of the sand particles were obtained from Hepworth Minerals and Chemicals Limited in Brookside Hall, Sandbach, Cheshire, CW11 0TR.

The particle size distribution was measured by taking a known mass of the sand and passing it though a series of Endecott BS410 Laboratory Test Sieves that were shaken using an Endecott 2MK1 Test Sieve Shaker. The mass of each sieve was noted when empty and at time intervals of 15 mins, 30 mins, 60 mins, 120 mins, etc. Once there was no further change between two consecutive measurements of the mass the experiment was stopped. The total mass of sand was checked at each time interval to ensure that no sand was lost during the sieving process. An example graph of how the mass on each sieve varied with time is shown in Figure 5.3:

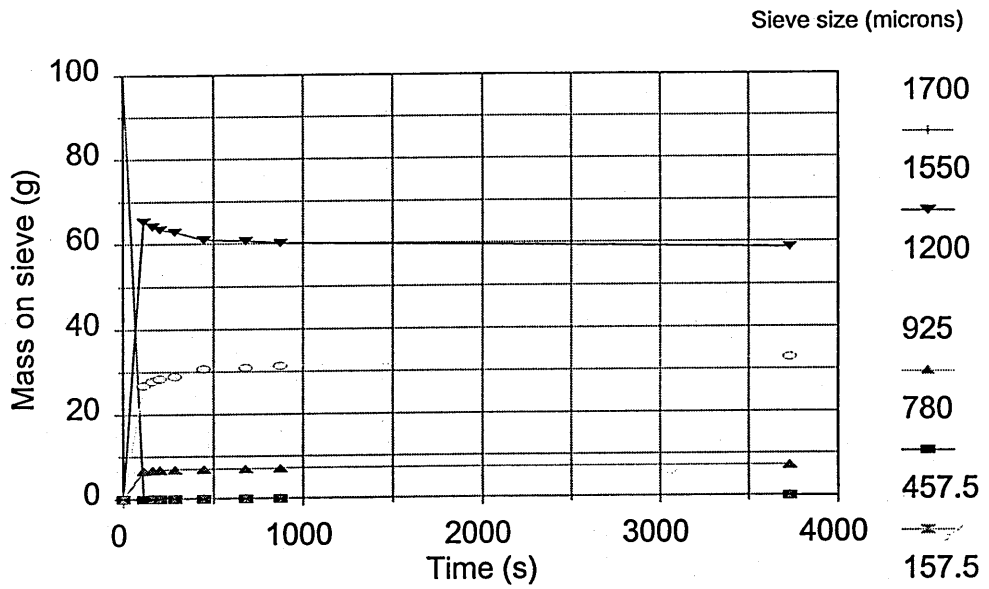

Figure 5.3. Sieve analysis of 1050μm diameter sand.

The particle size distribution of the sand particles can be seen in Figures 5.4-5.7. The sieve size analyses are presented as the mass in each interval divided by the size of the interval:

$$P(d) = \frac{M(d_i < d < d_{i+1})}{(d_{i+1} - d_i)} \tag{5.2}$$

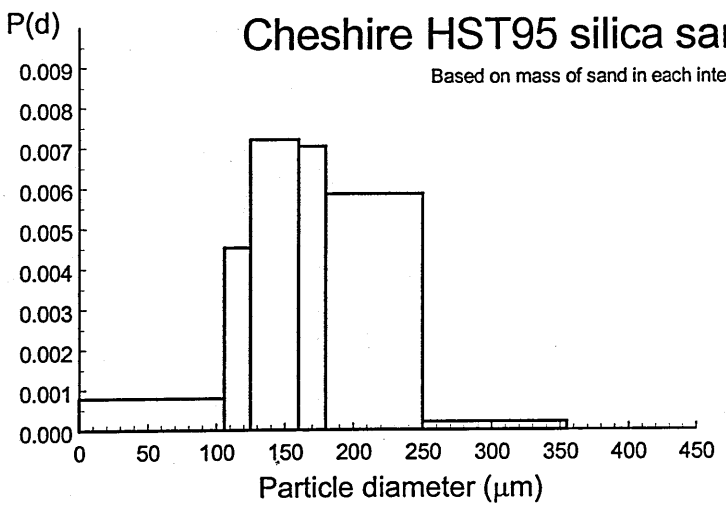

Figure 5.4. Sieve analysis of 150μm diameter sand.

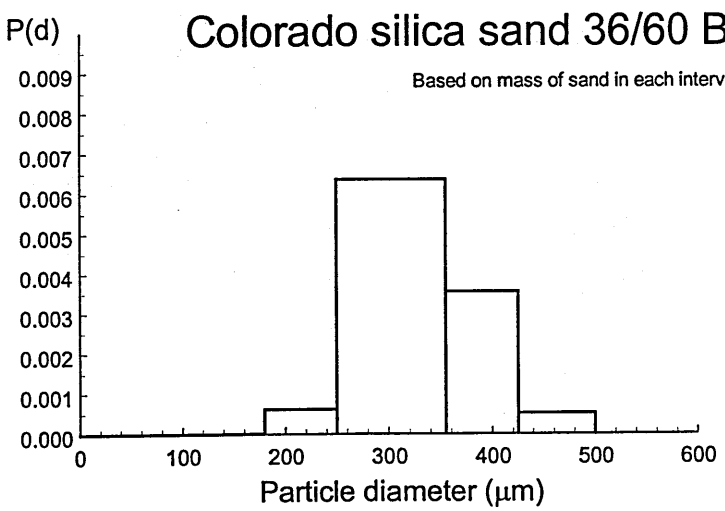

Figure 5.5. Sieve analysis of 320μm diameter sand.

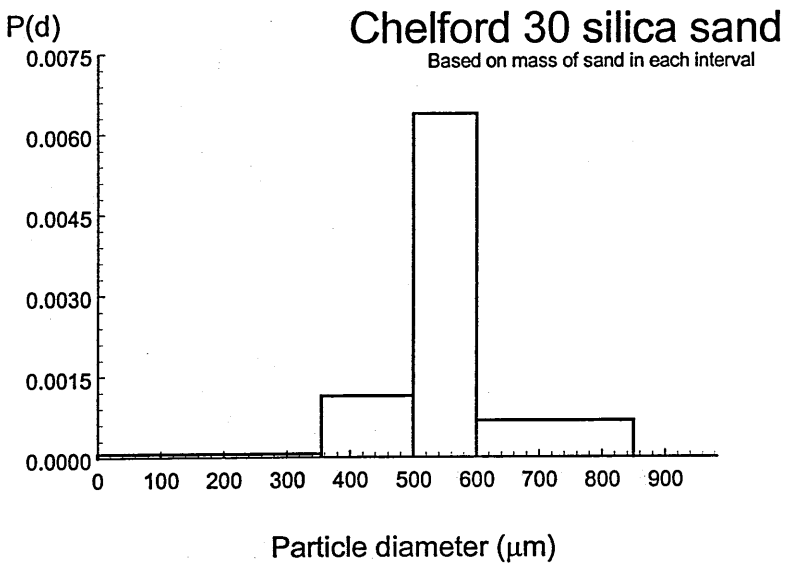

Figure 5.6. Sieve analysis of 590μm diameter sand.

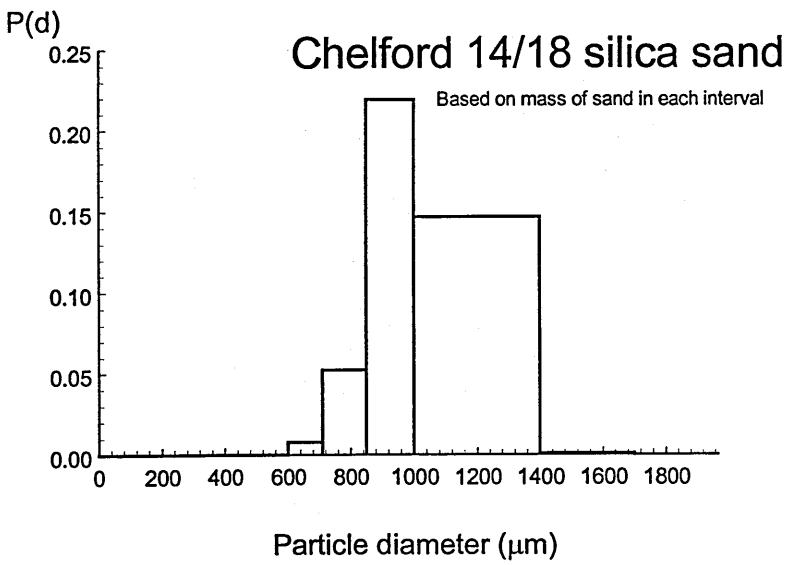

Figure 5.7. Sieve analysis of 1050μm diameter sand.

Throughout the experiments, tap water at room temperature was used. The temperature of the water varied between 9°C and 18°C. The tank-averaged sand concentration was 6.29%vol.

5.1.3 Impeller rotation speed

The impeller speed was measured in both vessels using a tachometer. The order of the speeds for the tests was randomly chosen to randomise any time variant errors due to effects such as the variation of system temperature which may have effected the liquid viscosity.

5.1.4 Torque measurement

The torque was measured in both vessels using strain gauge bridges which produced an output voltage which was proportional to the applied torque. Both systems were regularly calibrated by applying known torques and measuring the output voltage,

The power input was obtained from the measured speed, N, and torque, Λ, from:

$$P = 2\ \pi\ N\ \Lambda \tag{5.3}$$

5.1.5 Solids concentration measurement

a) Solids concentration probe

The local solids concentration was measured using a horse-shoe shaped conductivity probe. A diagram of this probe is shown in Figure 5.8.

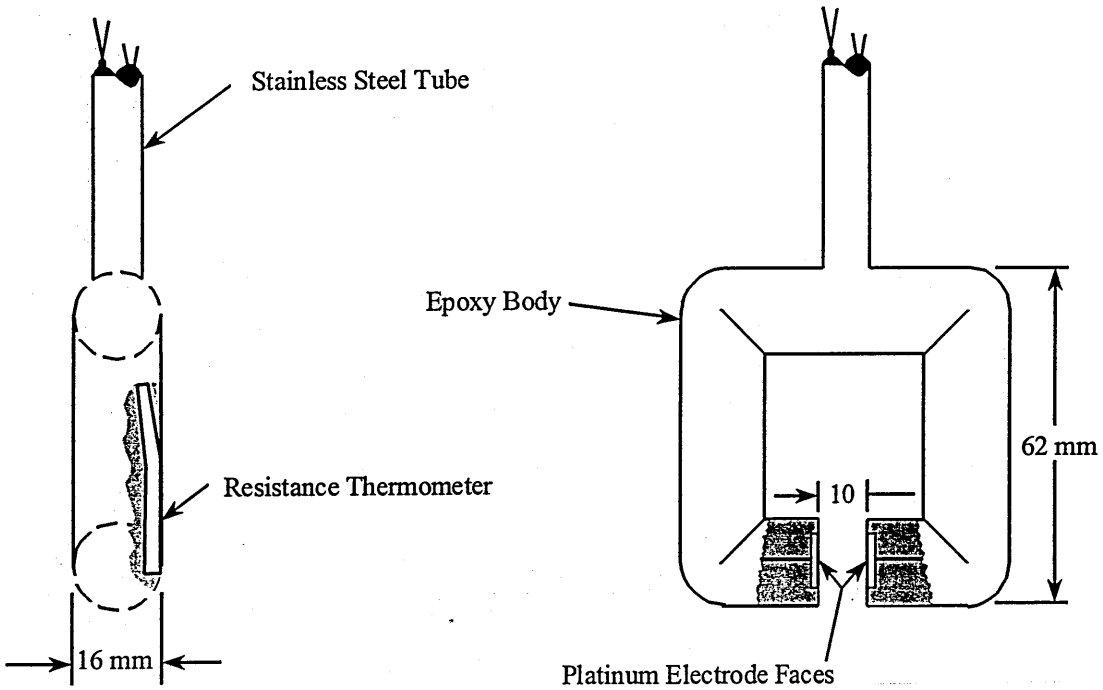

Figure 5.8. Solids concentration probe

The probe was equipped with a platinum resistance thermometer to enable the measurement of temperature. This allowed for the changes in liquid phase conductivity with temperature to be corrected.

A linear relationship between conductivity and local solids concentration was found during the calibration of the probe using a fluidised bed (Mak 1992).

b) Probe location and orientation

The probe was clamped in different positions with its closed side facing the vessel radius (Figure 5.9).

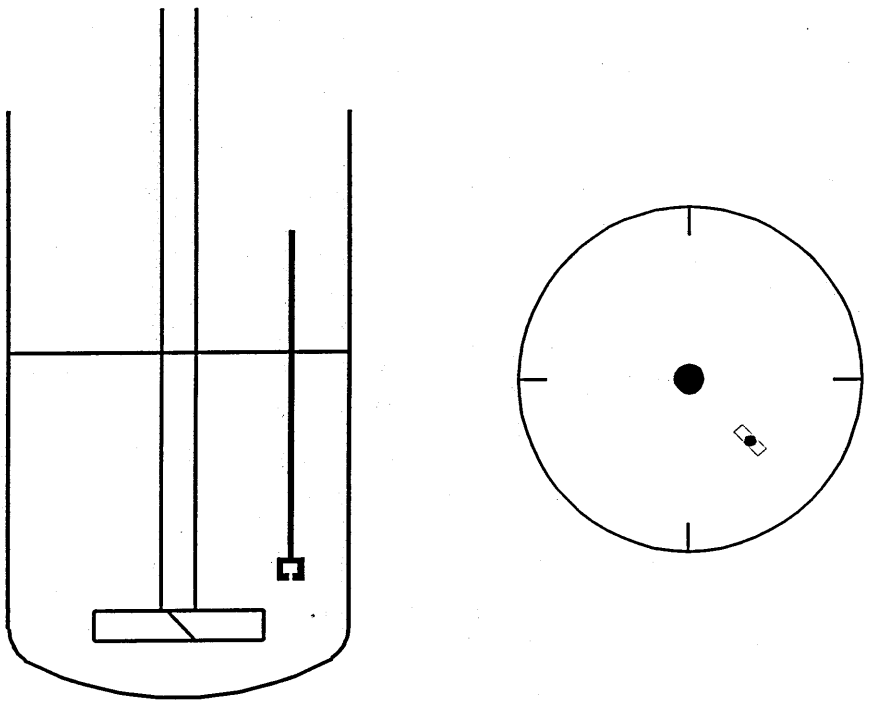

Figure 5.9. Solids concentration probe orientation.

All measurements were made in the plane equidistant between two adjacent baffles. Figure 5.10 shows the range of positions covered in most of this work. A particular position was identified by the radial distance from the shaft normalised by the vessel radius and the height above the vessel base normalised by the fill height.

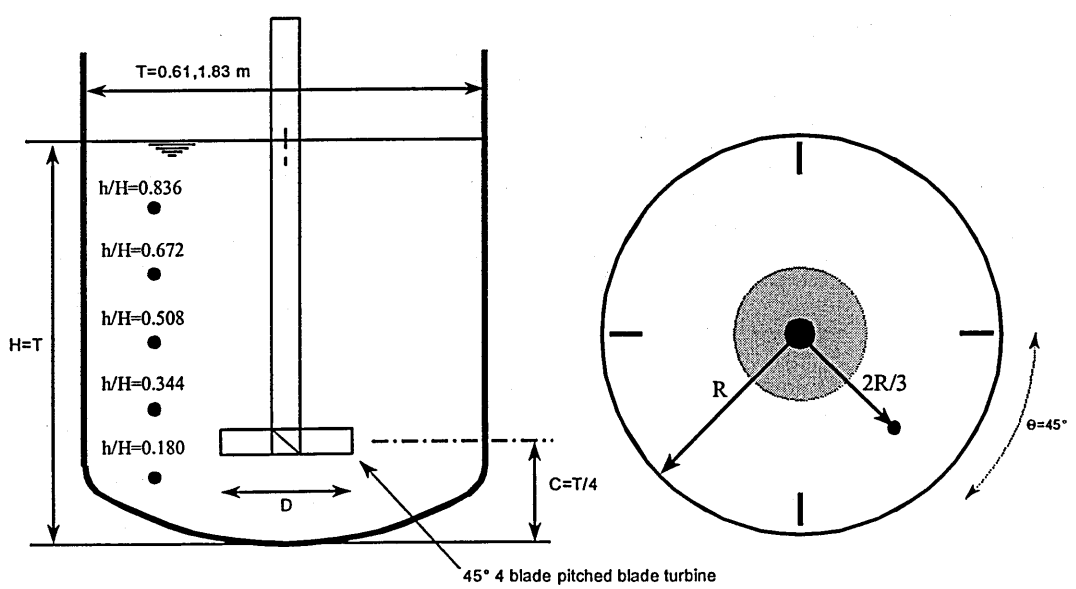

Figure 5.10. Measurement positions for most tests.

The measurement positions for the PBT ($D=T/2$) and PBT ($D=T/3$) in T=0.61m to examine the effect of impeller diameter included some additional positions so that the variation in concentration across a whole plane could be seen. These are shown in Figure 5.11. Some measurements were performed beneath the impeller to examine whether there was a region of high concentration there.

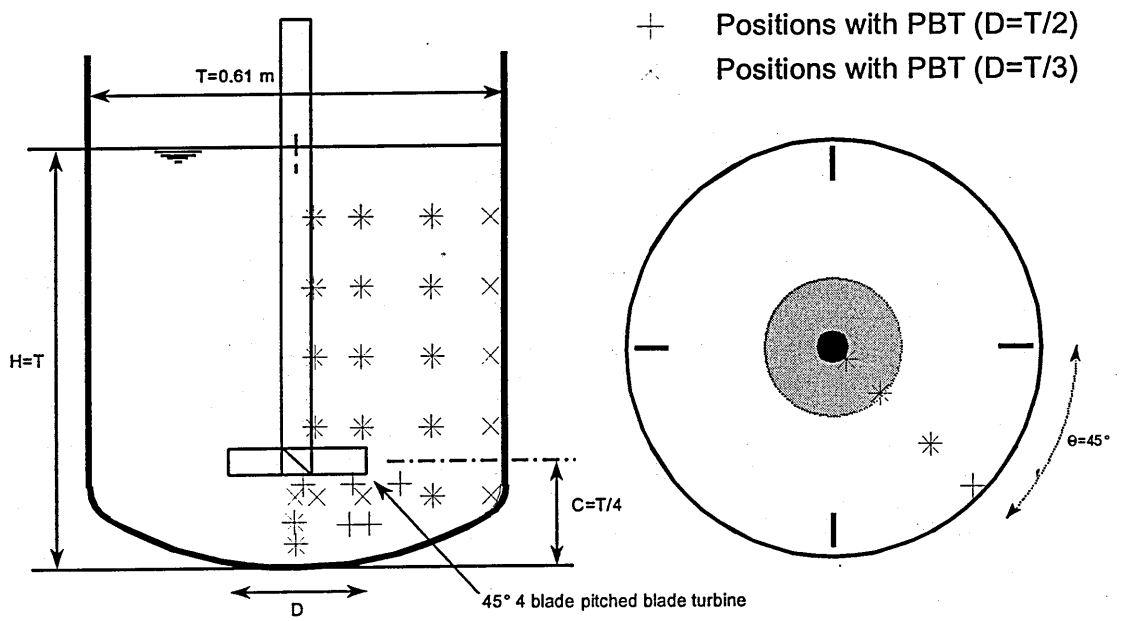

Figure 5.11. Measurement positions for 45°PBT4 (D=T/3, T/2), d=590 μm in T=0.61m.

Detailed experiments were also performed in the 0.61m vessel using the 150 μm sand. These experiments were performed so that the effect of particle size on the solids concentration profile could be evaluated. The measurement positions for these tests are shown in Figure 5.12.

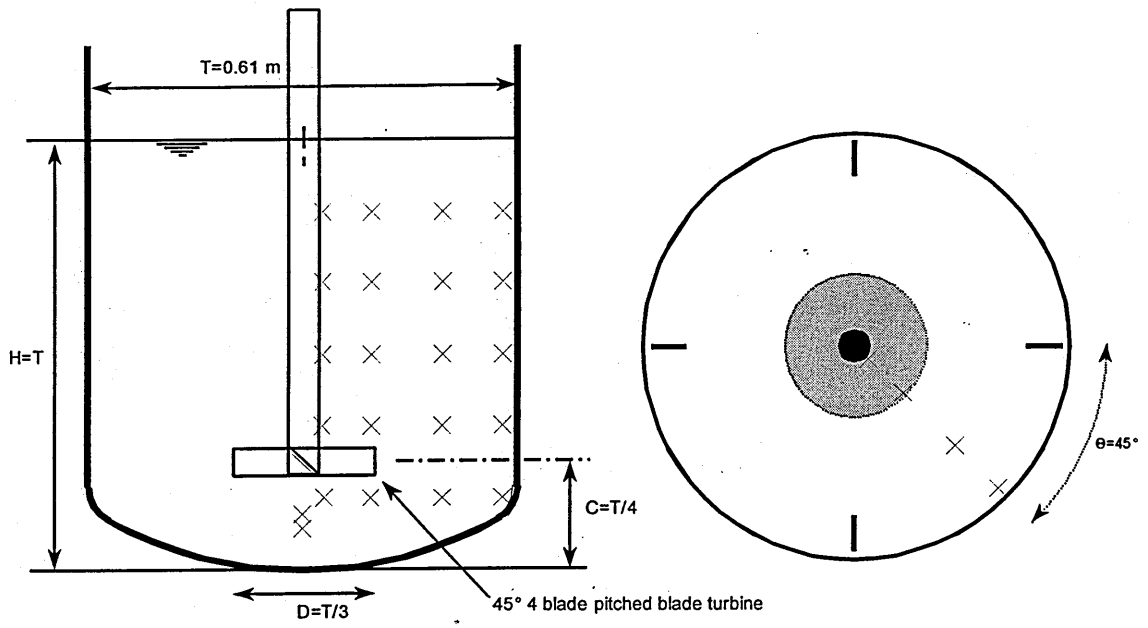

Figure 5.12. Measurement positions for 45°PBT4 (D=T/3, T/2), d=150μm in T=0.61m.

5.1.6 Data acquisition system

A Yokagowa SC200S conductivity meter processed the signal from the probe. This provided a voltage signal to the 16 channel analogue-to-digital converter in a *Tulip AT compact 2* personal computer with a 286 chip. This signal was then converted by the PC into a conductivity reading and then into a particle concentration value based on the calibration curve.

The background conductivity was measured while running the impeller very slowly to ensure flow of liquid over the probe without any solids passing through. This was repeated after a measurement of concentration was taken so that the error in the background conductivity could be estimated. The background conductivity was measured for 3 minutes in the T=1.83 m vessel and 1 minute in the T=0.61 m vessel.

It was found that the particle concentration in the 0.61m vessel reached equilibrium after about 1 minute following a step change in impeller speed. The apparatus was allowed to equilibrate for 3 minutes between changes in impeller speed to ensure that equilibrium was achieved, before taking a measurement. In the T=1.83m diameter tank, the equilibrium time was found to be 5 minutes, so a rest period of 15 minutes was allowed between changes in impeller speed.

5000 measurements were taken over a fixed period of 3 minutes in the T=1.83 m vessel and 1 minute in the T=0.61 m vessel so that a representative sample could be obtained. The mean concentration and standard deviation were calculated. From these, the 95% confidence interval was calculated. This was then combined with the background error to give an estimate of the 95% confidence limit for the concentration value.

CHAPTER 6.EXPERIMENTAL RESULTS

6.1 Experiments performed

6.1.1 Effect of impeller diameter, impeller design and vessel scale

The time-variant particle concentrations were measured at each of the impeller speeds shown in Table 6.1. The results have been normalised by the vessel-averaged particle concentration and listed as C/C_0 values in Appendix 4.

Table 6.1. Experiments performed to examine the effect of impeller diameter, impeller design and vessel scale.

d (μm)	T (m)	Impeller	D/T	N (rpm)	Results
590	0.61	PBT	0.33	360, 380, 390, 400, 420, 445	Table A4.1
590	0.61	PBT	0.5	200, 220, 240, 260, 280, 300	Table A4.2
590	1.83	PBT	0.33	60, 80, 100, 110, 120, 130, 140, 150, 160, 170, 180, 190, 200	Table A4.4
590	1.83	PBT	0.5	10, 20, 30, 40, 50, 60, 70, 80, 90, 100, 110, 120, 130	Table A4.5
590	1.83	A310	0.33	60, 80, 100, 120, 140, 160, 180, 200, 220, 240, 260, 280, 300	Table A4.6

6.1.2 Effect of particle size

The time-variant particle concentrations were measured at each of the impeller speeds shown in Table 6.2 and the C/C_0 values listed in Appendix 4.

Table 6.2. Experiments performed to examine the effect of particle diameter.

d (μm)	T (m)	Impeller	D/T	N (rpm)	Results
150	0.61	PBT	0.33	190, 200, 220, 240, 260, 280, 300	Table A4.6
150	1.83	PBT	0.33	75, 80, 85, 90, 100, 110, 120, 130	Table A4.7
320	1.83	PBT	0.33	40, 60, 80, 100, 105, 110, 115, 120, 125, 130, 135, 140, 145, 150, 160, 170, 180, 190, 200	Table A4.8
1050	1.83	PBT	0.33	80, 100, 110, 120, 130, 135, 140, 145, 150, 155, 160, 165, 170, 175, 180, 185, 190, 200	Table A4.9

6.2 Measurements made

The measurement positions have been identified by the normalised radial direction, r/R, and the normalised height above the vessel base, h/H, and are detailed in Section 5.1.5. The particle concentration at each of these points was monitored for a period of 1 minute in the 0.61m diameter vessel and 3 minutes in the 1.83m diameter vessel. The data acquisition system presented the data in the form of a mean particle concentration over that time frame and the standard deviation about the mean of the data.

The temperature was measured halfway through each of the tests and recorded. The effect of temperature was found to be negligible and has not been presented in Appendix 4.

The voltage from the strain gauge bridge was recorded during the period of the test and the time-averaged voltage was recorded in the experimental log book.

6.3 Manipulation of data

The particle concentration data was normalised by the tank-averaged particle concentration. Particle concentrations less that 1.00 represent concentrations below the tank-averaged concentration, those greater than 1.00 represent positions with particle concentrations greater than the tank-averaged particle concentration.

The standard deviation about the mean of the concentration data was converted by multiplying by 1.96 (Chatfield, 1997) to give the 95% confidence interval for the mean particle concentration. This too was normalised by the tank-averaged particle concentration to give the 95% confidence interval on the normalised particle concentration and has been presented with the data in Appendix 4.

The voltage measured across the strain gauge bridge was converted to torque using the conversion factors obtained during the frequent calibrations of the strain gauges on the shaft. The shaft torque was then converted to power using Equation 5.3 and presented as supplied shaft power per volume of vessel in Appendix 4.

To examine the effect of impeller diameter, impeller design and vessel scale, the normalised data has been plotted against impeller tip speed and power per unit volume so that the data sets can be compared on these bases. To examine the effect of particle size, the normalised data has been plotted as a function of impeller speed and particle size.

Some qualitative comparisons of the effect of particle size and impeller diameter were performed using the data sets from the 0.61m diameter vessel. The data was plotted as a bubble plot across the plane midway between the baffles. These comparisons should only be used qualitatively.

CHAPTER 7.DISCUSSION

Data was obtained using a variety of impellers and at two vessel diameters and a variety of particle sizes were used. These data have been presented so that the effect of scale, impeller design, impeller diameter and particle size could each be examined. A variety of data methods have been attempted with varied degrees of success.

7.1 Concentration profiles - General points

7.1.1 Different degrees of suspension

The plots of normalised particle concentration against impeller speed all show a similar trend at the measurement positions in the lower half of the vessel. Figure 7.1 shows one example of the effect of N on C/C_0 where the data was obtained using a 4PBT45 (D=T/3) in T_{183} at (r/R=0.67, h/H=0.34) and using particles of d_{32}=590 μm.

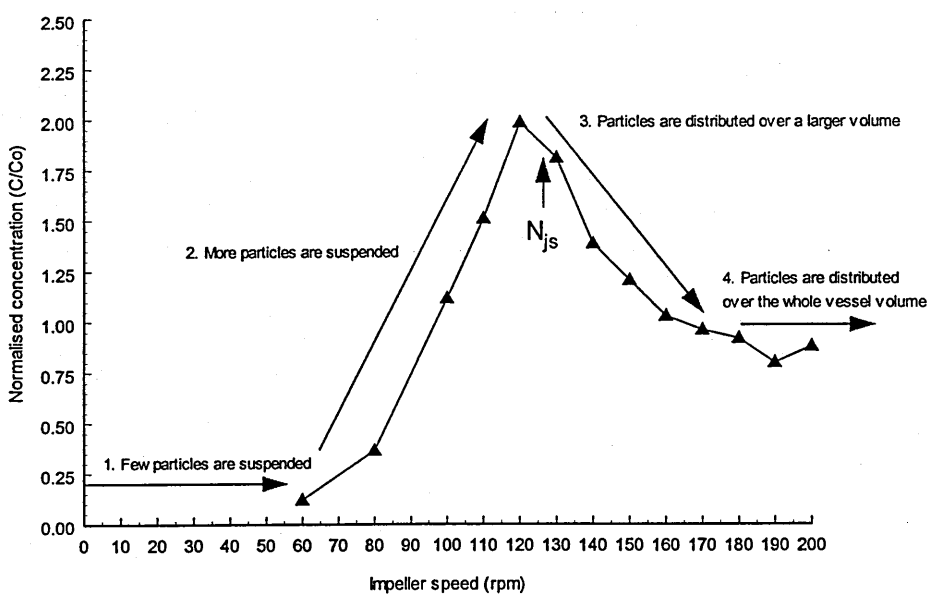

Figure 7.1. Features of a solids distribution curve.

The main characteristics of the change of C/C_0 with N are:

1. The particle concentration is zero when the impeller is stationary.
2. As the speed is increased up to N_{js}, more solids are picked up and suspended in the liquid. Therefore, the solids concentration rises as the impeller speed is increased.
3. Once all the solids have been suspended, the concentration then falls as solids are suspended to higher points in the vessel and hence over a larger volume.
4. An impeller speed is finally reached at which the solids occupy all regions of the tank and so the vessel is effectively homogeneous and no further change in concentration is noted.

Figure 7.1 also shows that N_{js} can be determined from the maximum in the plot provided that the increase in concentration due to suspension is faster than the rate at which the concentration falls due to suspension into higher points in the vessel. A conductivity probe near to the vessel base could allow determination of N_{js}. Since this method is more objective than the traditional method of visual observation of the impeller speed where particles remain stationary on the vessel base for no longer than 1-2 seconds (Zwietering, 1958), the disagreement between different observers would be significantly reduced. Musil and Vlk (1978) successfully used this method to measure N_{js}.

7.1.2 Mass balance

The total mass in the vessel was calculated using the solids concentration measurements. The vessel was divided up into a series of volumes whose centres lie at the measurement points for this purpose.

Figure 7.2 shows how the calculated mass balance varied with impeller speed during the experiments in T_{183} with a 4PBT45 (D=T/3) to suspend solids with d_{32}=150 μm. It was found that there was some scatter in the calculated mass balance due to the coarseness of the measuring matrix in T_{183}. When the mass balances between 80 and 130 rpm were averaged, which corresponds to the conditions above N_{js}, a value of 98% was obtained.

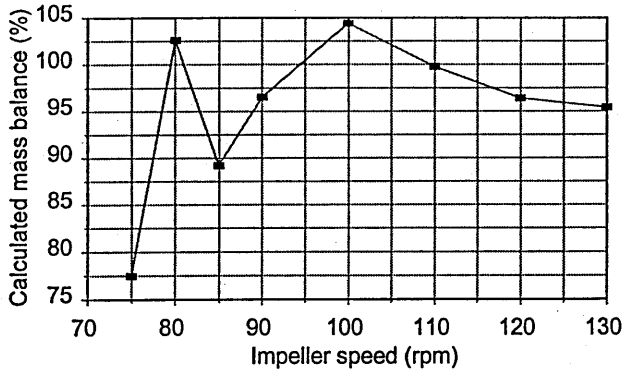

Figure 7.2. Plot of calculated mass balance with impeller speed (T=1.83m, d=150 μm, 4PBT45, D=T/3, C=T/4).

When the results obtained using the large-diameter PBT in T_{61} to suspend solids with d_{32}=590 μm were examined, a mass balance of 90% was calculated. Figure 7.3 shows how the apparent mass in the vessel varied with the number of measurement positions that were considered. It can be seen that as the number of measurement positions was increased for this impeller, the amount of solids that were accounted for also increased. From this trend further improvements in the mass balance would be observed as more measurement positions were introduced.

Localised high concentration regions have been found beneath the impeller as well as near to the vessel wall. The large concentration gradients that were observed in T_{61} when solids with d_{32}=590 μm were used resulted in a poor mass balance. These positions needed to be investigated more thoroughly to obtain a better mass balance. The large concentration gradients were not observed in the experiments performed using the small sand (d_{32}=150 μm) and this problem was not apparent.

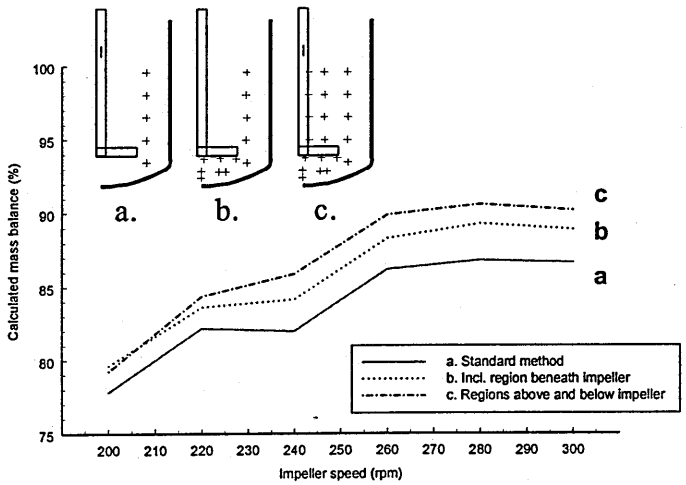

Figure 7.3. Plot of calculated mass balance with impeller speed (T=0.61m, d=590 μm, 4PBT45, D=T/2, C=T/4).

7.2 Empirical analysis of data

The literature review has demonstrated that a variety of predictive methods for scale-up have been found that range from impeller tip speed to specific power. Tank mean and RMS velocities have been found to scale with impeller tip speed (Musgrove, 1998). If kinematic similarity was important, then impeller tip speed would be expected to be a useful criterion for solid-liquid systems. An alternative mechanism that might be important is the energy supplied to the suspension, which prevents settling. In the literature, data analysis has been performed at these extremes and also at predictions in between these two extremes. This work has made comparisons between these two predictions. This allowed the experimental data obtained to be analysed in the same way as was presented by Mak (1992) who examined the variation of RSD with impeller speed and specific power.

RSD has been used in the past because it is a single value that represents the homogeneity of the whole tank. This allowed the effect of impeller speed and specific power on the tank homogeneity to be quantified. The parameter says nothing about the point tank concentrations. Analysing the data at different positions provides more information than does RSD for industrial design purposes.

In this study, all of the comparisons between the data sets were performed at impeller speeds greater than N_{js} and before the solids suspension level had reached the liquid surface. This meant that two effects, caused by the partial suspension of solids, could be removed from the physics of the distribution of solids:

1. As the impeller speed is increased, some of the energy that is supplied to the vessel is used to suspend the settled solids.
2. Since the solids are partially suspended the average particle concentration will be lower than expected and the effect of varying C_0 would have to be included in the analysis. The literature review (Section 3.2.3) on the effect of C_0 has shown that there is a small effect in this respect.

7.3 Effect of Scale

The variation of concentration, at different h/H and r/R=0.67, for the PBT ($D=T/2$) in the 0.61 m and 1.83 m diameter vessels was evaluated on the basis of power per unit volume as shown in Figure 7.4 and the impeller tip speed as shown in Figure 7.5. The graphs show that equal power per unit volume (Figure 7.4) was a better scale-up criterion than impeller tip speed (Figure 7.5). A similar conclusion was drawn when Figure 7.6 and Figure 7.7 were compared for a PBT of $D=T/3$. When Figure 7.8 and Figure 7.9 were compared for an A310 of $D=T/3$ the comparisons were not as good on either basis but P/V was better than V_{tip} especially at h/H=0.180 and h/H=0.344 where, above N_{js}, the two data sets were well correlated.

The data for the A310 in T_{61} was obtained from Mak (1988). The conditions were identical to the tests in T_{183} except that d=605 μm.

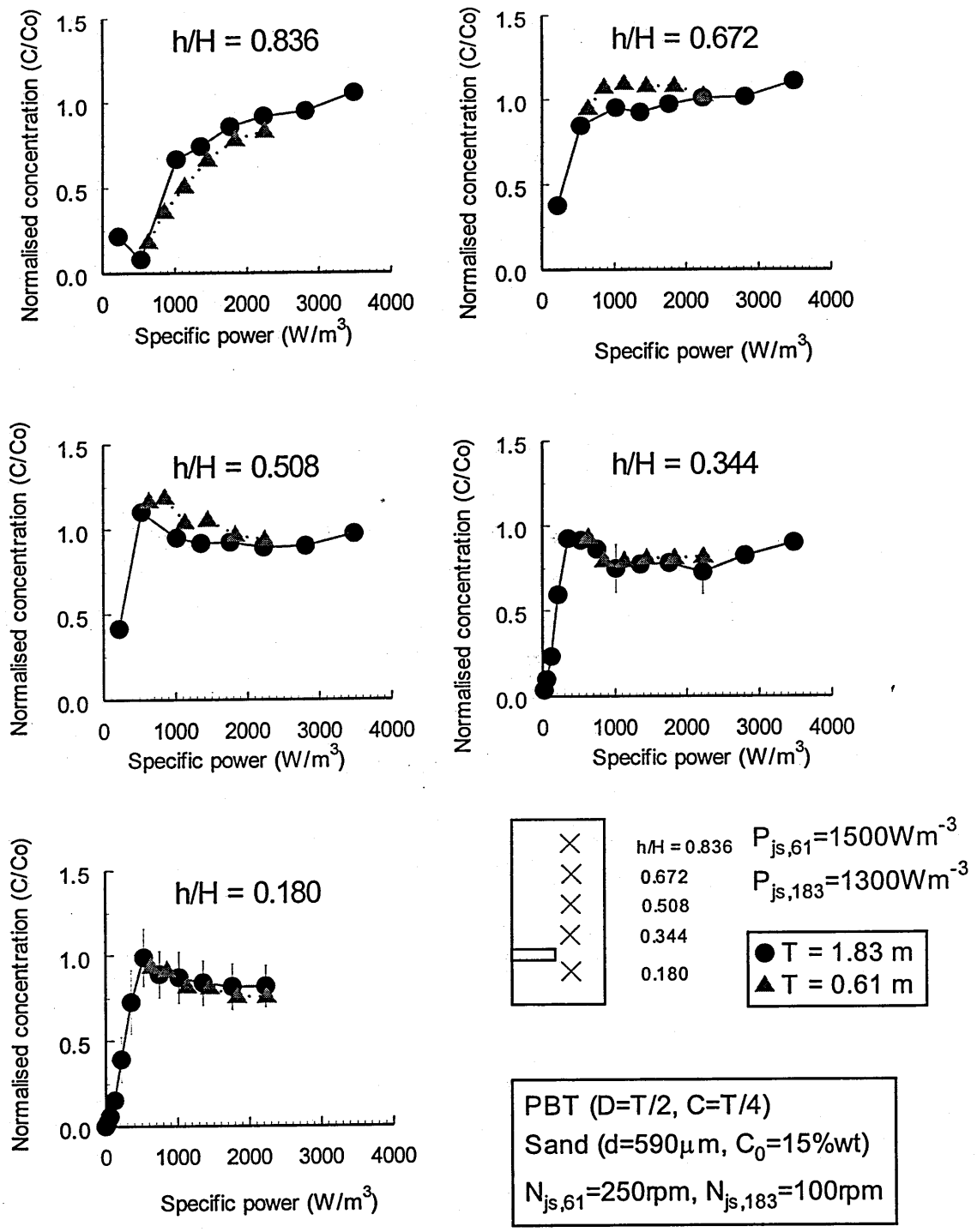

Figure 7.4. Scaling-up on the basis of P/V (45°PBT4, D=T/2).

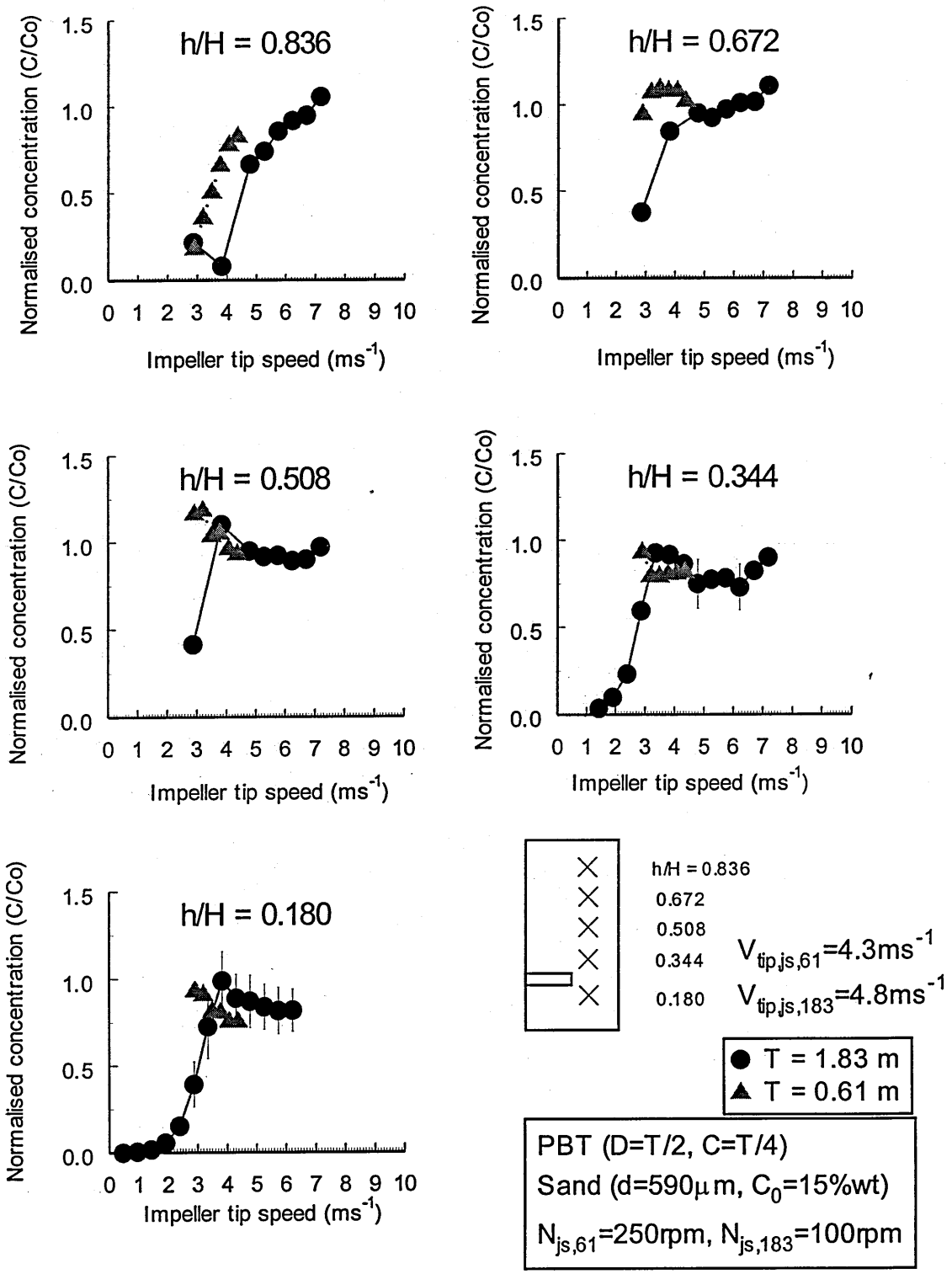

Figure 7.5 Scaling-up on the basis of V_{tip} (45°PBT4 (D=T/2)).

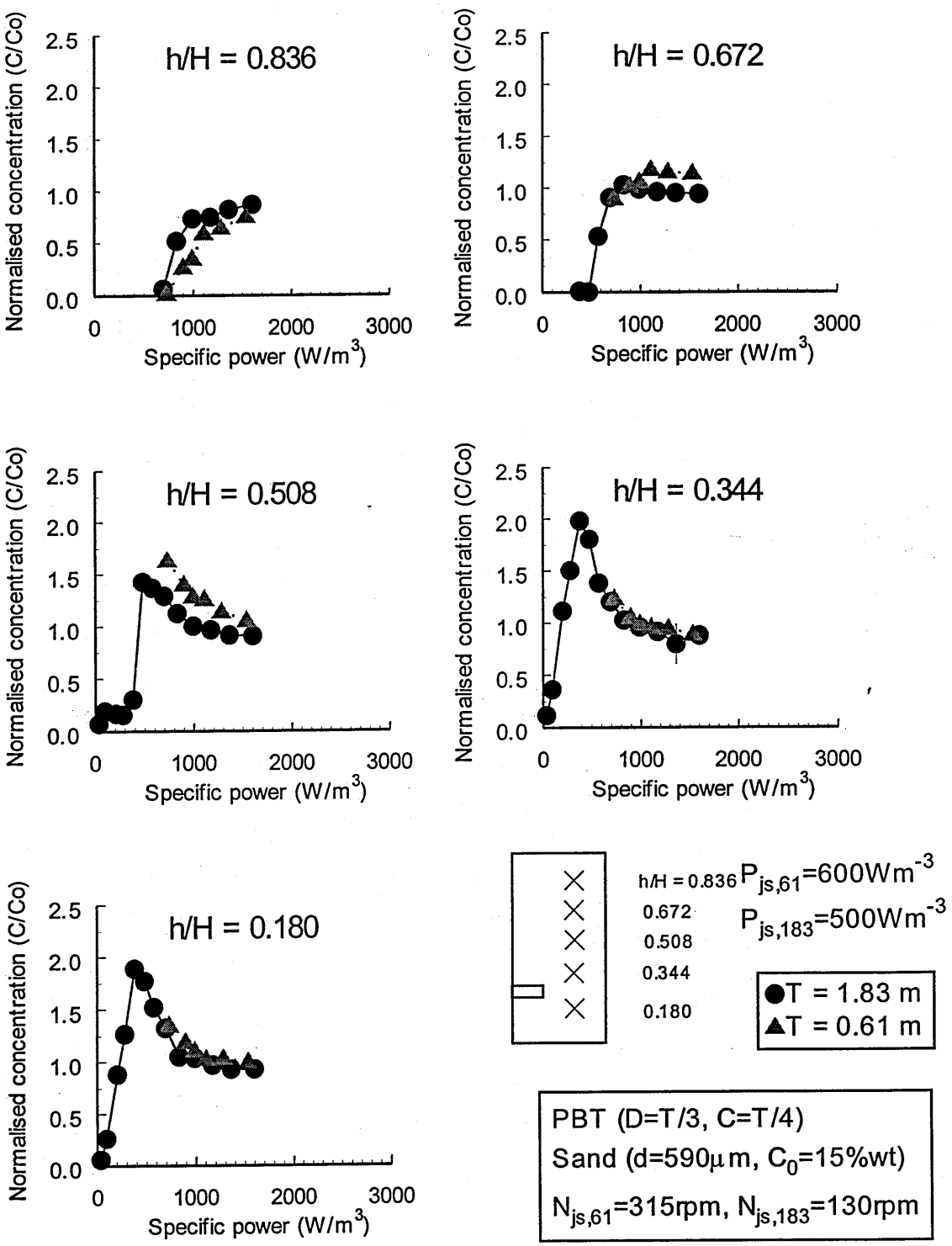

Figure 7.6. Scaling-up on the basis of P/V (45°PBT4 (D=T/3)).

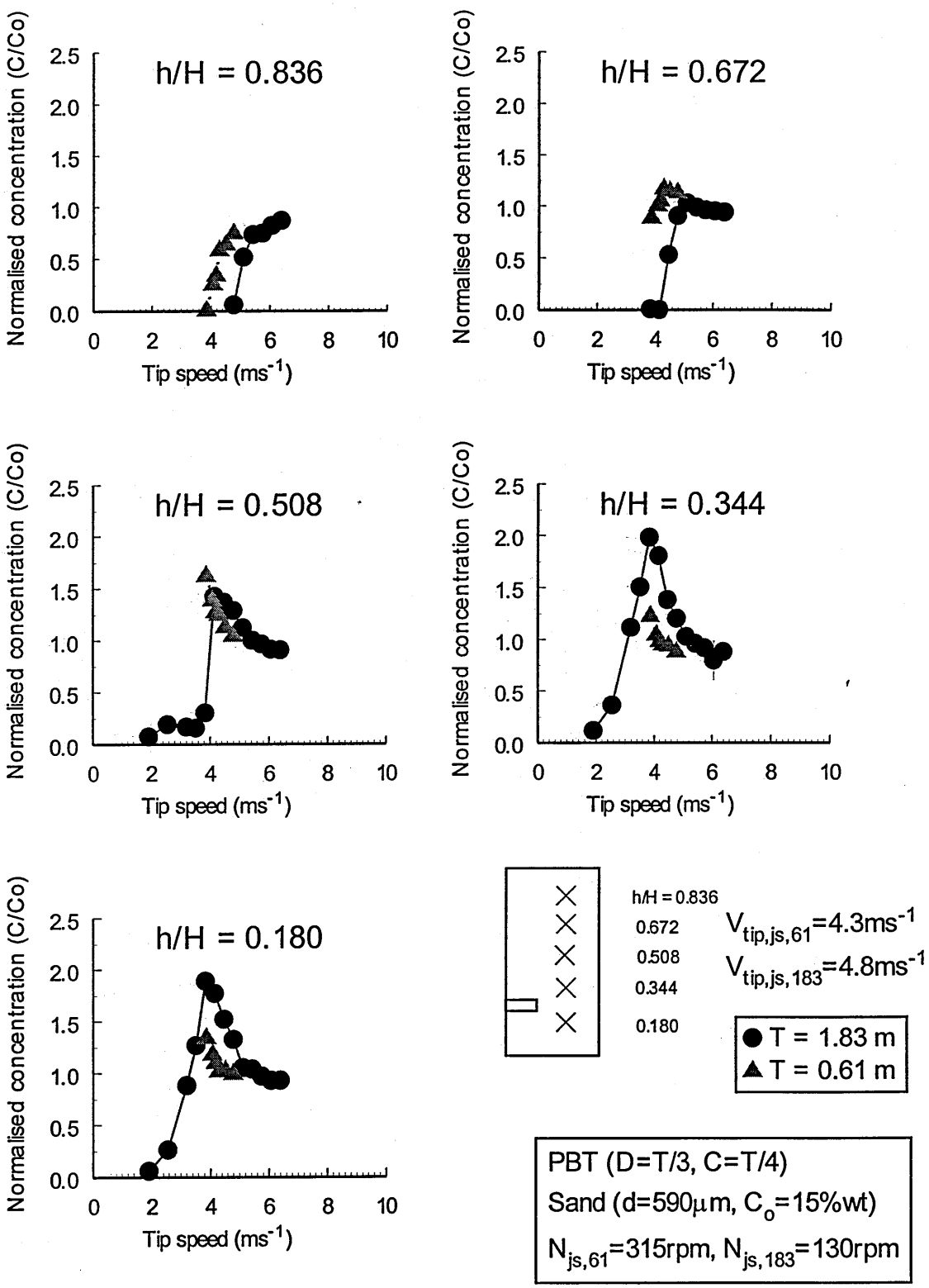

Figure 7.7. Scaling-up on the basis of V_{tip} (45°PBT4 (D=T/3)).

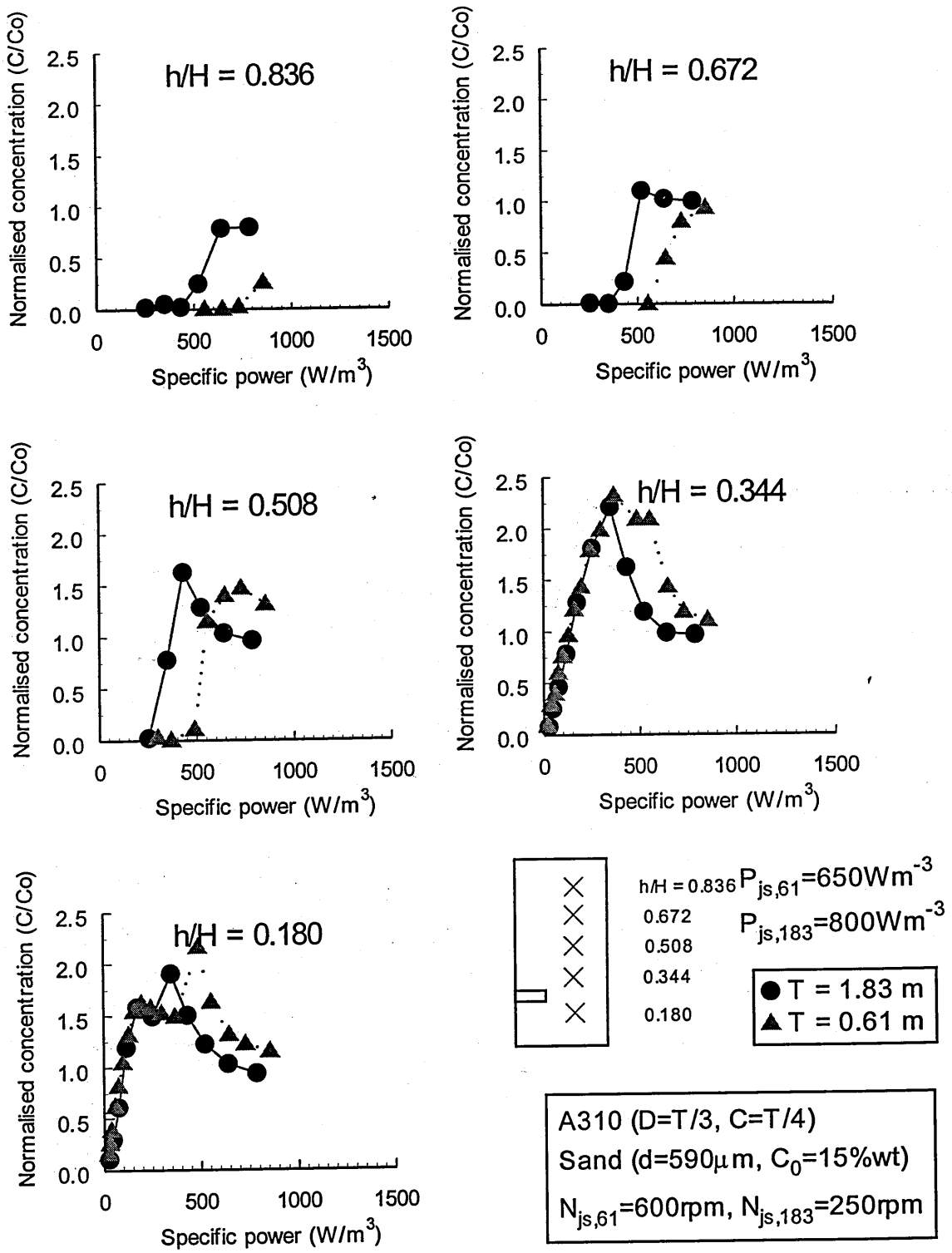

Figure 7.8. Scaling-up on the basis of P/V (A310 (D=T/3)).

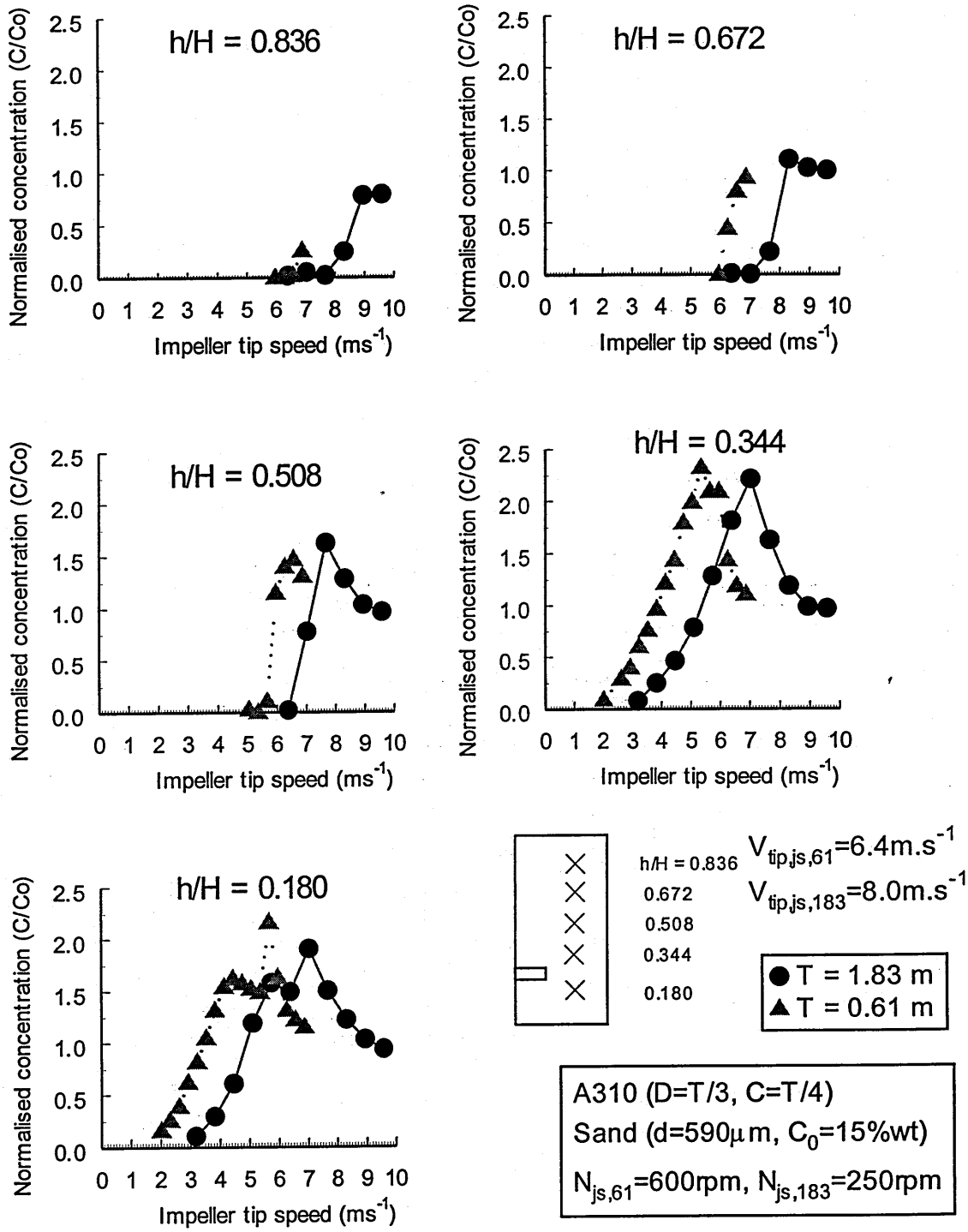

Figure 7.9. Scaling-up on the basis of V_{tip} (A310 (D=T/3)).

7.4 Effect of impeller design

The effect of impeller design was examined by comparing the results obtained using an A310 and a PBT. Both impellers had a diameter of $D=T/3$ and mounted at a clearance, $C=T/4$. The data set was obtained in the 1.83m diameter vessel at various values of h/H and r/R=0.67. Comparisons between these two impellers on the basis of impeller specific power (Figure 7.10) showed that this is a good method of comparing these two impellers. The same data sets were also compared on the basis of the impeller tip speed (Figure 7.11), showing that the two impellers produced very different concentration profiles at the same impeller tip speeds.

At a given specific power, the A310 will operate at a lower torque than the PBT. The A310 may therefore be the preferred impeller design for the distribution of solids since this would result in a lower capital cost for the gearbox. On the other-hand, at a given P/V, the A310 will rotate at a much higher impeller speed than the PBT, which may not be desirable for certain processes or products where high velocities result in a reduction in quality.

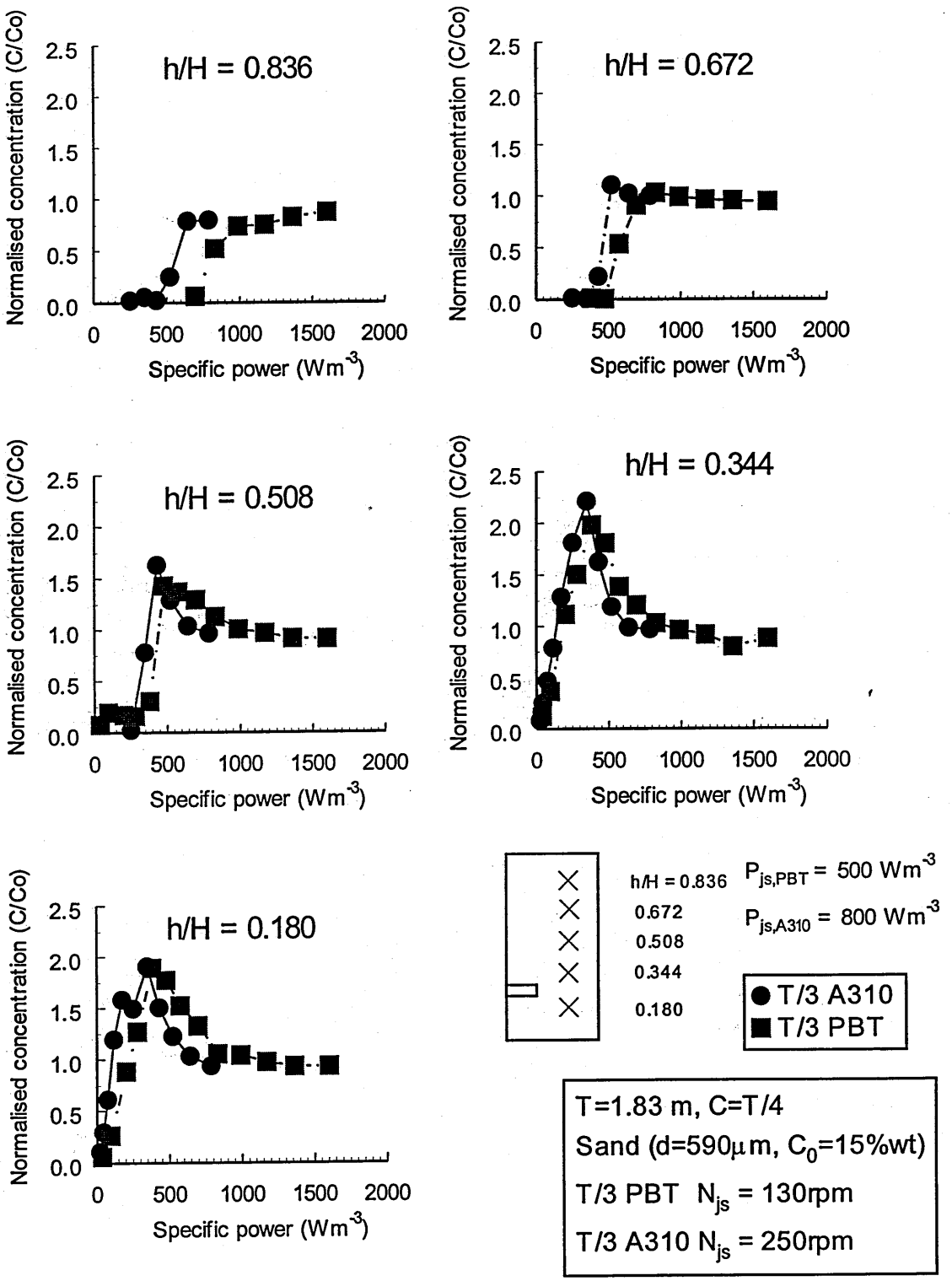

Figure 7.10. Effect of impeller design on the basis of P/V (A310, 45°PBT4 (D=T/3)).

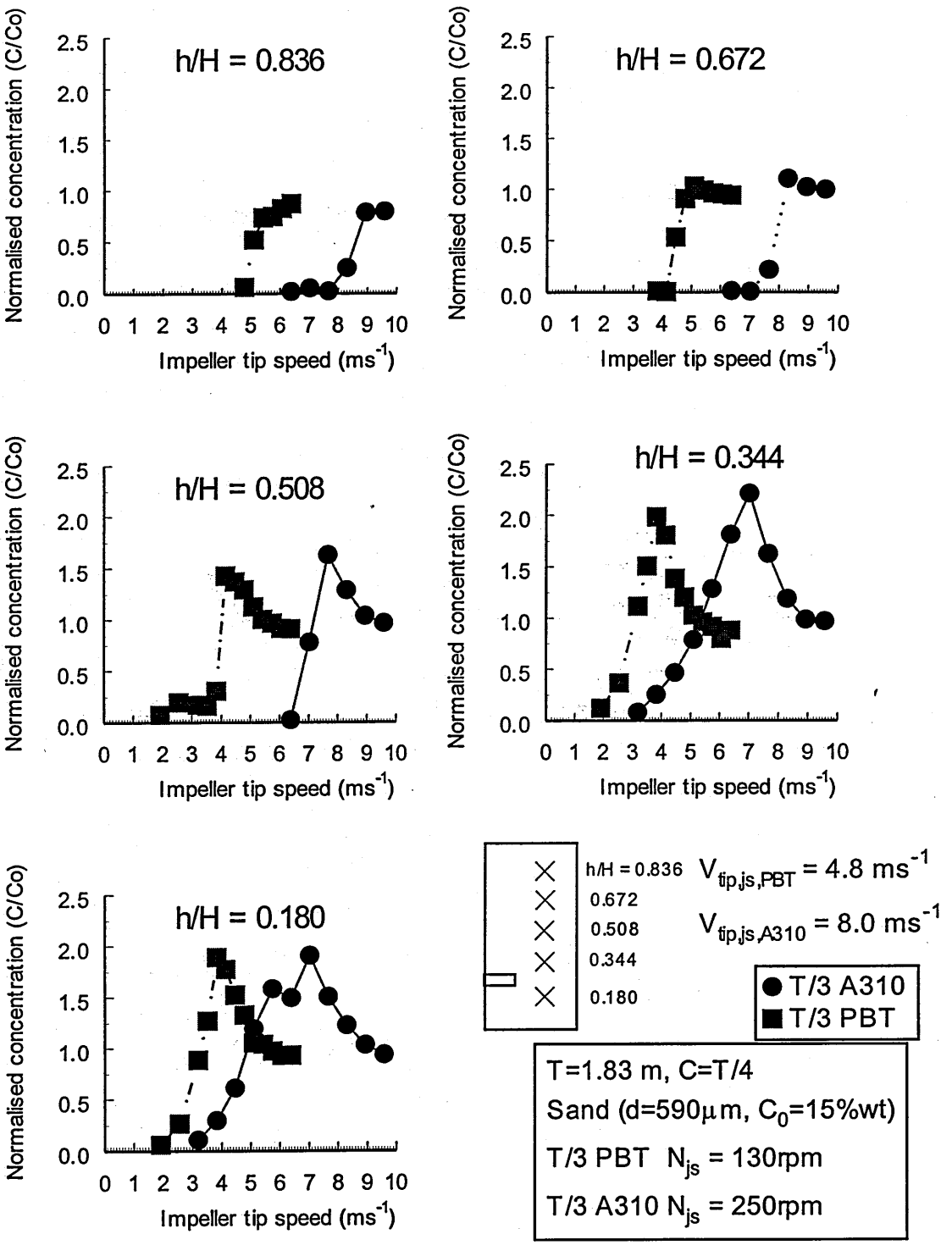

Figure 7.11. Effect of impeller design on the basis of V_{tip} (A310, 45°PBT4 (D=T/3)).

7.5 Effect of impeller diameter

The effect of impeller-to-tank diameter ratio was examined in both the 0.61 m and 1.83 m diameter vessels using PBTs of *D=T/2* and *D=T/3*. The particle size was 590 μm for all of these comparisons.

Figure 7.12 and Figure 7.13 show that P/V is better than V_{tip} for correlating the data obtained in T_{183}. It can be seen in both figures that between h/H=0.18-0.51 the maximum concentration that was measured was much lower when the suspension was stirred with the PBT with D/T=0.5 than when stirred with a PBT with D/T=0.33. This was due to the high concentration region that was found beneath both impellers. The region of high concentration was a result of the up-flowing slurry beneath the PBTs as shown in Figure 2.2(b) that acts in a similar way to a moving bed. The higher particle concentration was observed in T_{61} (Figure 7.14) when the vessel was stirred with either the D=T/2 or D=T/3 impellers. Since the D=T/2 impeller has a larger volume beneath it and produced a more radial flow pattern, the concentration that was measured at r/R=0.67 was much lower than when experiments were performed with the D=T/3 impeller. This effect resulted in a relatively poor mass balance for the D=T/2 impeller as was discussed in Section 7.1.2.

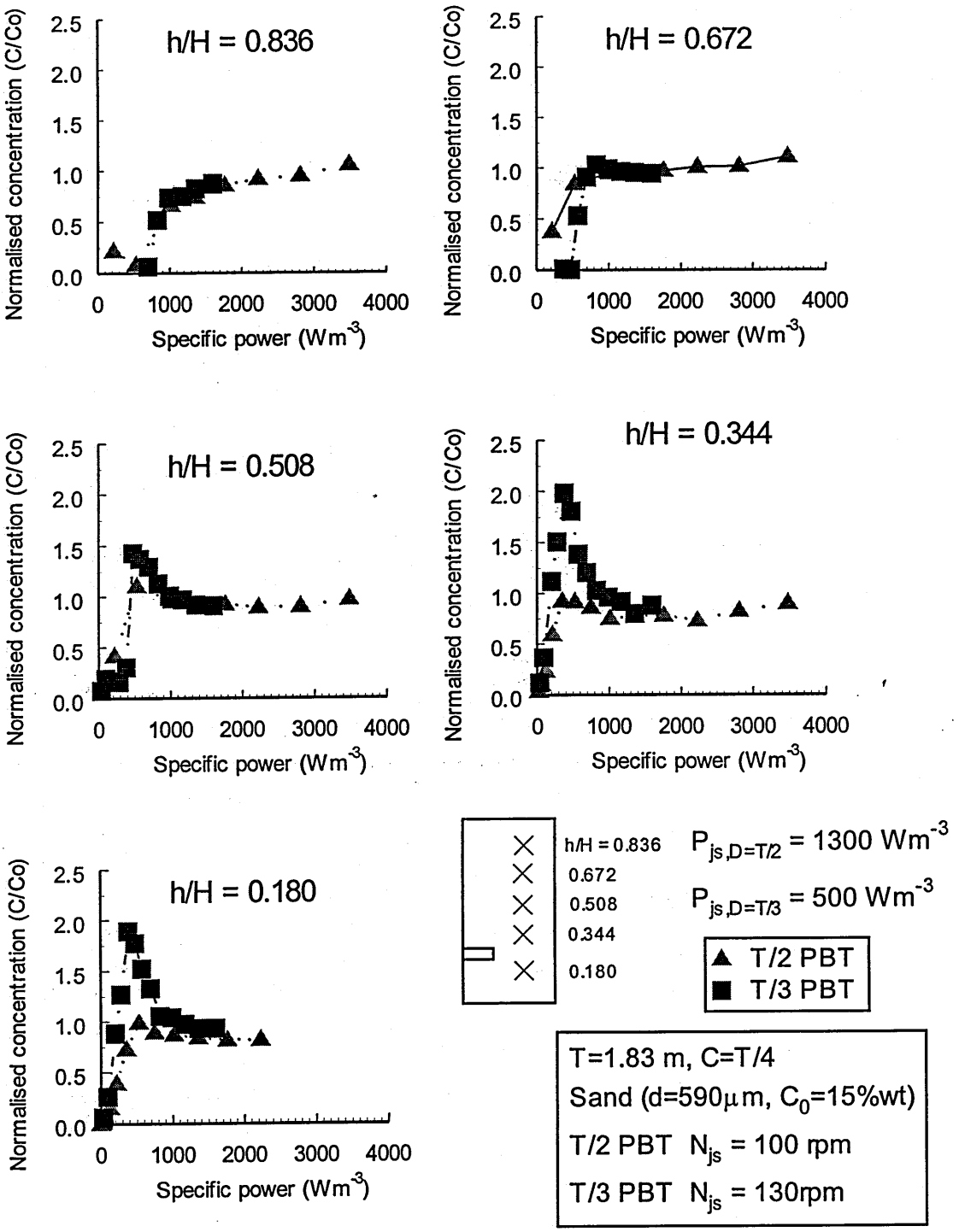

Figure 7.12. Effect of impeller diameter on the basis of P/V (45°PBT4 (D=T/2, T/3)).

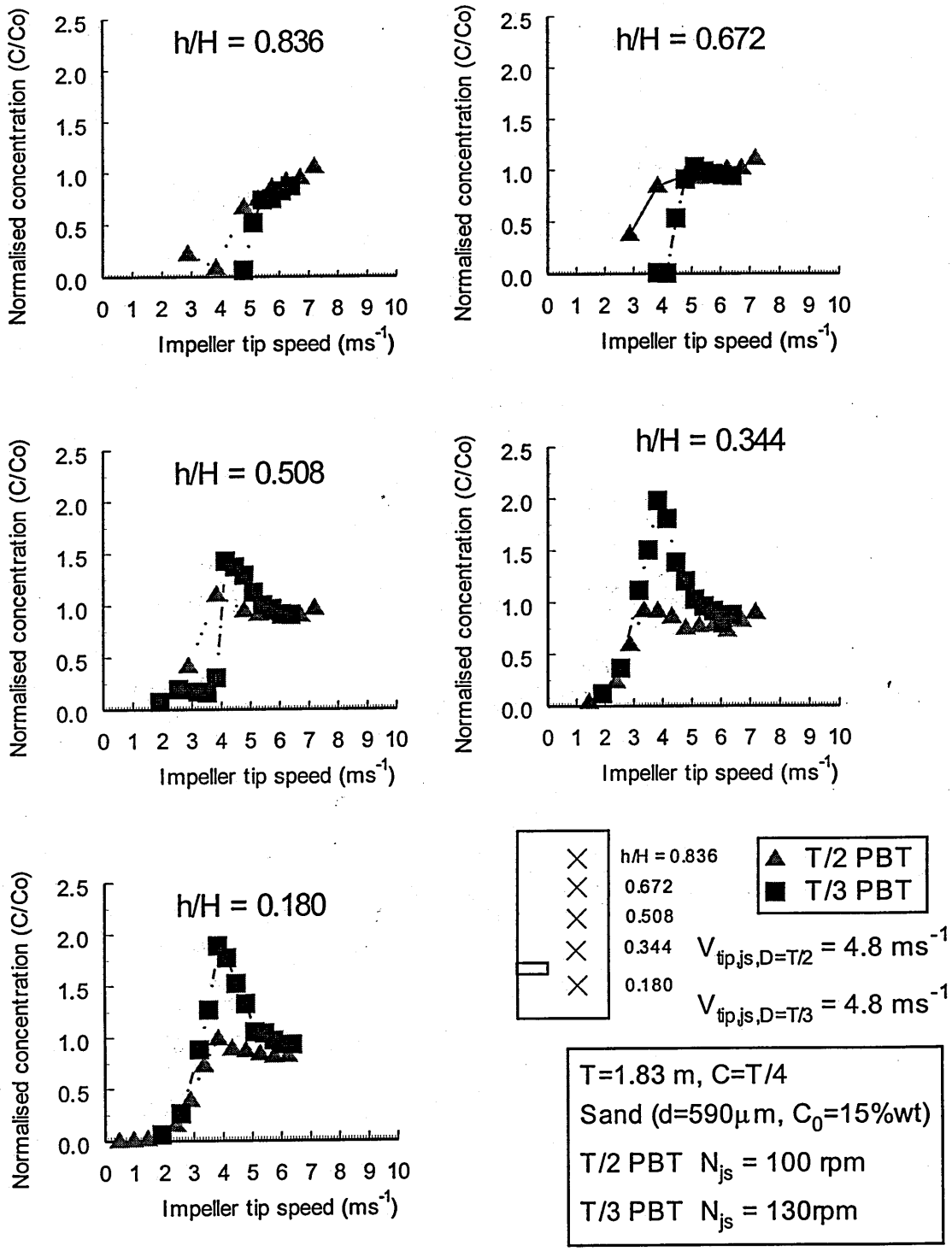

Figure 7.13. Effect of impeller diameter on the basis of V_{tip} (45°PBT4 (D=T/2, T/3)).

In addition to the large-scale studies in T_{183}, experiments were performed in T_{61}. These experiments were performed to give qualitative information on the distribution produced by the D=T/2 and D=T/3 PBTs. The measurement positions are shown in Figure 7.14 and Figure 7.15, the colour of the measurement position is proportional to the concentration with blue representing no solids and red representing a position with $C/C_0 \geq 2$. The results that have been presented cover a range of normalised radii and heights.

Examples of the results obtained in T_{61} have been presented in Figure 7.14 and Figure 7.15. These results show that the concentration profiles produced by the two impellers differed significantly. These differences appear in comparisons on the basis of both impeller specific power and impeller tip speed. The differences arise as a result of the larger circulation loop produced by the *D=T/2* PBT. The larger loop reduces the solids at (r/R=0.67, h/H=0.51). The concentration at the centre of the circulation loop with the *D=T/2* PBT was found to be much lower than that found during the experiments with the D=T/3 PBT. A spot of high concentration was also found at (*r/R*~0.7, *h/H*~0.7) when the D=T/2 PBT was used. This region of higher than average concentration corresponded to the position where plumes of solids, that were carried up the baffle and then swept away by the flow field, crossed the plane halfway between the baffles. The time-averaged effect of these plumes results in the region of high concentration that was observed.

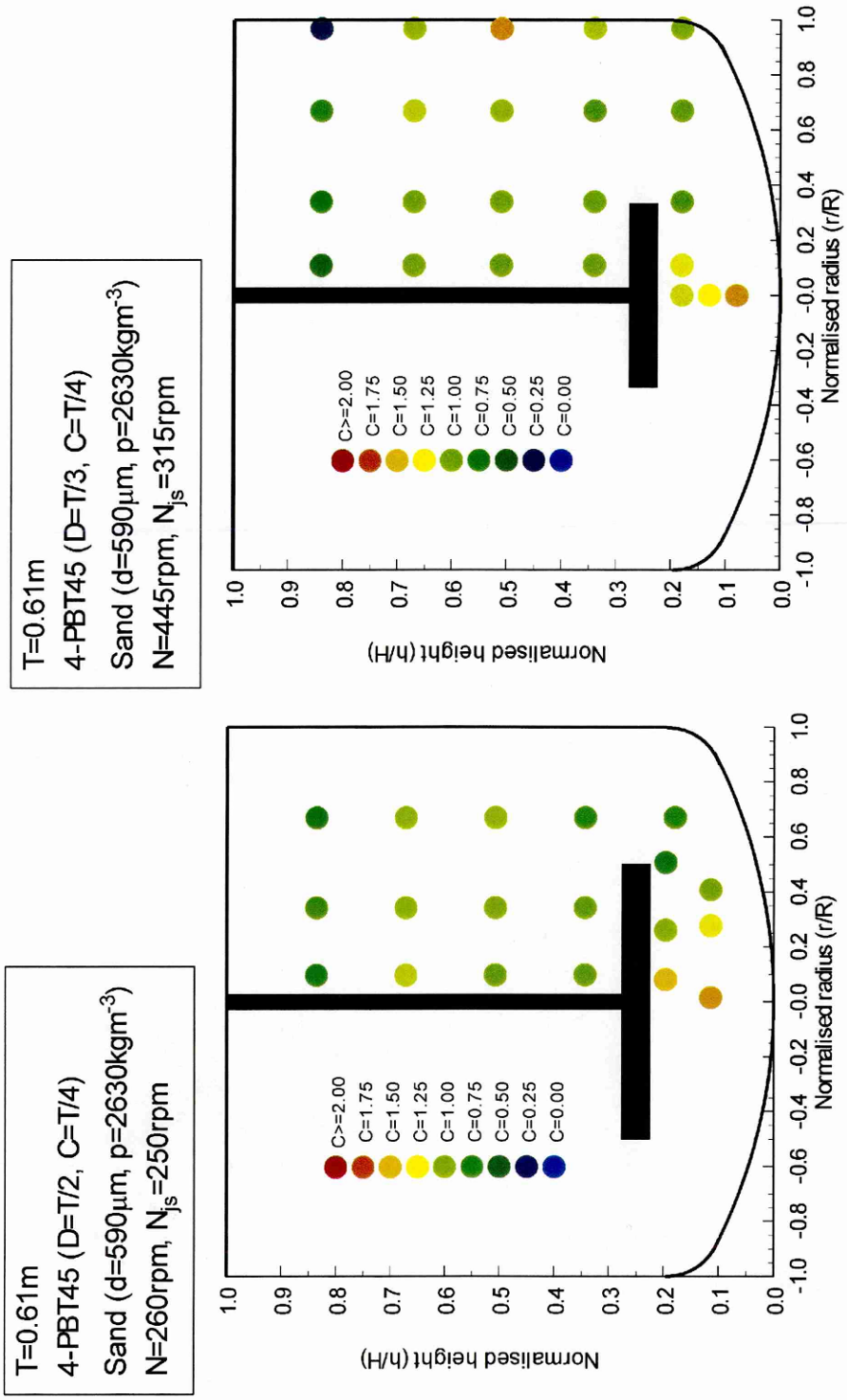

Figure 7.14. Comparison of the concentration profiles for 4PBT45 (D=T/2) and 4PBT45(D=T/3) at the same P/V.

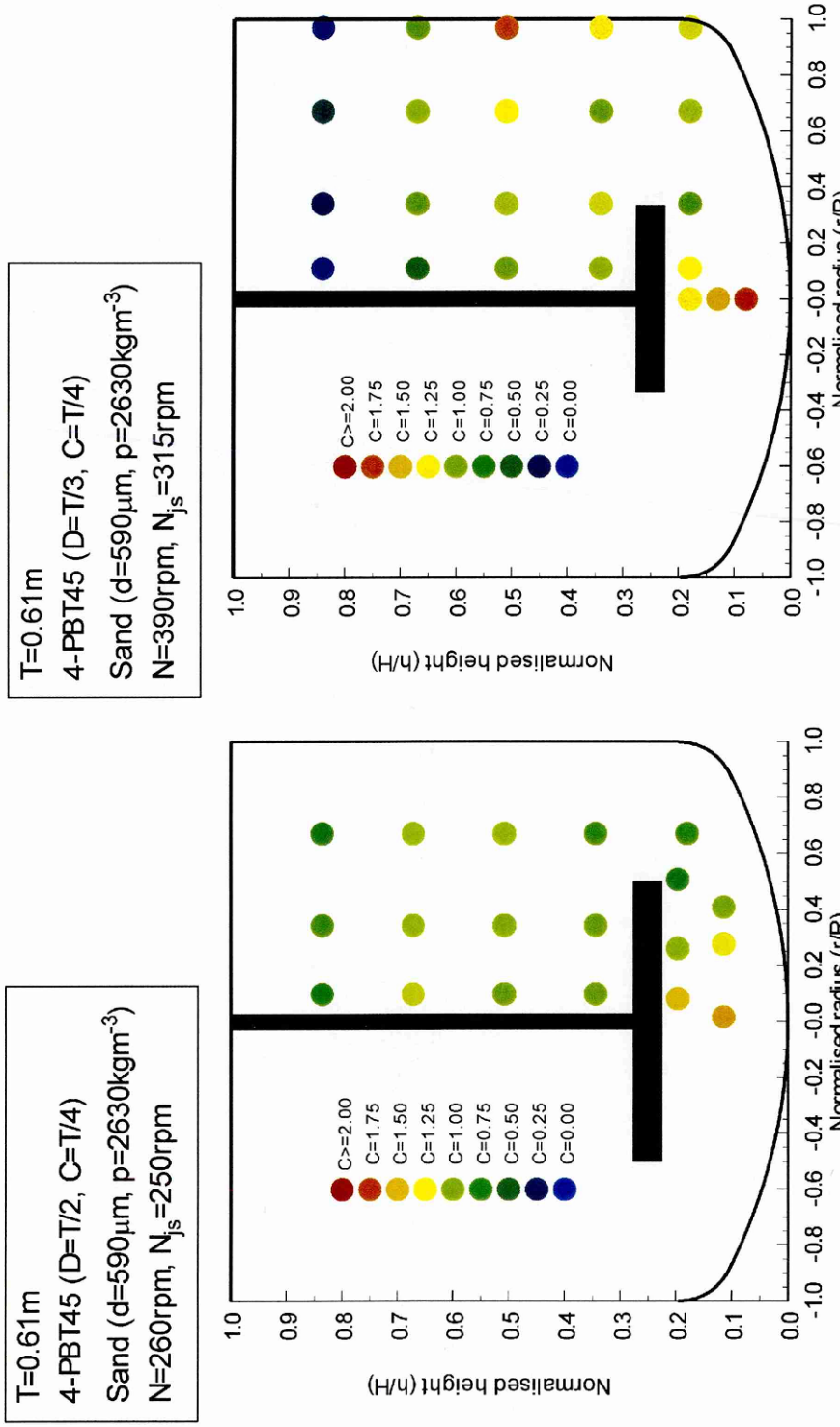

Figure 7.15. Comparison of the concentration profiles for 4PBT45 (D=T/2) and 4PBT45(D=T/3) at the same Vtip.

7.6 Effect of particle diameter

Experiments were performed in T_{183} using particles with different d_{32} values between 150-1050 μm. By performing measurements using different particle sizes, it was hoped that a design procedure could be developed that covered a variety of particle sizes as well as vessel scales. In T_{61} the solids concentration profiles produced by particles of 150 μm and 590 μm were measured. The data was correlated together so that the effects of particle size and power input were included.

7.6.1 Regression of data

The experiments that have been performed on the effect of particle size were at two scales and a range of particle sizes. When the regression of the experimental data was performed, both the effect of particle size and the effect of scale on the distribution of solids in a stirred tank had to be included. The discussion on the effect of vessel scale has shown that scaling-up on the basis of power per unit volume was very successful. Therefore, this was chosen as the baseline for the analysis. Power per unit volume is given in Equation 7.1:

$$\frac{P}{V} = \frac{Po\rho N^3 D^5}{V} \tag{7.1}$$

Assuming that power per unit volume is a successful scale-up criterion, it is expected that the relationship in Equation 7.2 will be valid:

$$\frac{\left(\frac{P}{V}\right)_1}{\left(\frac{P}{V}\right)_2} = \left(\frac{Po_1}{Po_2}\right)\left(\frac{N_1}{N_2}\right)^3\left(\frac{D_1}{D_2}\right)^5\left(\frac{V_1}{V_2}\right)^{-1} \tag{7.2}$$

Here, the subscripts 1 and 2 represent the respective variable at scale 1 and 2. Since it was found that power per unit volume was a successful scale-up criterion, the impeller speed for a concentration, C, N(C), would obey Relationship 7.3:

$$N(C) \propto \left(VPo^{-1}D^{-5}\right)^{1/3} \tag{7.3}$$

Assuming also that the impeller speed for a given particle concentration is proportional to the particle diameter raised to some power, gives Relationship 7.4:

$$N(C) \propto d^{-a}\left(VPo^{-1}D^{-5}\right)^{1/3} \tag{7.4}$$

Where it was expected that a<0.

For each data set, the impeller speed for a particular particle concentration was noted. This was performed by plotting particle concentration against impeller speed and linearly interpolating between adjacent data points to read off the impeller speed for a given concentration. This data was tabulated as a spreadsheet in the form of particle concentration and impeller speed for that concentration. In the next column the modified impeller speed for that concentration was placed. This modified impeller speed, N_{mod}, was given by Equation 7.5:

$$N_{mod} = N(C)d^{a}\left(VPo^{-1}D^{-5}\right)^{b}. \tag{7.5}$$

Here, a and b were both variables that the built-in optimisation program in Microsoft Excel 97 could vary. The average value of N_{mod} for each normalised concentration was calculated together with the standard deviation of the N_{mod}s for each normalised concentration. The sum of the standard deviations, σ_{sum}, was calculated using Equation 7.6. This parameter gave a measure of the average error at each of the positions examined.

$$\sigma_{sum} = \frac{1}{n}\sum_{C_j}\left(\frac{n\sum_{i=1}^{n}N_{mod}(C_j)_i^2 - \left(\sum_{i=1}^{n}N_{mod}(C_j)_i\right)^2}{n(n-1)\left(\frac{1}{n}\sum_{i=1}^{n}N_{mod}(C_j)_i\right)^2}\right)^{1/2} \tag{7.6}$$

Here, $N_{mod}(C_j)_i$ was defined as the impeller speed for a given concentration modified by particle size raised to the power a and power per unit raised to the power b for condition i. Condition i is defined by a particular vessel diameter and particle size. n is the total number of conditions where an impeller speed for a particular concentration, C_j, could be interpolated. The standard deviation for each C_j was then summed over each of the conditions j to give σ_{sum}.

The variables a and b were varied so that the sum of the standard deviations of N_{mod} between the data sets was minimised. The data presented covers a variety of particle and vessel sizes.

The minimisation procedure was performed in four ways:

1. The raw data was plotted (a=0, b=0) (Section 7.6.1(a)).
2. The assumption of power per unit volume was forced but the exponent on particle size was allow to vary (a varies, b=-0.33) (Section 7.6.1(b)).
3. The assumption of power per unit volume was dropped and both exponents were allowed to vary (a varies, b varies) at each position in the vessel. (Section 7.6.1(c))
4. Both a and b were allowed to vary (a varies, b varies) but were not allowed to vary between different points in the vessel. (Section 7.6.1(d))

The measurement points that were used in this analysis are only those where the solids concentration was measured in T_{183} (Figure 5.10). Therefore, some of the data that was gathered has not been used in the analysis. Later on, this analysis has been used to compare the concentration profiles for two particle sizes. Since there are 5 positions, an extra degree of freedom was introduced. This allowed for any variability in the effect of particle size or scale between measurement points. The final minimisation was performed by forcing the exponent on particle size and vessel scale to be invariant between measurement positions.

In each case that has been analysed the data for each condition has been plotted as N_{mod} vs. C/C_0 with the average $N_{mod}(C)$ and $N_{mod}(C)$ plus and minus one standard deviation overlaying the data points. The overlaid lines give an indication of the range of the values for $N_{mod}(C)$ that corresponded to a particular concentration when the plots are read horizontally. When read vertically the plots show the range of concentrations that correspond to a particular $N_{mod}(C)$.

7.6.1(a) Raw data plots (a=0, b=0)

Figures 7.16-7.20 show how the particle concentration at each of the points investigated varied with impeller speed. It can be seen that the impeller speed that was required for a given particle concentration decreased with increasing vessel scale at constant particle diameter and increased with particle diameter at constant scale. At larger scales, lower impeller speeds are required for a given concentration since to maintain power per unit volume constant, $N \propto T^{-0.67}$. In Section 7.3, power per unit volume was shown to be a reliable scale-up criterion for a range of impeller designs and impeller diameters. Intuitively, any increase in particle diameter will result in a higher settling velocity which will require higher mean and turbulent velocities to remain suspended in the vessel and thus higher impeller speeds would be needed.

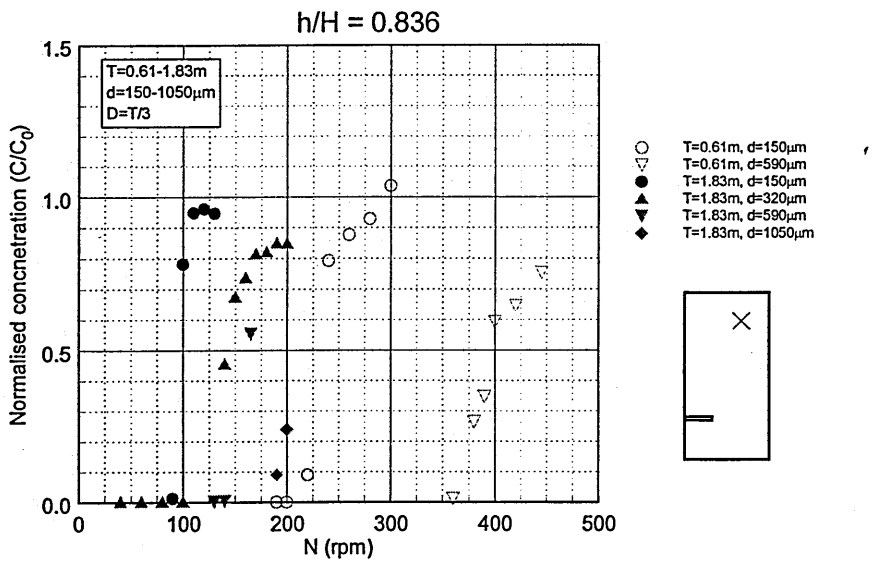

Figure 7.16. Variation of concentration at h/H=0.836 with impeller speed for 45°PBT4(D=T/3)s at T=0.61 and 1.83m.

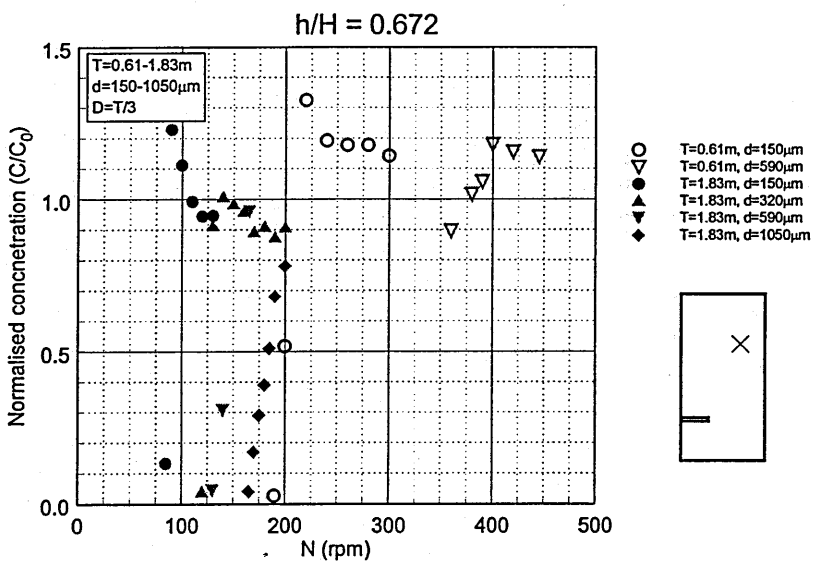

Figure 7.17. Variation of concentration at h/H=0.672 with impeller speed for 45°PBT4(D=T/3)s at T=0.61 and 1.83m.

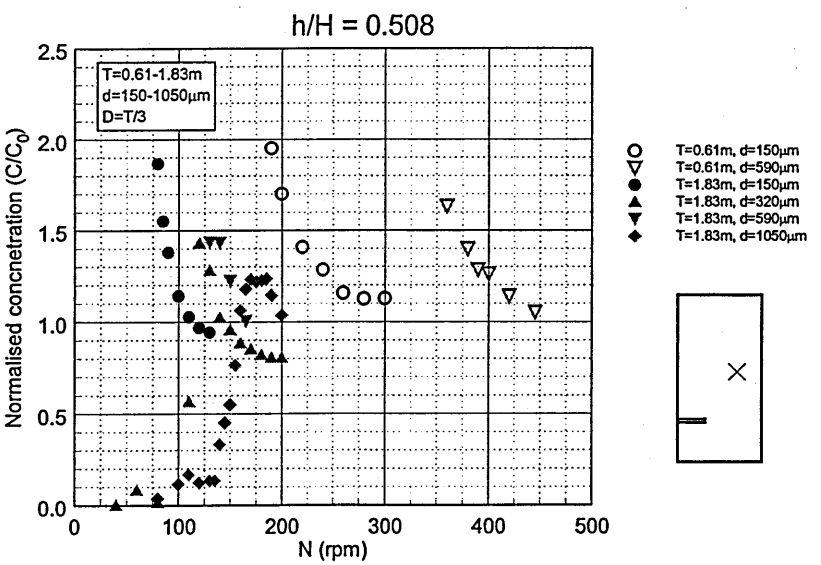

Figure 7.18. Variation of concentration at h/H=0.508 with impeller speed for 45°PBT4(D=T/3)s at T=0.61 and 1.83m.

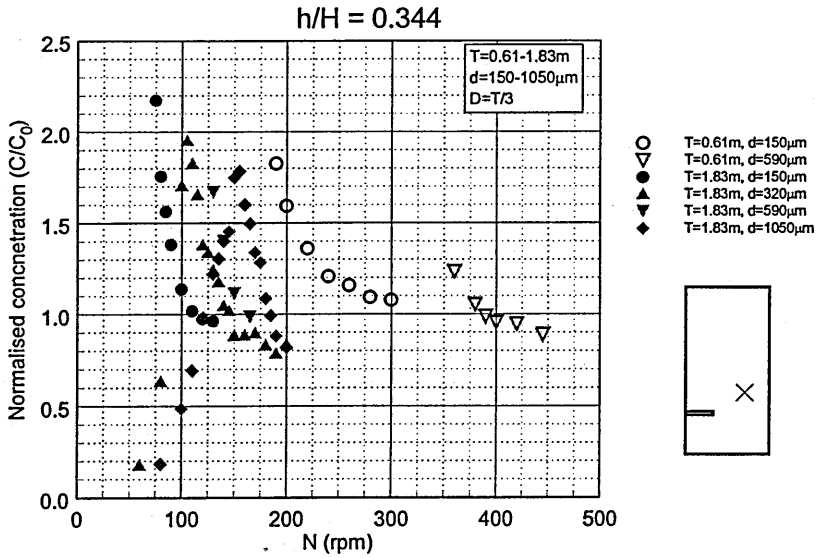

Figure 7.19. Variation of concentration at h/H=0.344 with impeller speed for 45°PBT4(D=T/3)s at T=0.61 and 1.83m.

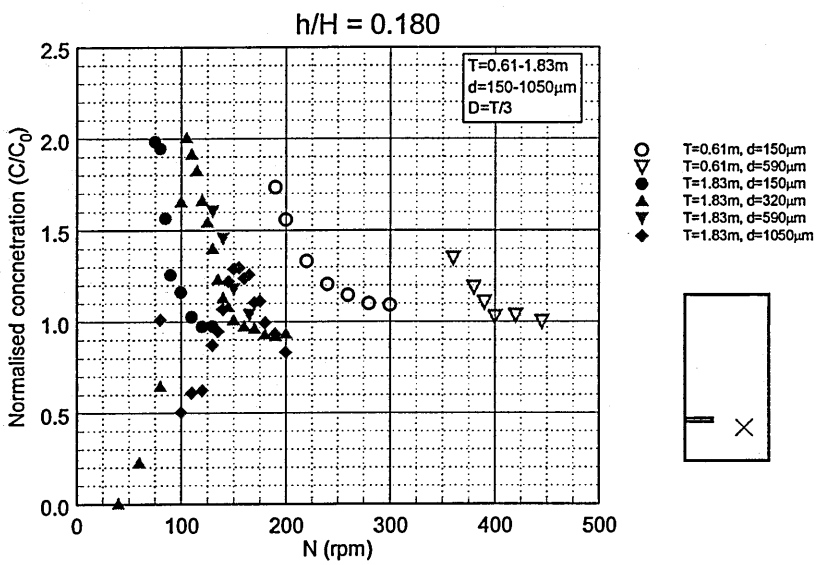

Figure 7.20. Variation of concentration at h/H=0.180 with impeller speed for 45°PBT4(D=T/3)s at T=0.61 and 1.83m.

Due to the large variation in impeller speeds for a given concentration, constant impeller speed was found to be a very poor method of examining the effect of scale and particle diameter together. The value of σ_{sum} for each position is shown in Table 7.1.

Table 7.1. Values of σ_{sum} for comparisons of raw data.

h/H	σ_{sum}
0.836	0.13
0.672	0.087
0.508	0.10
0.344	0.07
0.180	0.069
Total	0.46

7.6.1(b) Correlation of concentration with particle size and constant power per unit volume (a varies, b=-0.33)

Power per unit volume is an appropriate method to examine the effect of scale-up for a variety of impeller designs and impeller diameters. In this section, power per unit volume has been enforced for the effect of scale. The exponent on particle size was allowed to vary at each point in the vessel to see whether there was any variation between points in the vessel. Figure 7.21 to Figure 7.25 show how C/C_0 varied with N_{mod} at each position, when power per unit volume was forced upon the correlation. Table 7.2 shows the correlation that was used at each position.

Table 7.2. Correlations for particle size data where P/V has been forced.

h/H	Correlation (N_{mod}=)	Shown in which Figure
0.836	$N(C)d^{-0.40}\left(VPo^{-1}D^{-5}\right)^{-0.33}$	Figure 7.21
0.672	$N(C)d^{-0.37}\left(VPo^{-1}D^{-5}\right)^{-0.33}$	Figure 7.22
0.508	$N(C)d^{-0.32}\left(VPo^{-1}D^{-5}\right)^{-0.33}$	Figure 7.23
0.344	$N(C)d^{-0.28}\left(VPo^{-1}D^{-5}\right)^{-0.33}$	Figure 7.24
0.180	$N(C)d^{-0.25}\left(VPo^{-1}D^{-5}\right)^{-0.33}$	Figure 7.25

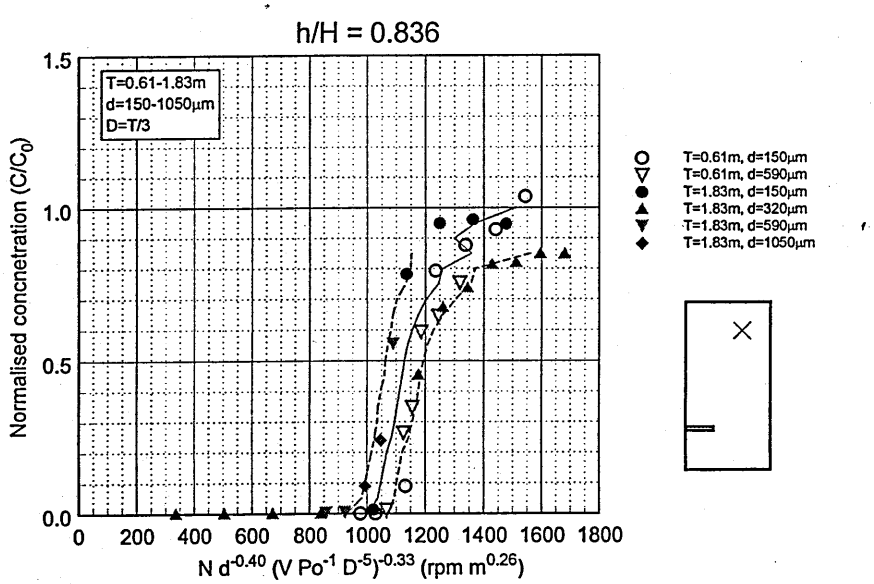

Figure 7.21. Variation of concentration at h/H=0.836 with N_{mod} for 45°PBT4(D=T/3)s at T=0.61 and 1.83m.

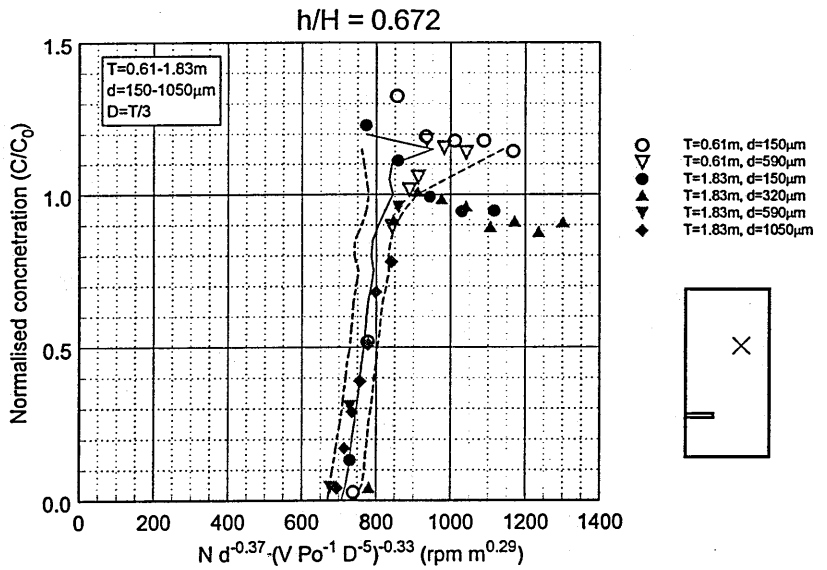

Figure 7.22. Variation of concentration at h/H=0.672 with N_{mod} for 45°PBT4(D=T/3)s at T=0.61 and 1.83m.

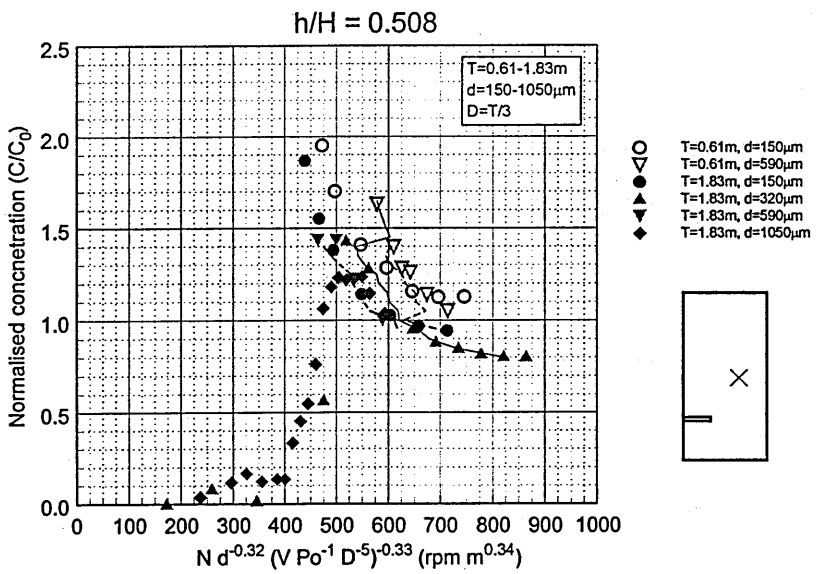

Figure 7.23. Variation of concentration at h/H=0.508 with N_{mod} for 45°PBT4(D=T/3)s at T=0.61 and 1.83m.

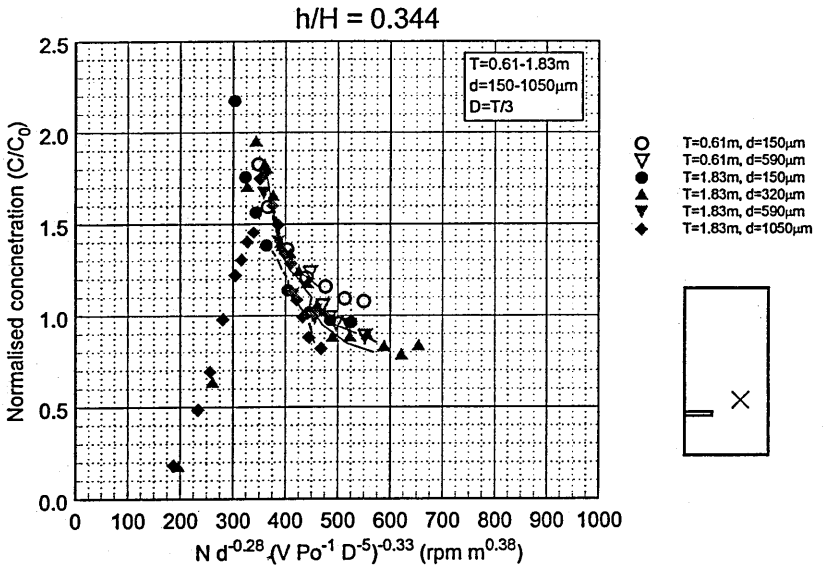

Figure 7.24. Variation of concentration at h/H=0.344 with N_{mod} for 45°PBT4(D=T/3)s at T=0.61 and 1.83m.

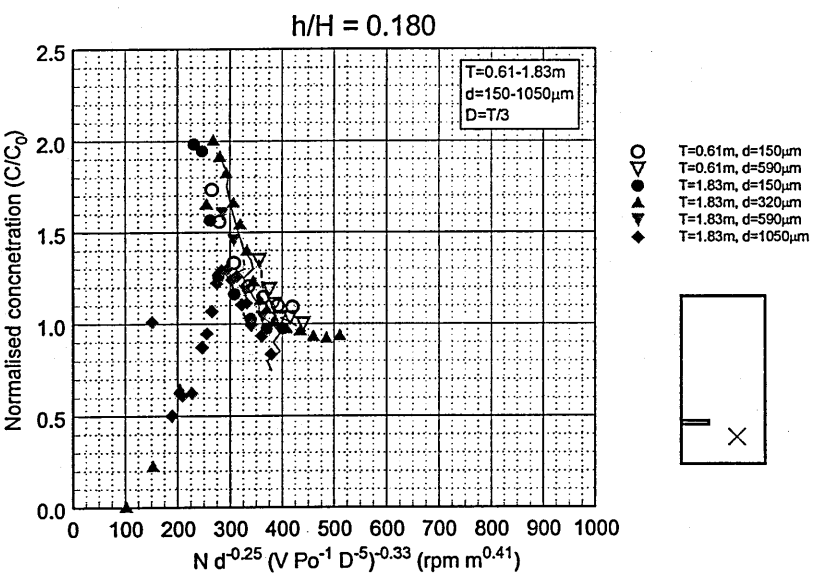

Figure 7.25. Variation of concentration at h/H=0.180 with N_{mod} for 45°PBT4(D=T/3)s at T=0.61 and 1.83m.

This method of data analysis was successful in bringing the data together well but the exponent on the particle diameter increased significantly from bottom to top from (-0.25) to (-0.40). This implies that, near the surface, the particle size has a more pronounced effect. This can be attributed to the observation that in the upper parts of the vessel the particles are transported primarily by intermittent large scale turbulent eddies. These eddies moved large packets of particles from the bulk of the vessel and placed them in the upper parts of the vessel. These particles were then observed to settle through the quiescent clear layer above the suspension back into the suspension. The larger particles resulted in a higher particle settling velocity. Since the particles passed through the probe volume faster, the time averaged particle concentration was much lower with the larger particles. This would have resulted in an increased effect of d on the solids concentration at the highest points in the vessel. Elsewhere in the vessel, the suspension was dominated more by the flow that was generated by the impeller.

The value of σ_{sum} for each position is shown in Table 7.3.

Table 7.3. Values of σ_{sum} for comparisons with P/V forced.

h/H	σ_{sum}
0.836	0.015
0.672	0.015
0.508	0.016
0.344	0.0089
0.180	0.011
Total	0.066

7.6.1(c) Correlation of concentration with particle size and power per unit volume (a and b both vary, position dependent)

This method of correlating the data has the greatest number of variables to change. The exponents on particle size, as well as power per unit volume, were allowed to vary at each of the measurement positions.

The correlations for each measurement position are shown in Table 7.4. The plots for the variations of C/C_0 with the correlations are shown in Figure 7.26-Figure 7.30.

Table 7.4. Best correlations for particle size data.

h/H	Correlation (N_{mod}=)	Shown in Figure
0.836	$N(C)d^{-0.38}\left(VPo^{-1}D^{-5}\right)^{-0.36}$ (7.12)	Figure 7.26
0.672	$N(C)d^{-0.36}\left(VPo^{-1}D^{-5}\right)^{-0.37}$ (7.13)	Figure 7.27
0.508	$N(C)d^{-0.32}\left(VPo^{-1}D^{-5}\right)^{-0.41}$ (7.14)	Figure 7.28
0.344	$N(C)d^{-0.28}\left(VPo^{-1}D^{-5}\right)^{-0.37}$ (7.15)	Figure 7.29
0.180	$N(C)d^{-0.23}\left(VPo^{-1}D^{-5}\right)^{-0.37}$ (7.16)	Figure 7.30

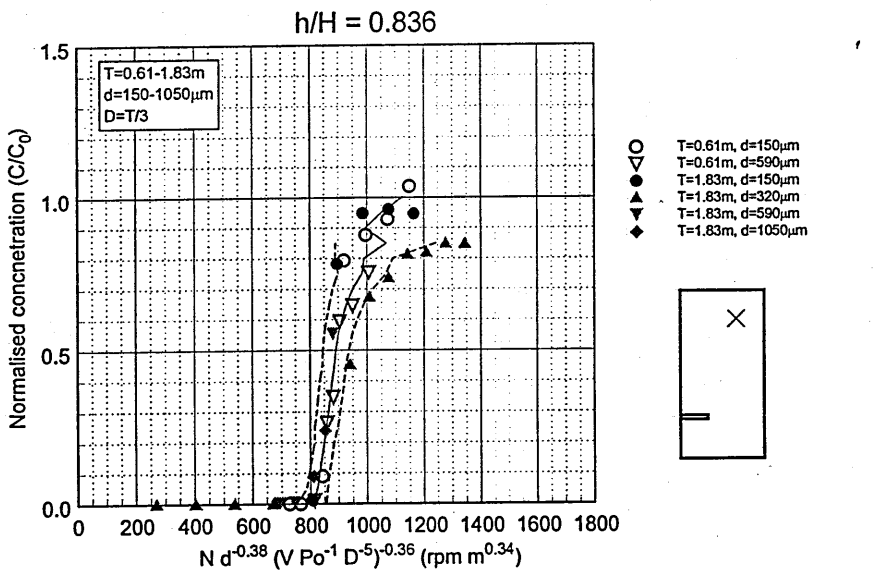

Figure 7.26. Variation of concentration at h/H=0.836 with N_{mod} for 45°PBT4(D=T/3)s at T=0.61 and 1.83m.

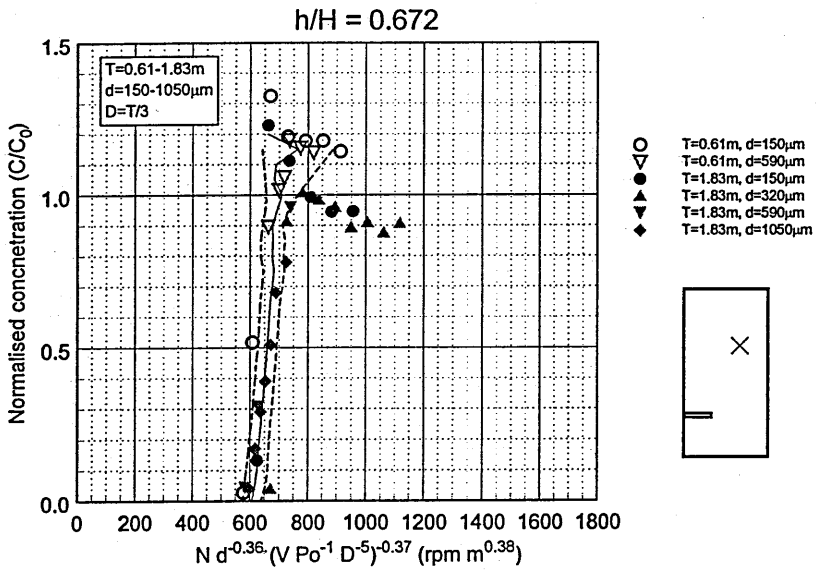

Figure 7.27. Variation of concentration at h/H=0.672 with N_{mod} for 45°PBT4(D=T/3)s at T=0.61 and 1.83m.

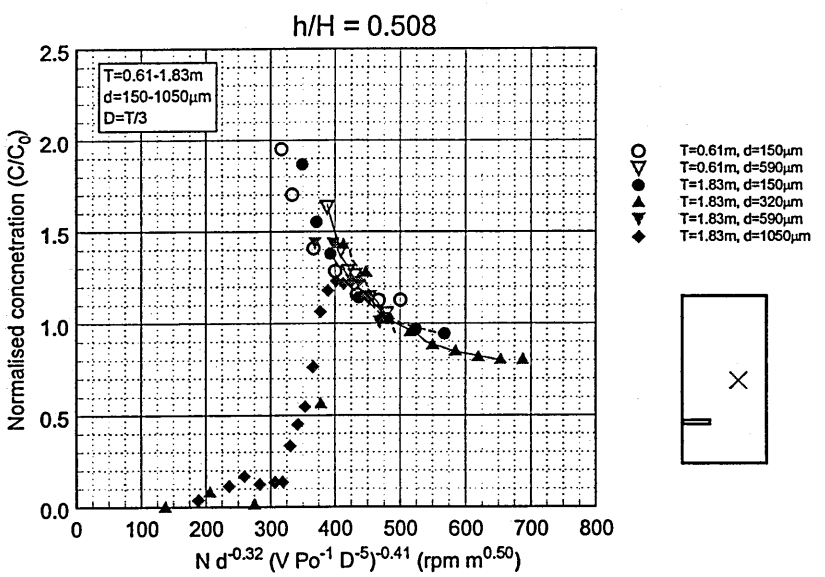

Figure 7.28. Variation of concentration at h/H=0.508 with N_{mod} for 45°PBT4(D=T/3)s at T=0.61 and 1.83m.

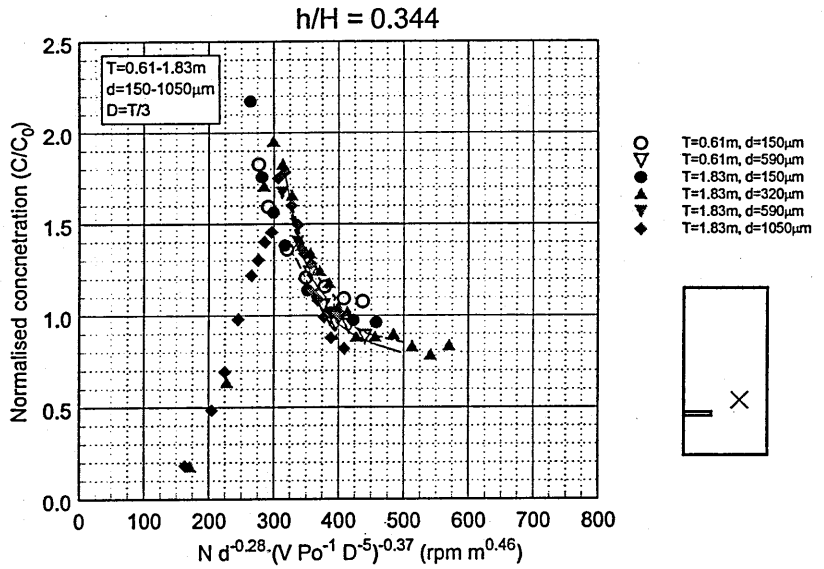

Figure 7.29. Variation of concentration at h/H=0.344 with N_{mod} for 45°PBT4(D=T/3)s at T=0.61 and 1.83m.

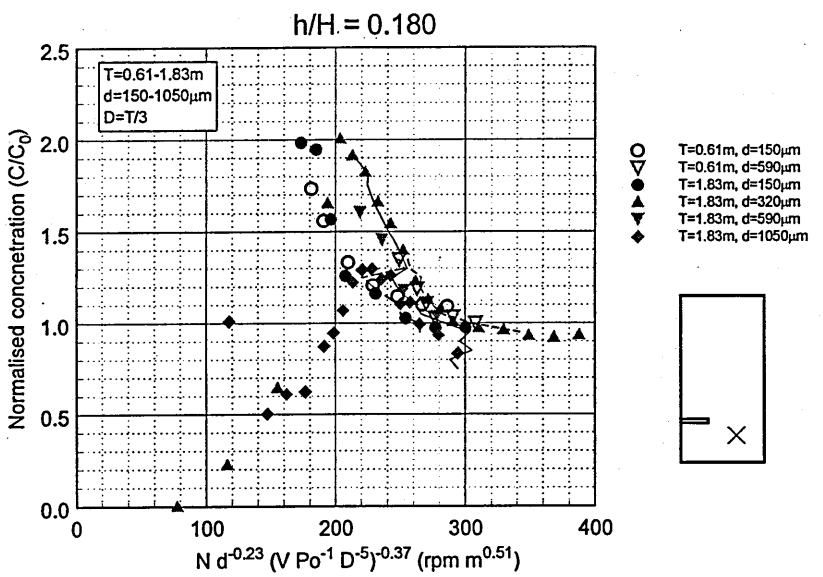

Figure 7.30. Variation of concentration at h/H=0.180 with N_{mod} for 45°PBT4(D=T/3)s at T=0.61 and 1.83m.

The value of σ_{sum} for each position is shown in Table 7.5.

Table 7.5. Values of σ_{sum} for comparisons where a,b are position dependent.

h/H	σ_{sum}
0.836	0.014
0.672	0.015
0.508	0.0058
0.344	0.0068
0.180	0.008
Total	0.050

Since each of the variables was changeable independently, it was found that this method of data analysis gave the narrowest band between the upper and lower lines on the correlations.

7.6.1(d) Correlation of concentration with particle size and power per unit volume (a and b both vary, position independent)

The exponents on particle size, as well as power per unit volume, were allowed to vary but were forced to be the same at each of the measurement positions.

The correlations for each measurement position are shown in Table 7.6.

Table 7.6. Correlations for particle size data where a,b are position independent.

h/H	Correlation (N_{mod}=)		Shown in which Figure
0.836	$N(C)d^{-0.32}\left(VPo^{-1}D^{-5}\right)^{-0.39}$	(7.17)	Figure 7.31
0.672	$N(C)d^{-0.32}\left(VPo^{-1}D^{-5}\right)^{-0.39}$	(7.18)	Figure 7.32
0.508	$N(C)d^{-0.32}\left(VPo^{-1}D^{-5}\right)^{-0.39}$	(7.19)	Figure 7.33
0.344	$N(C)d^{-0.32}\left(VPo^{-1}D^{-5}\right)^{-0.39}$	(7.20)	Figure 7.34
0.180	$N(C)d^{-0.32}\left(VPo^{-1}D^{-5}\right)^{-0.39}$	(7.21)	Figure 7.35

The plots for the variations of C/C_0 with the correlations are shown in Figure 7.31-Figure 7.35.

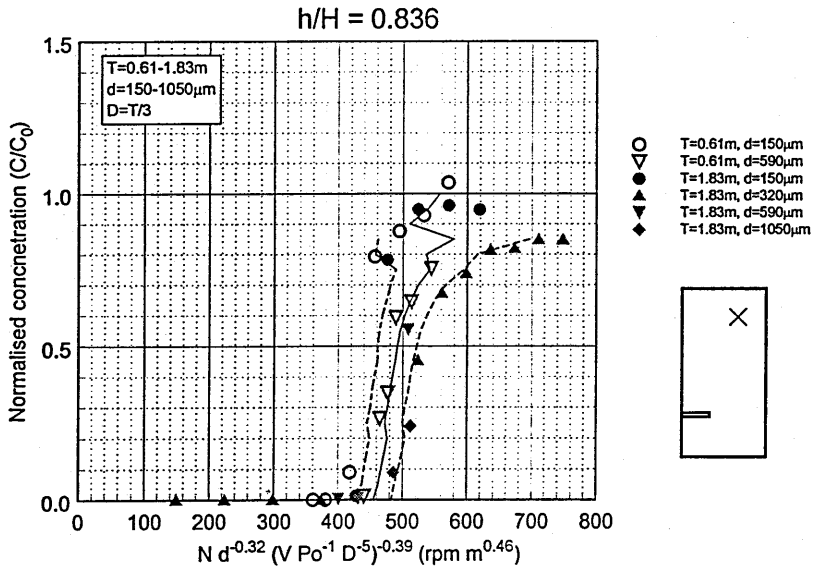

Figure 7.31. Variation of concentration at h/H=0.836 with N_{mod} for 45°PBT4(D=T/3)s at T=0.61 and 1.83m.

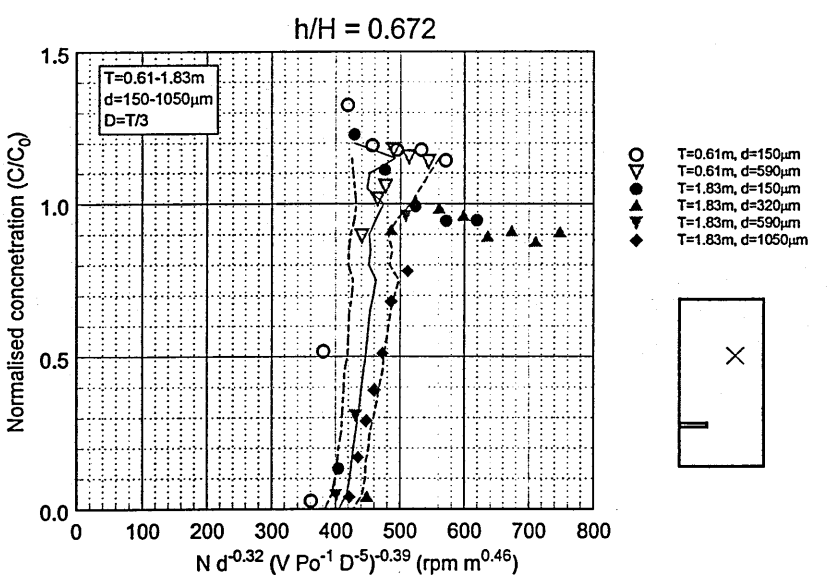

Figure 7.32. Variation of concentration at h/H=0.672 with N_{mod} for 45°PBT4(D=T/3)s at T=0.61 and 1.83m.

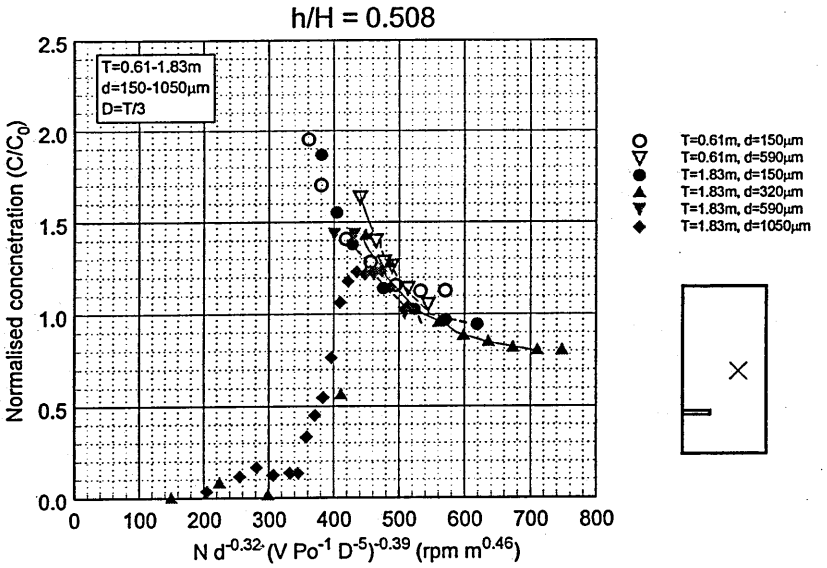

Figure 7.33. Variation of concentration at h/H=0.508 with N_{mod} for 45°PBT4(D=T/3)s at T=0.61 and 1.83m.

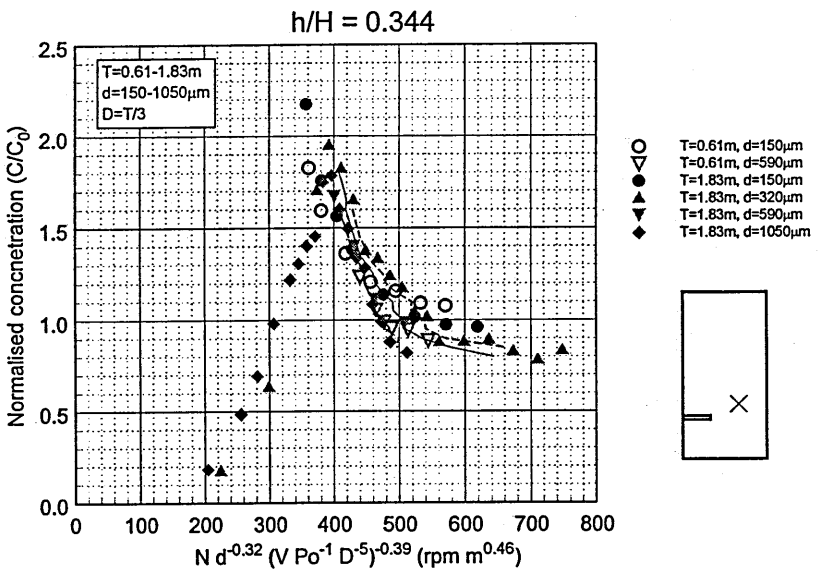

Figure 7.34. Variation of concentration at h/H=0.344 with N_{mod} for 45°PBT4(D=T/3)s at T=0.61 and 1.83m.

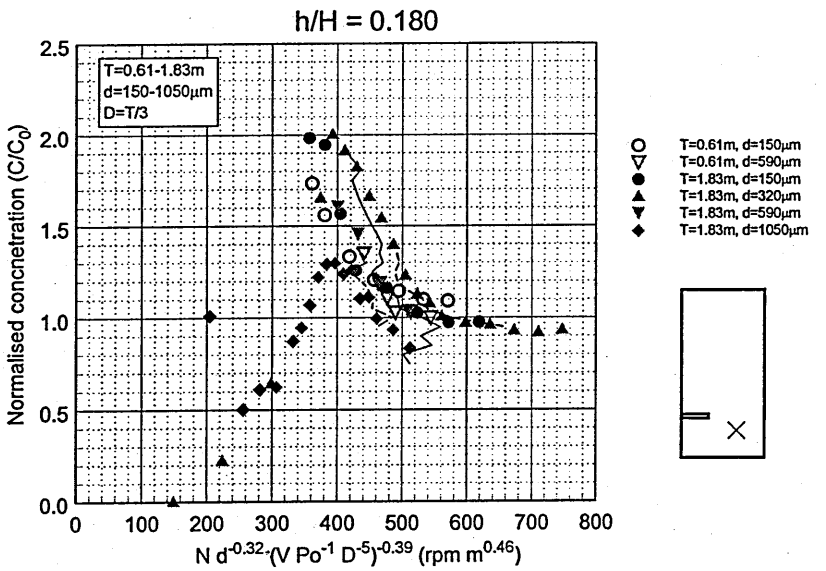

Figure 7.35. Variation of concentration at h/H=0.180 with N_{mod} for 45°PBT4(D=T/3)s at T=0.61 and 1.83m.

The value of σ_{sum} for each position is shown in Table 7.7.

Table 7.7. Values of σ_{sum} for comparisons where a and b are position independent.

h/H	σ_{sum}
0.836	0.017
0.672	0.017
0.508	0.0070
0.344	0.0095
0.180	0.011
Total	0.061

The correlations were found to be poorer than when a and b were position dependent. It can be seen that the maximum and minimum values for each of the correlations is much broader than was found in Section 7.6.1(c).

7.6.1(e) Conclusions

A summary of the correlations used in these analyses and the errors associated with each one have been shown in Table 7.8.

Table 7.8 shows that the sum of the relative errors are virtually the same except for the correlation on the basis of the raw data. The observation that the total relative error does not change by a large amount when P/V was forced to be the scale-up rule is strong support for this to be generally applied. However, a more accurate correlation where the exponents on particle size and vessel diameter have both been optimised has been developed and it is this that has been chosen for the design calculations shown in Section 7.9.

Table 7.8. Summary of correlations and relative errors.

Section	h/H	Correlation (N_{mod}=)	n	σ_{sum}	Sum (σ_{sum})
7.6.1(a)	0.836	N(C)	81	0.13	0.46
	0.672	N(C)	89	0.087	
	0.508	N(C)	52	0.10	
	0.344	N(C)	76	0.07	
	0.180	N(C)	67	0.069	
7.6.1(b)	0.836	$N(C)d^{-0.40}\left(VPo^{-1}D^{-5}\right)^{-0.33}$	81	0.015	0.066
	0.672	$N(C)d^{-0.37}\left(VPo^{-1}D^{-5}\right)^{-0.33}$	89	0.015	
	0.508	$N(C)d^{-0.32}\left(VPo^{-1}D^{-5}\right)^{-0.33}$	52	0.016	
	0.344	$N(C)d^{-0.28}\left(VPo^{-1}D^{-5}\right)^{-0.33}$	76	0.0089	
	0.180	$N(C)d^{-0.25}\left(VPo^{-1}D^{-5}\right)^{-0.33}$	67	0.011	
7.6.1(c)	0.836	$N(C)d^{-0.38}\left(VPo^{-1}D^{-5}\right)^{-0.36}$	81	0.014	0.050
	0.672	$N(C)d^{-0.36}\left(VPo^{-1}D^{-5}\right)^{-0.37}$	89	0.015	
	0.508	$N(C)d^{-0.32}\left(VPo^{-1}D^{-5}\right)^{-0.41}$	52	0.0058	
	0.344	$N(C)d^{-0.28}\left(VPo^{-1}D^{-5}\right)^{-0.37}$	76	0.0068	
	0.180	$N(C)d^{-0.23}\left(VPo^{-1}D^{-5}\right)^{-0.37}$	67	0.008	
7.6.1(d)	0.836	$N(C)d^{-0.32}\left(VPo^{-1}D^{-5}\right)^{-0.39}$	81	0.017	0.061
	0.672	$N(C)d^{-0.32}\left(VPo^{-1}D^{-5}\right)^{-0.39}$	89	0.017	
	0.508	$N(C)d^{-0.32}\left(VPo^{-1}D^{-5}\right)^{-0.39}$	52	0.0070	
	0.344	$N(C)d^{-0.32}\left(VPo^{-1}D^{-5}\right)^{-0.39}$	76	0.0095	
	0.180	$N(C)d^{-0.32}\left(VPo^{-1}D^{-5}\right)^{-0.39}$	67	0.011	

7.6.2 Comparisons of plots of concentration across a plane

The comparisons of geometrical effects in Sections 7.3-7.5 have shown that power per unit volume was a suitable scale-up criterion for the distribution of solids in a stirred vessel. The results from Section 7.6.1(b) have shown that when power per unit volume is used as the scale-up criterion, the exponent on particle diameter varied between 0.25 at the lowest point where concentration was measured and 0.40 at highest point. The data obtained in T_{61} using particles of d=150μm and 590μm have been analysed using these two exponents in order to examine qualitatively the predictions from the two values. When the data was analysed on the basis of $N(C) \propto d^{0.40}$ (Figures 7.36 and 7.37), good agreement was found between the bubble plots of the data.

The level to which particles were suspended and the region around (r/R=0.2, h/H=0.7), which has a lower concentration than the positions closer to the vessel wall, were well correlated by an exponent of -0.4 on the particle size.

When the data was analysed on the basis of $N(C) \propto d^{0.28}$ (Figures 7.38 and 7.39) the comparisons were found to be generally very poor.

In Figure 7.39 the level to which the solids were suspended, which could be considered to be the position where the normalised concentration had a value of 0.5, were very different. The 590 μm sand was suspended to about h/H=0.7 whereas the experiments with the 150 μm sand suggest that the particles were suspended all the way to the liquid surface.

The qualitative comparisons will be dominated by the strong gradient of particle concentration with increasing height above the vessel base. It would be expected therefore that use of the exponents near to the surface would result in a better qualitative comparison than those lower down. This means that the qualitative comparisons would be more of a measure of the suspension height in the vessel rather than the concentration profile at each point in the vessel. For the purposes of design, it is more important that the concentration profile at each point in the vessel be examined individually which is why the design procedure (Section 7.9) uses the individual exponents for each position in the vessel, as was presented in Section 7.6.1(c).

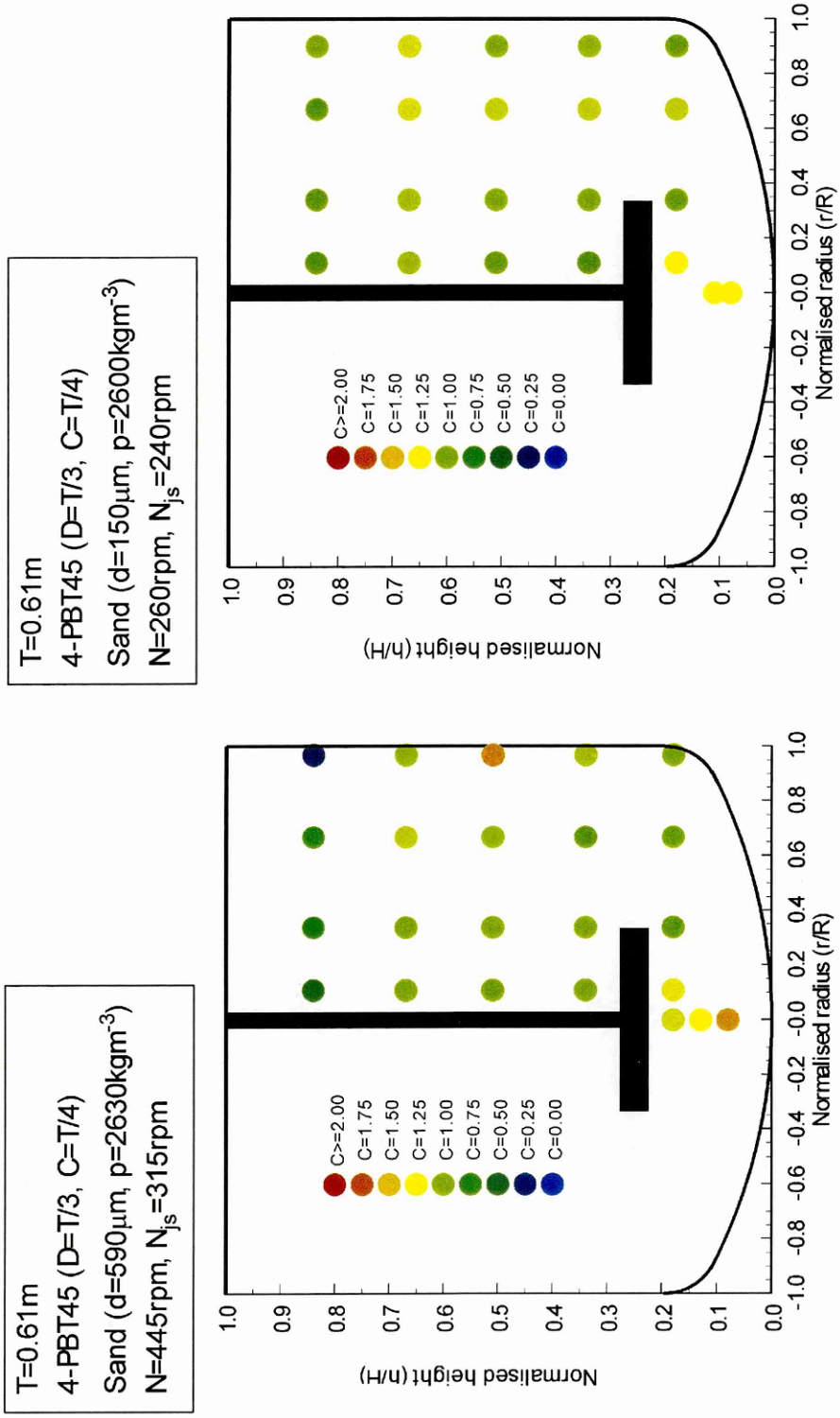

Figure 7.36. Comparison of data obtained in T_{61} on the basis of $N(C)\alpha d^{0.40}$.

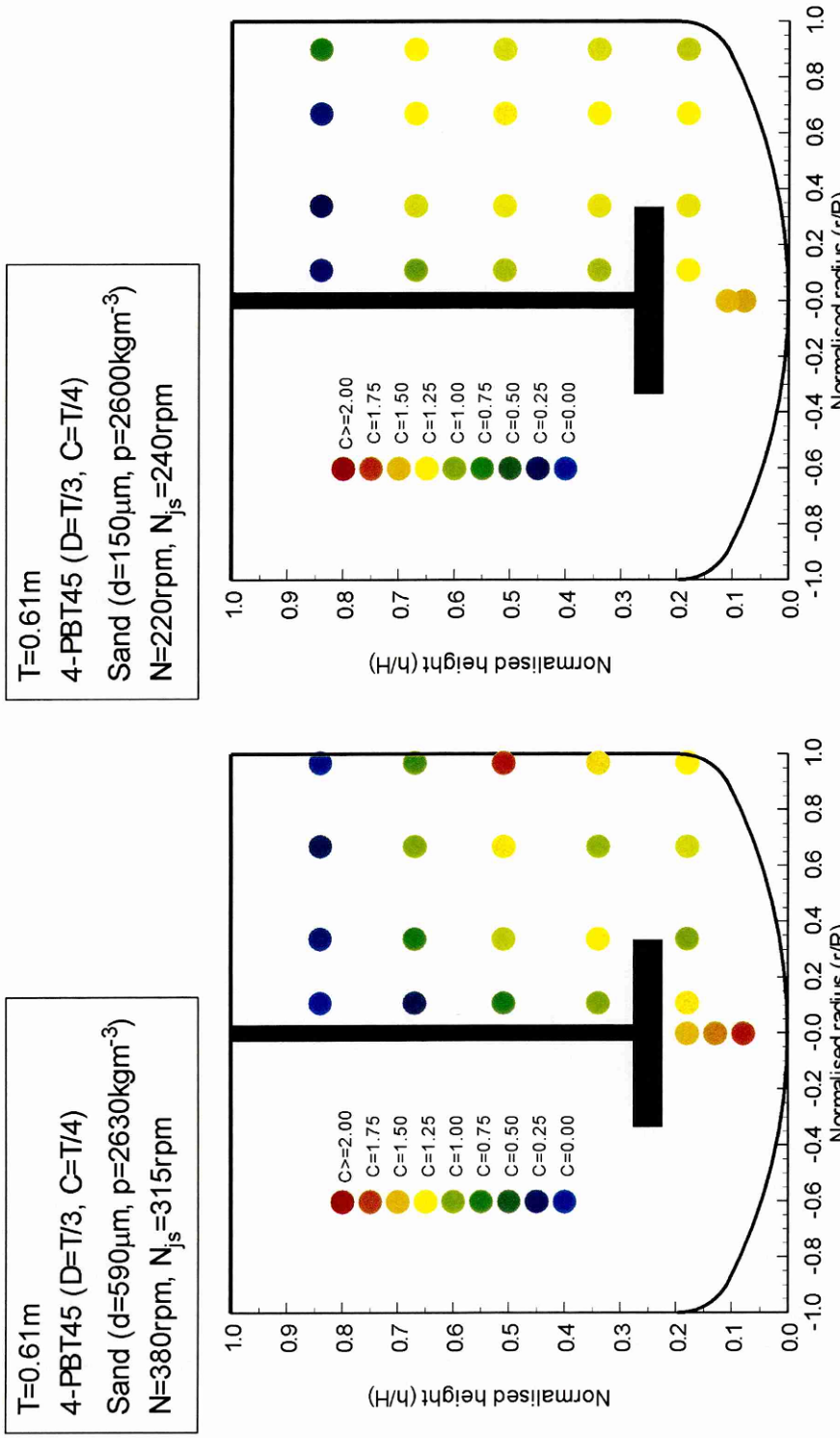

Figure 7.37. Comparison of data obtained in T_{61} on the basis of $N(C)\alpha d^{0.40}$.

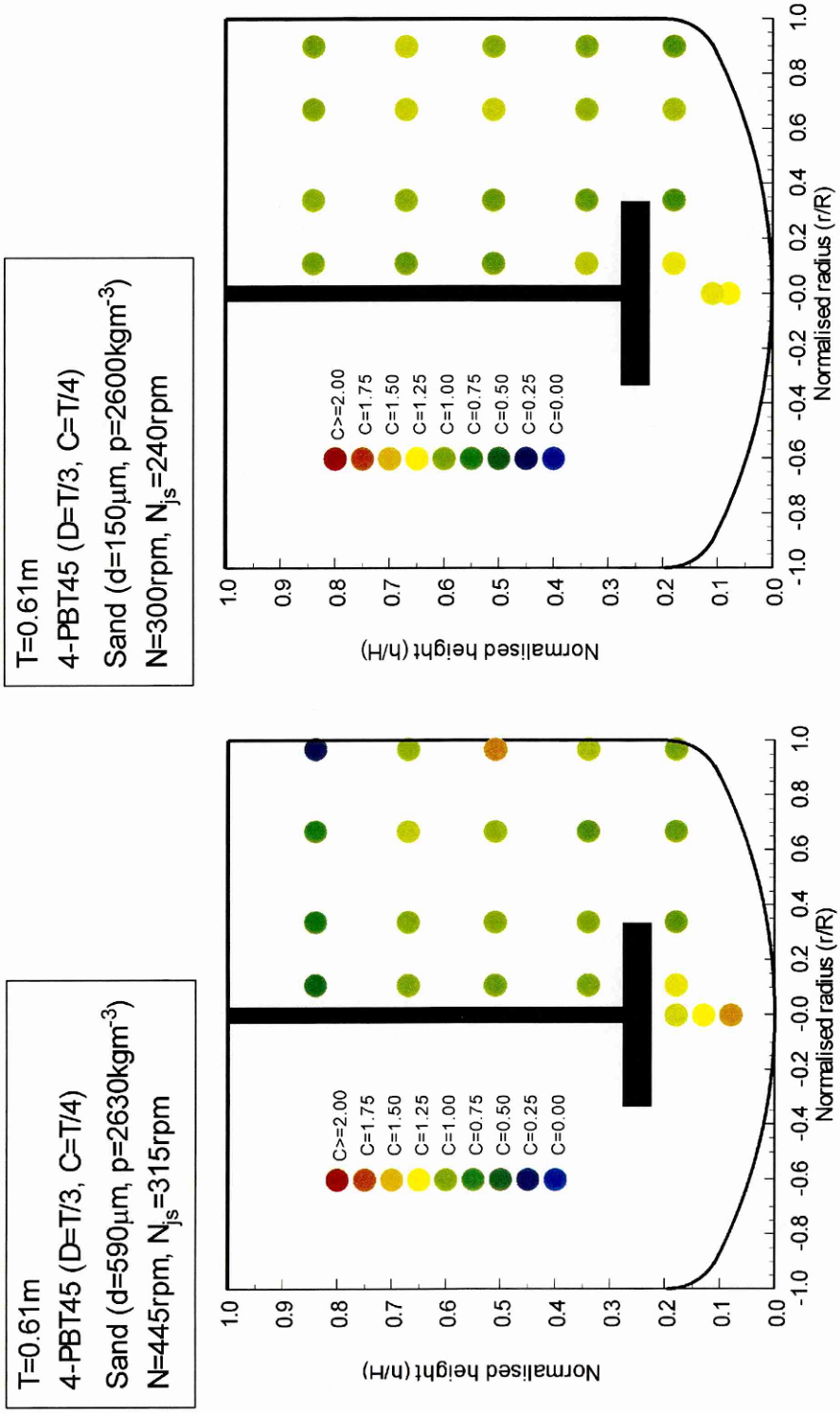

Figure 7.38. Comparison of data obtained in T_{61} on the basis of $N(C)\alpha d^{0.25}$.

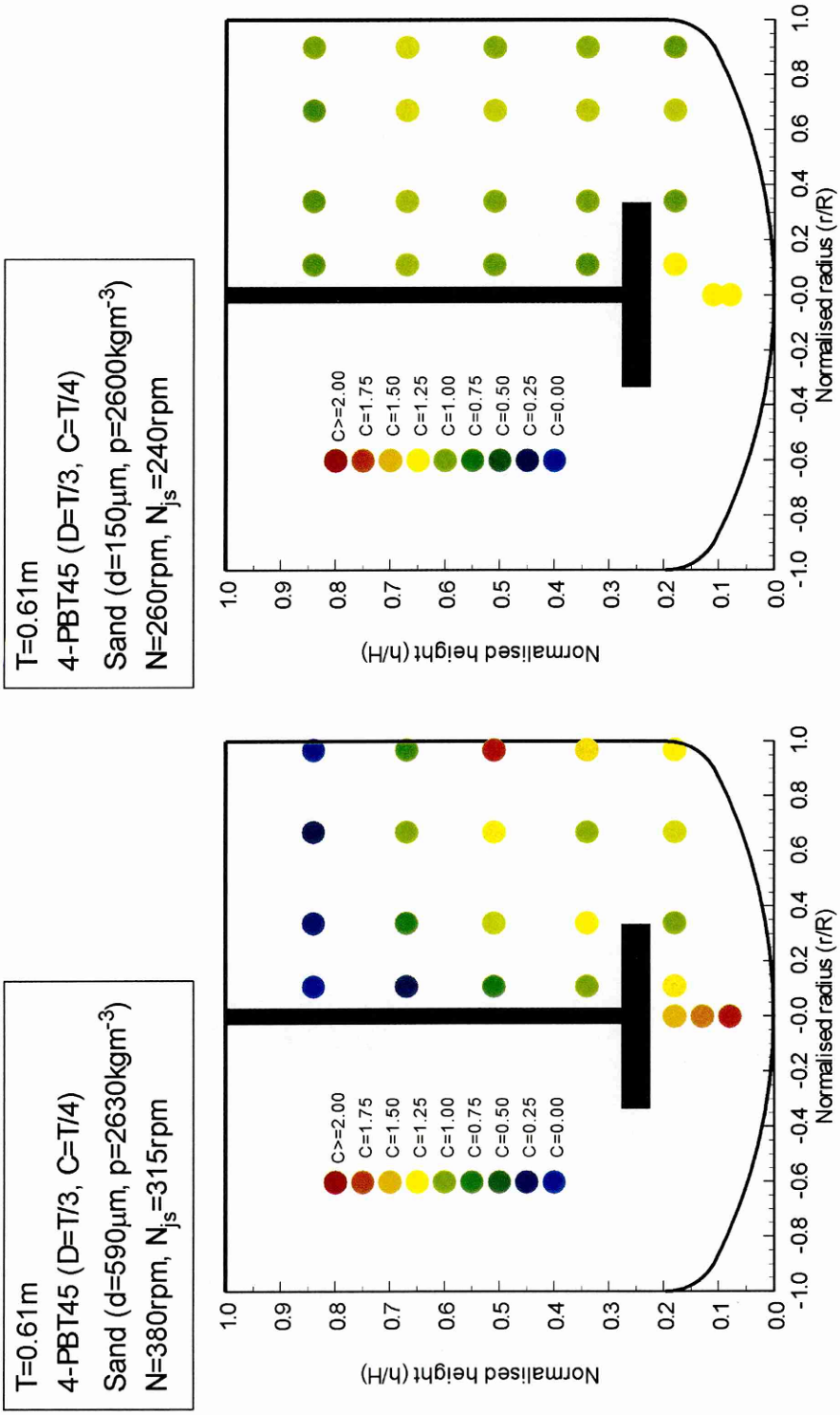

Figure 7.39. Comparison of data obtained in T_{61} on the basis of $N(C)\alpha d^{0.25}$.

7.7 Modelling the solids concentration as an array of oscillating spheres

The comparisons so far have been empirical which says little about the underlying physics that occur in a stirred vessel. This simple model was developed to see what could be said from the theoretical view of particle-particle interactions.

This method of analysis models the particles in the stirred vessel as though they are gas molecules in a vacuum. Since the particles are colliding with eddies and each other, they exert a pressure on their surroundings. The force that prevents the particles from expanding to fill the vessel is the gravitational force and this is equated in the model with the dispersive force of the particles.

Bagnold (1954) produced a correlation relating the force that causes particles to separate as they shear inside an annular shear cell. This paper was used to examine whether a simple model that equates the dispersive forces due to shear with the settling force due to gravity could be developed:

$$F_G = F_D \tag{7.22}$$

Here, F_G and F_D are the gravitational (Equation 7.23) and dispersive forces, respectively.

$$F_G = \Delta\rho g V \tag{7.23}$$

The relationship in the "grain-inertia region" for the "granular pressure", P_D was modelled by Bagnold (1954):

$$P_D = 0.042(Ld)^2 \dot{\gamma}^2 \cos\alpha_i \rho_S \tag{7.24}$$

Here, L is the ratio of the particle diameter, d, to the distance between particle surfaces, x_s, as illustrated in Figure A2.1. It can be shown (Appendix 2) that, for a close-packed array of spheres, L is given by Equation A2.7:

$$L = \frac{\alpha}{\sqrt{2}}\left(\frac{2\pi}{3C}\right)^{1/3} - 1 \tag{A2.7}$$

The local shear rate, $\dot{\gamma}$, is difficult to define in a stirred tank. The best approximation is to say that for isotropic turbulence, the mean square velocity over distance, d (Harnby *et al.*, 1999) is given by Equation 7.25:

$$u^2 = C_1(\varepsilon_m d)^{2/3} \tag{7.25}$$

Since the velocity fluctuations are occurring over a distance d, it was assumed that the local shear rate of the particles could be given by Equation 7.26.

$$\frac{u}{d} = \dot{\gamma} = \left(\frac{\beta\bar{\varepsilon}}{d^2}\right)^{1/3} \tag{7.26}$$

The parameter β was included so that the effect of varying localised energy dissipation rates and the constant, C_1, could be included in the analysis.

The relationship between P_D and F_D is shown in Equation 7.27:

$$\frac{F_D}{P_D} = \tan\alpha_i \tag{7.27}$$

Experimentally it was found by Bagnold (1957) that $\tan\alpha_i = 0.32$. Equation 7.24 can be rearranged as an expression for the dispersive force due to the intergranular pressure and the shear rate as shown in Equation 3.49:

$$F_D = 0.0128L^{-2}d^2\dot{\gamma}^2 A\rho_S \tag{3.49}$$

Where A is the area occupied by a particle in a close-packed plane as shown in Appendix A2. A is given by Equation A2.12:

$$A = \frac{\sqrt{3}}{2}\left(\frac{\pi^2}{18C^2}\right)^{1/3}\alpha^2 d^2 \tag{A2.12}$$

Equation 3.49 can now be rearranged to give Equation 7.28:

$$F_D = 0.0128\left[\frac{\alpha}{\sqrt{2}}\left(\frac{2\pi}{3C}\right)^{1/3} - 1\right]^{-2} d^2\left(\frac{\beta\bar{\varepsilon}}{d^2}\right)^{2/3}\frac{\sqrt{3}}{2}\left(\frac{\pi^2}{18C^2}\right)^{1/3}\alpha^2 d^2\rho_S = \Delta\rho g\frac{\pi d^3}{6} \tag{7.28}$$

From Equation 7.28, it can be seen that for a given set of particle properties the concentration can be calculated at different impeller speeds or power inputs provided that α and β are known. This model of the physics of what is happening in a stirred vessel was applied to the results from the measurement positions at h/H=0.180 and 0.344 in T_{183}. The analysis was only applied to the results from the experiments performed with particles of diameter 320 μm, 590 μm and 1050 μm. The data has been plotted in Figure 7.40 to Figure 7.45 as the impeller speed for a given concentration versus the calculated impeller speed for each of the data sets.

The parameters α and β were calculated at each measurement position by varying them such that the square of the difference between the measured and calculated values of the impeller speed for a given particle concentration was minimised.

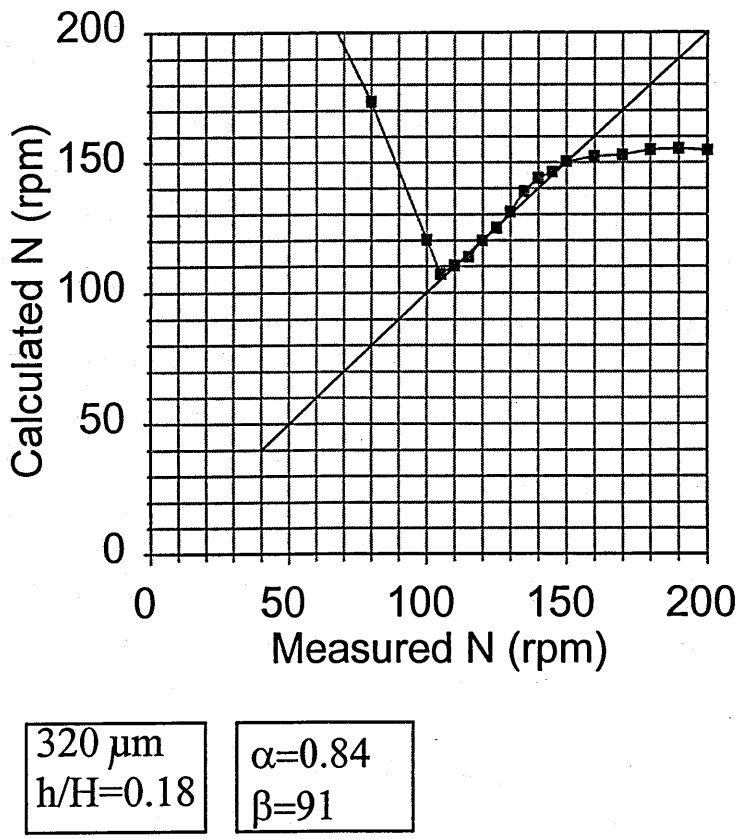

Figure 7.40. Comparison of measured vs. predicted impeller speeds from the Bagnold model (d=320 μm, h/H=0.180).

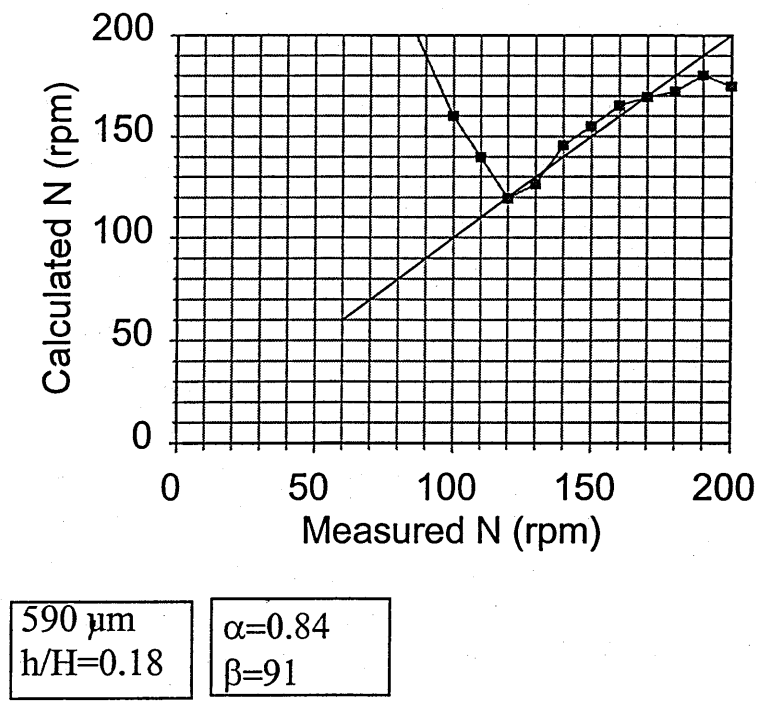

Figure 7.41. Comparison of measured vs. predicted impeller speeds from the Bagnold model (d=590 µm, h/H=0.180).

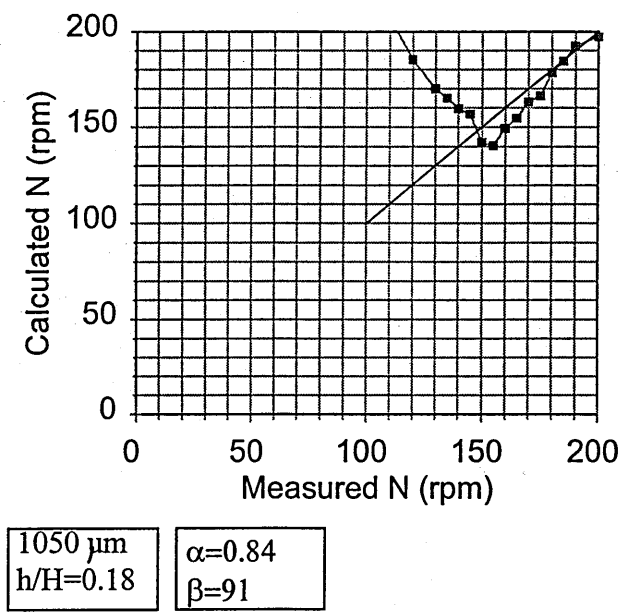

Figure 7.42. Comparison of measured vs. predicted impeller speeds from the Bagnold model (d=1050 µm, h/H=0.180).

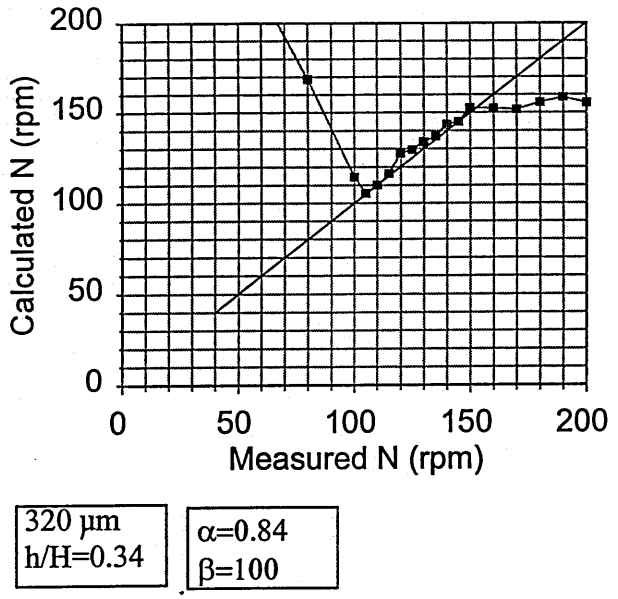

Figure 7.43. Comparison of measured vs. predicted impeller speeds from the Bagnold model (d=320 µm, h/H=0.344).

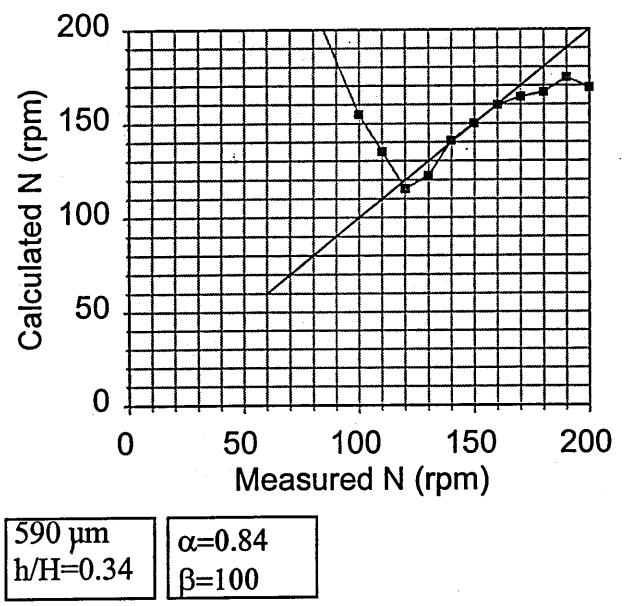

Figure 7.44. Comparison of measured vs. predicted impeller speeds from the Bagnold model (d=590 µm, h/H=0.344).

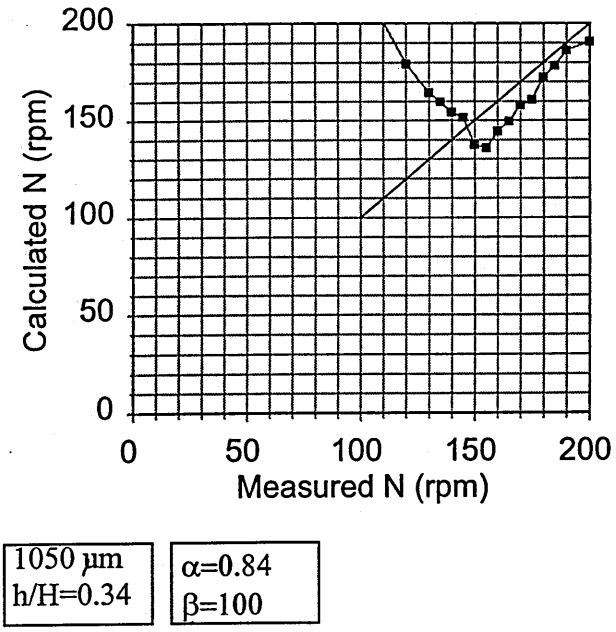

Figure 7.45. Comparison of measured vs. predicted impeller speeds from the Bagnold model (d=1050 µm, h/H=0.344).

The results from this analysis were close to those that were measured although the model under-predicted the impeller speed for a given concentration when the d=1050 µm data was analysed. Below N_{js} or above N_{homo}, this model over- and under-predicts the required impeller speed for a given particle concentration, respectively.

It can be seen that α=0.84 as expected that this value was found to be close to 1, the value for a close-packed structure of solids. The value of β was found to be very high. This indicates that the local energy dissipation rate in the slurry is about 100 times that when averaged over the whole vessel. This is clearly wrong since particles are suspended to at least 50% of the vessel volume, so the maximum value of β would be 2. The origin of this error is almost certainly in the assumption that the characteristic shear rate is a result of the turbulent eddies in the inertial sub-range. The required shear rate for a given concentration was found to be of the order of 500 s^{-1} for the Bagnold-based model to be true. It is possible that this major problem could be overcome by using the collision frequency of particles as the characteristic shear rate.

7.8 Modelling of data using 1-d sedimentation – dispersion model

The one dimensional sedimentation dispersion model was described in Section 3.1.1. This model assumes that the opposing velocities of sedimentation and turbulent dispersion are balanced at each point in the vessel. Since the forces are balanced, this model is a steady state model. The concentration profile that resulted from this model is shown in Equation 3.7:

$$\frac{C(z)}{C_0} = \frac{Pe(H)e^{-Pe(z)}}{1-e^{-Pe(H)}} \tag{3.7}$$

Equation 3.7 has been used by Fajner *et al.* (1985). In this equation the Peclet number, Pe (z) is defined in Equation 3.6:

$$Pe(z) = \frac{(u_t - u)z}{D_S} \tag{3.6}$$

Since the upward flow of liquid through a cross-section through the vessel is zero (u=0), Equation 3.6 reduces to Equation 7.29:

$$Pe(z) = \frac{u_t z}{D_S} \tag{7.29}$$

The value for D_S has been calculated using the correlation from Pinelli *et al.* (1996) as shown in Equation 7.30.

$$\frac{D_S}{ND^2} = \begin{cases} 0.13, & Re \geq 10\,000, \\ 0.0217\ \mathrm{Ln}(Re) - 0.0699, & Re < 10\,000. \end{cases} \tag{7.30}$$

There is a difference between the settling velocities of particles in a quiescent medium (u_t) and those in a turbulent flow (u_s) (Fajner *et al.*, 1985). The effect of the reduction of the particle settling velocity by the turbulent flow field has been included using the correlation from Pinelli *et al.* (1996) which is shown in Equation 7.31.

$$\frac{u_S}{u_t} = 201 \tanh\left(6.05\frac{\lambda_K}{d} + 3.14\right) - 200 \tag{7.31}$$

Here, the Kolmogorov length scale, λ_K, is given by Equation 7.32:

$$\lambda_K = \left(\frac{\upsilon^3}{\bar{\varepsilon}}\right)^{0.25} \tag{7.32}$$

Here, υ is the kinematic viscosity of the liquid and $\bar{\varepsilon}$ is the tank-averaged energy dissipation rate. The local energy dissipation rate should be used in the calculation of λ_K but since this is not well defined due to the modification of the turbulent flow field by the particles, the global energy dissipation rate has been used. Measurement of the liquid and particle flow velocities using refractive-index matched LDA would be of great use in gathering data on the turbulent flow fields with different particle sizes. An alternative method would be to use a chemical probe, in which the products of a reaction are sensitive to the local dissipation rate and so measurement of the reaction products would give an indication of the energy dissipation rates at different measurement positions.

The impeller Reynolds number was greater than 10,000 for each of the measurements obtained. The normalised dispersion coefficient in Equation 7.30 always had the value of 0.13. Since the normalised dispersion coefficient is constant, the dispersion coefficient will increase with impeller speed and impeller diameter. In Figure 7.46 to Figure 7.50 the measured normalised particle concentration has been plotted against to the normalised concentration that was calculated using Equation 3.7. At impeller speeds below N_{js}, the average particle concentration in the vessel was less than C_0. This was not taken into account which resulted in the measured concentration being much less than that calculated. To remove this affect from the analysis, the analysis was restricted to impeller speeds above N_{js}.

The comparisons were generally poor at each measured position. The calculated particle concentration was under-predicted significantly for some conditions. In Figure 7.46, the measured particle concentration was as high as 2.0 whereas the predicted concentration for this condition was about 1.2. Similar under-predictions were seen from the results from each of the other positions (Figure 7.47 - Figure 7.50).

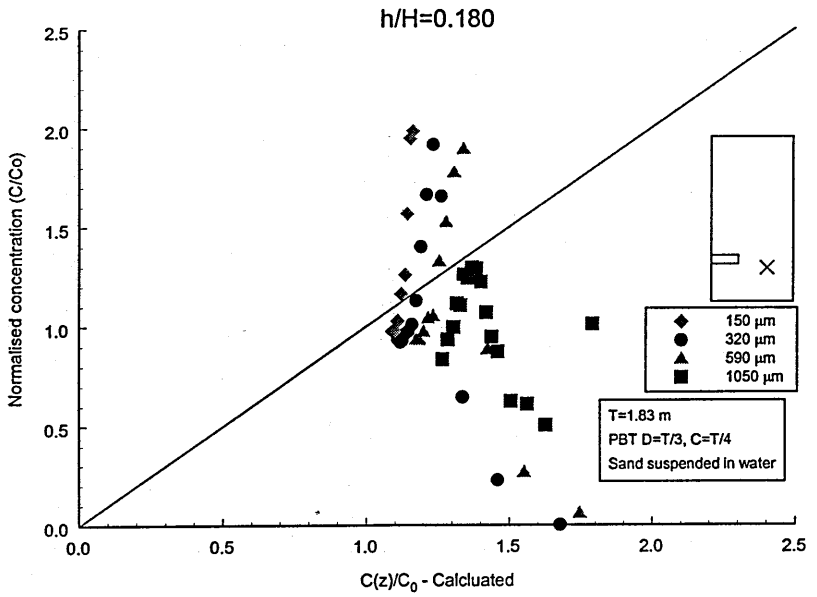

Figure 7.46. Comparison of measured vs. predicted concentrations from the 1d sedimentation-dispersion model (h/H=0.180).

The analysis of the results the from measurement position at h/H=0.344 were particularly poor. The predicted concentration for this position was 1.1 over all the impeller speeds that were tested whereas concentrations of up to 2.2 were measured.

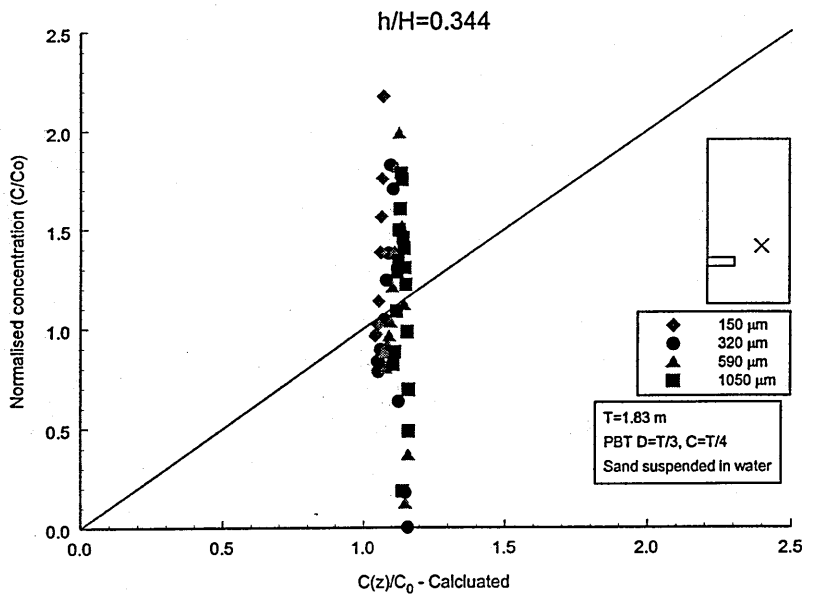

Figure 7.47. Comparison of measured vs. predicted concentrations from the 1d sedimentation-dispersion model (h/H=0.344).

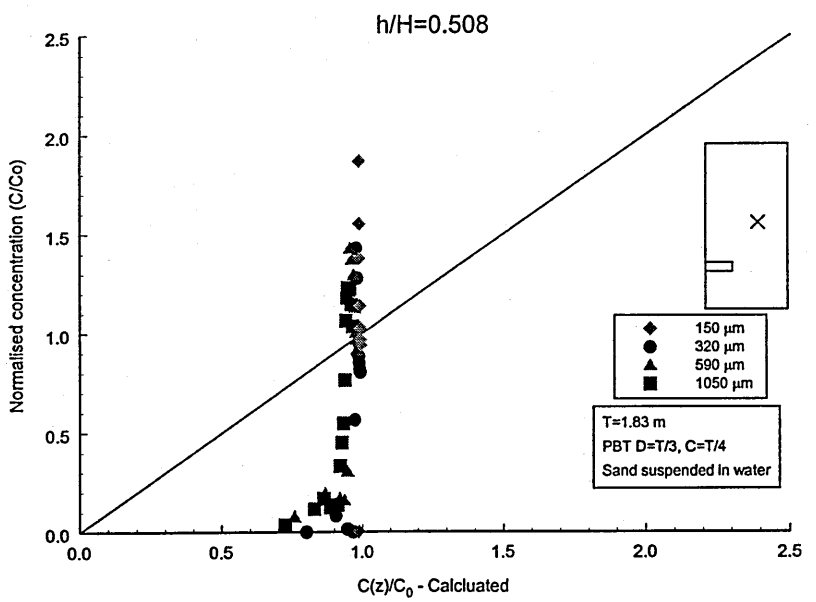

Figure 7.48. Comparison of measured vs. predicted concentrations from the 1d sedimentation-dispersion model (h/H=0.508).

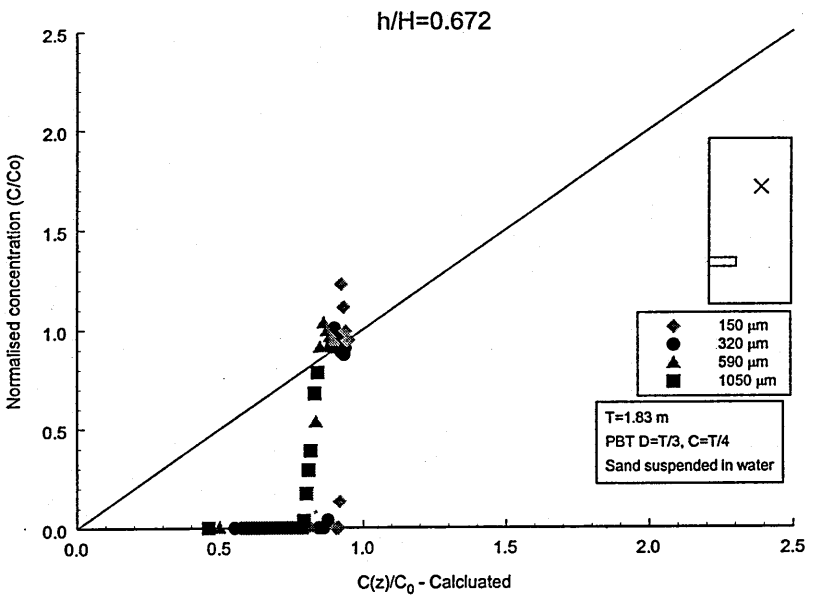

Figure 7.49. Comparison of measured vs. predicted concentrations from the 1d sedimentation-dispersion model (h/H=0.672).

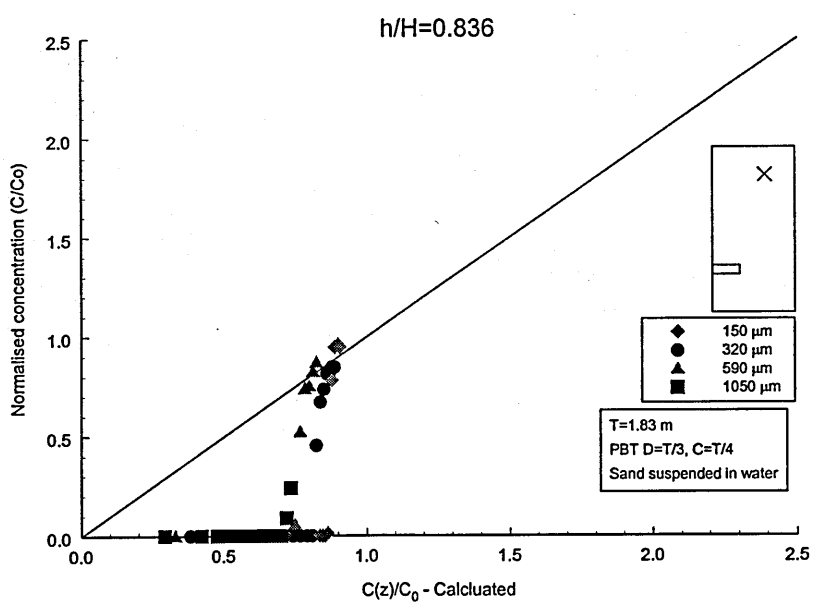

Figure 7.50. Comparison of measured vs. predicted concentrations from the 1d sedimentation-dispersion model (h/H=0.836).

The 1d sedimentation-dispersion model is a steady-state model with an exponential decay of concentration with height above the vessel base. This is in opposition to what was observed during the experimental work. During the experiments, it was observed that the slurry interface was clear cut and fluctuated significantly as particles were swept high into the vessel by large-scale flow structures. The problems with the ability of this model to predict concentrations is probably due to the conflicts between the observed and theoretical results from this model.

Another problem with the model is, in its simplest form, that D_S was assumed to be position invariant. In reality, the value of D_S will vary significantly and this could only be measured experimentally by a method such as positron emission particle tracking. This experiment would involve labelling one particle with a radioactive isotope and monitoring its spatial position and velocity with time. The value of D_S at different positions could be estimated during the data analysis by examining where the particle is a short time later. The standard deviation of the positions about the mean position sometime later would give a measure of the value for D_S.

7.9 Design procedures for solids concentration

There are a variety of ways in which a design engineer could use the data that has been generated during this project:

1. To specify the required impeller speed or draw-off position for the particle concentration to be *at least* a particular value.
2. To specify the required impeller speed or draw-off position for the particle concentration to be *at most* a particular value.
3. To specify the required impeller speed or draw-off position for the particle concentration to be approximately a particular concentration but with a known range of concentrations that could occur.

Examples for each of the above cases has been illustrated below. In each case, the correlation that has been used is that which has been presented in Section 7.6.1(c) where the exponents on particle size and specific power were allowed to vary with position. The correlation for each position is shown in Equations 7.12 to 7.16.

h/H=0.836:

$$N_{mod} = N(c)d^{-0.38}\left(VPo^{-1}D^{-5}\right)^{-0.36} \quad (7.12)$$

h/H=0.672:

$$N_{mod} = N(c)d^{-0.36}\left(VPo^{-1}D^{-5}\right)^{-0.37} \quad (7.13)$$

h/H=0.508:

$$N_{mod} = N(c)d^{-0.32}\left(VPo^{-1}D^{-5}\right)^{-0.41} \quad (7.14)$$

h/H=0.344:

$$N_{mod} = N(c)d^{-0.28}\left(VPo^{-1}D^{-5}\right)^{-0.37} \quad (7.15)$$

h/H=0.180:

$$N_{mod} = N(c)d^{-0.23}\left(VPo^{-1}D^{-5}\right)^{-0.37} \quad (7.16)$$

Example 1. Specification of a maximum concentration allowed at a given position.
A 4PBT45 (D=T/3, C=T/4, Po=1.3) is to be used in a T=1.2 m vessel (H=T, V=1.27m^3) to suspend particles with d=825μm, Δρ=1630 kgm^{-3} and C_0=6.3%v/v (N_{js} = 193rpm). The maximum allowable concentration at h/H=0.836 is C/C_0=0.5. What is the range of impeller speeds within which this vessel may be operated?

Answer to 1.
Using Figure 7.26, N_{mod} is read off and found to be N_{mod}=850. The impeller speed for N_{mod}=850 is given by Equation 7.33.

$$N = \frac{N_{mod}}{d^{-0.38}\left(VPo^{-1}D^{-5}\right)^{-0.36}} = \frac{850}{(825x10^{-6})^{-0.38}\left([1.27][1.3^{-1}][0.4^{-5}]\right)^{-0.36}} = 295rpm \quad (7.33)$$

The range of allowable operating speeds for the impeller is therefore 193-295 rpm.

Example 2. Specification of a minimum concentration allowed at a given position.

A 4PBT45 (D=T/3, C=T/4, Po=1.3) is to be used in a T=1.2 m vessel (H=T, V=1.27m^3) to suspend particles with d=825μm, Δρ=1630 kgm^{-3} and C_0=6.3%v/v (N_{js} = 193rpm). The minimum allowable concentration at h/H=0.836 is C/C_0=0.5. What is the minimum impeller speed at which this vessel may be operated?

Answer to 2.

Using Figure 7.26, N_{mod} is read off to be N_{mod}=950. The impeller speed for N_{mod}=950 is given by Equation 7.34.

$$N = \frac{N_{mod}}{d^{-0.38}\left(VPo^{-1}D^{-5}\right)^{-0.36}} = \frac{950}{(825x10^{-6})^{-0.38}\left([1.27][1.3^{-1}][0.4^{-5}]\right)^{-0.36}} = 330rpm \qquad (7.34)$$

This impeller speed is greater than N_{js} (193rpm) and so is a valid answer.

This vessel should be operated at a speed of no less than 330rpm.

Example 3. Specification of the concentration profile for an existing vessel.

A 4PBT45 (D=T/3, C=T/4, Po=1.3) is to be used in a T=1.2 m vessel (H=T, V=1.27m^3) to suspend particles with d=825μm, Δρ=1630 kgm^{-3} and C_0=6.3%v/v (N_{js} = 193rpm).

a. What is the concentration profile at a speed of 250 rpm?

b. What is the concentration profile at a speed of 300 rpm?

Answer to 3a.

Using Figure 7.26 to Figure 7.30, C/C_0 is read off for each measurement position. The values of N_{mod} for each position are given by Equations 7.35-7.39.

h/H=0.836

$$N_{mod} = Nd^{-0.38}\left(VPo^{-1}D^{-5}\right)^{-0.36} = 250(825x10^{-6})^{-0.38}\left([1.27][1.3^{-1}][0.4^{-5}]\right)^{-0.36} = 720rpmm^{0.34} \qquad (7.35)$$

h/H=0.672

$$N_{mod} = Nd^{-0.36}\left(VPo^{-1}D^{-5}\right)^{-0.37} = 250(825x10^{-6})^{-0.36}\left([1.27][1.3^{-1}][0.4^{-5}]\right)^{-0.37} = 600rpmm^{0.38} \qquad (7.36)$$

h/H=0.508

$$N_{mod} = Nd^{-0.32}\left(VPo^{-1}D^{-5}\right)^{-0.41} = 250(825x10^{-6})^{-0.32}\left([1.27][1.3^{-1}][0.4^{-5}]\right)^{-0.41} = 370rpmm^{0.50} \qquad (7.37)$$

h/H=0.344

$$N_{mod} = Nd^{-0.28}\left(VPo^{-1}D^{-5}\right)^{-0.37} = 250(825x10^{-6})^{-0.28}\left([1.27][1.3^{-1}][0.4^{-5}]\right)^{-0.37} = 340rpmm^{0.46} \quad (7.38)$$

h/H=0.180

$$N_{mod} = Nd^{-0.23}\left(VPo^{-1}D^{-5}\right)^{-0.37} = 250(825x10^{-6})^{-0.23}\left([1.27][1.3^{-1}][0.4^{-5}]\right)^{-0.37} = 240rpmm^{0.51} \quad (7.39)$$

The values of C/C_0 at each position are given in Table 7.9.

Table 7.9. Values of C/C_0 at each position for design example 3a.

h/H	C/C_0		
	Low	Mid	High
0.836	0.00	0.00	0.00
0.672	0.00	0.00	0.20
0.508	0.60	1.65	1.90
0.344	1.15	1.30	1.35
0.180	1.14	1.50	Not available

For h/H=0.180 there was not enough data available for the upper concentration to be measured. Further experiments would be needed to obtain this information. The predicted concentration profile is shown schematically in Figure 7.51.

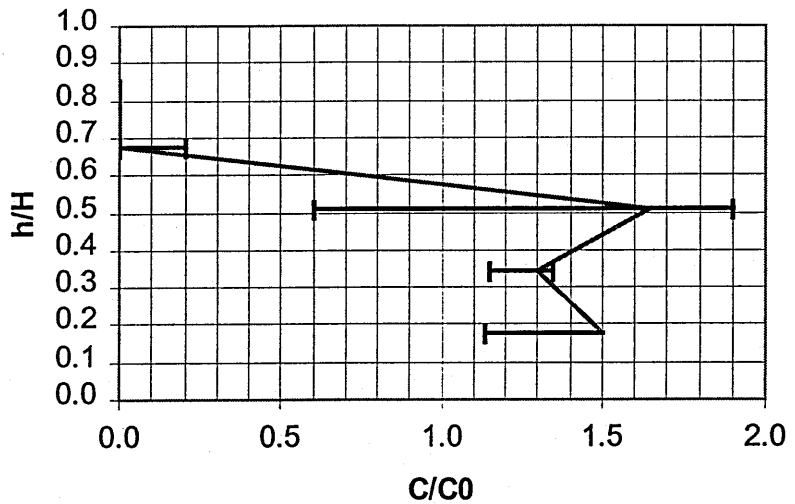

Figure 7.51. Predicted concentration profile from Example 3a.

The plot shows that at 250rpm, particles are suspended only up to about h/H=0.6. There is a large uncertainty in the concentration around h/H=0.5. The best place for a draw-off point would be below about h/H=0.4.

Answer to 3b.

Using Figure 7.26 to Figure 7.30, C/C_0 is read off for each measurement position. The values of N_{mod} for each position are given by Equations 7.40-7.44.

h/H=0.836

$$N_{mod} = Nd^{-0.38}\left(VPo^{-1}D^{-5}\right)^{-0.36} = 300(825x10^{-6})^{-0.38}\left([1.27][1.3^{-1}][0.4^{-5}]\right)^{-0.36} = 860rpmm^{0.34} \quad (7.40)$$

h/H=0.672

$$N_{mod} = Nd^{-0.36}\left(VPo^{-1}D^{-5}\right)^{-0.37} = 300(825x10^{-6})^{-0.36}\left([1.27][1.3^{-1}][0.4^{-5}]\right)^{-0.37} = 720rpmm^{0.38} \quad (7.41)$$

h/H=0.508

$$N_{mod} = Nd^{-0.32}\left(VPo^{-1}D^{-5}\right)^{-0.41} = 300(825x10^{-6})^{-0.32}\left([1.27][1.3^{-1}][0.4^{-5}]\right)^{-0.41} = 450rpmm^{0.50} \quad (7.42)$$

h/H=0.344

$$N_{mod} = Nd^{-0.28}\left(VPo^{-1}D^{-5}\right)^{-0.37} = 300(825x10^{-6})^{-0.28}\left([1.27][1.3^{-1}][0.4^{-5}]\right)^{-0.37} = 410rpmm^{0.46} \quad (7.43)$$

h/H=0.180

$$N_{mod} = Nd^{-0.23}\left(VPo^{-1}D^{-5}\right)^{-0.37} = 300(825x10^{-6})^{-0.23}\left([1.27][1.3^{-1}][0.4^{-5}]\right)^{-0.37} = 280rpmm^{0.51} \quad (7.44)$$

The values of C/C_0 at each position are given in Table 7.10.

Table 7.10. Values of C/C_0 at each position for design example 3b.

h/H	C/C_0		
	Low	Mid	High
0.836	0.00	0.20	0.50
0.672	0.80	1.10	Not available
0.508	1.10	1.15	1.30
0.344	Not available	0.95	1.00
0.180	Not available	1.00	1.05

The predicted concentration profile for N=300rpm is shown schematically in Figure 7.52

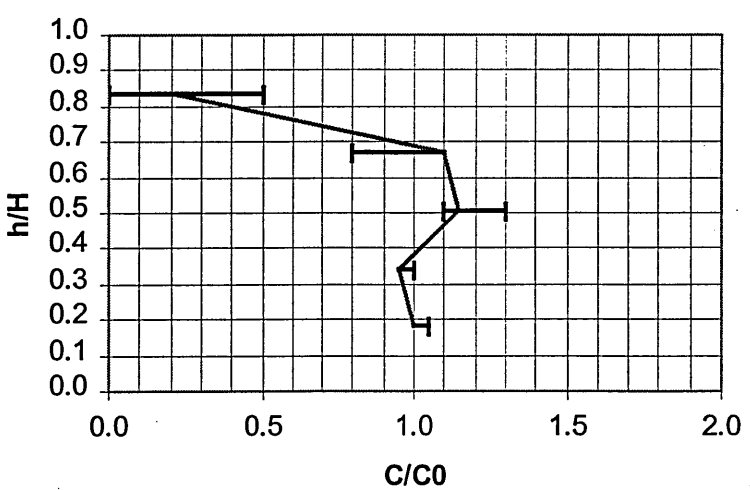

Figure 7.52. Predicted concentration profile from Example 3b.

The plot shows that it is likely that solids are suspended to about h/H=0.8 at N=300rpm. The familiar maximum in concentration is observed to be at about h/H=0.5. A draw off in this case could be positioned anywhere between h/H=0.0-0.7 but if it was positioned about h/H=0.4 and the slurry could be drawn-off iso-kinetically this would be representative of the overall vessel particle concentration. In a continuous flow situation, where solids could be added or formed, no increase or decrease of tank-averaged particle concentration would be observed.

7.10 Role of research within CFD development at BHR Group

BHR Group Limited has had a long interest in developing numerical models of complex three-dimensional fluid-dynamic systems. Within this area, work has been performed by Xiao-Dong (Sam) Yang, a Computational Fluid Dynamics (CFD) specialist, to develop a CFD model of solid-liquid mixing in mechanically stirred vessels. The development of this model has required experimental data to set the empirical constants in the model and to act as a benchmark against which the model could be judged. The CFD group used some of the data generated during this project to reach these objectives. Yang and Taylor (1998) (see Appendix 5) have presented comparisons between the experimental results and the CFD model.

The simulations were performed using CFX4.1 and its multiphase solver *SINCE*. In the model both the liquid and solid phases were considered to be a continuum for which the conservation equations of mass and momentum may be derived separately. The multi-fluid model solves the full set of conservation equations separately, together with the constitutive equations for the exchange of momentum between the two phases which was determined using an empirical particle drag coefficient.

The standard k-ε for single-phase flow was applied directly to the solid-liquid flow field in this simulation. The turbulent diffusion of the solids was determined using the eddy diffusivity hypothesis which states that the particle diffusion is proportional to the eddy viscosity as shown in Equation 7.45:

$$D_S = \frac{\mu_T}{\mathrm{Pr}_T} \tag{7.45}$$

Here, Pr_T is the turbulent Prantl number which had to be determined using experimental data and μ_T is the eddy viscosity.

A momentum source model was used to describe the impeller. This model uses experimental data and empirical correction factors to determine the average body force produced by the impeller.

The drag coefficient was determined using the standard drag curve (Equation 7.46):

$$C_D = \frac{24}{\mathrm{Re}} + \frac{5.48}{\mathrm{Re}^{0.573}} + 0.36 \tag{7.46}$$

Here, Re_P is the particle Reynolds number which is given by Equation 3.64:

$$\mathrm{Re}_P = \frac{\rho_L u_t d}{\mu} \tag{3.64}$$

It was also assumed that there were no particle-particle interactions. Therefore, the particle concentration has to be low which was not always the case which could lead to errors in the regions of high concentration. This is a steady state model and, as such, cannot show the transient behaviour that was observed in the experimental work. The liquid surface was described as a flat, frictionless surface. Since the model does not describe the suspension of particles from the vessel base it is only applicable to situations above N_{js}.

The model of T_{61} had about 70,000 cells and T_{183}, 90,000 cells. No change in the results was found when a greater density of cells was used which showed that the condition of grid independence applied. The computational grid is shown in Figure 7.53.

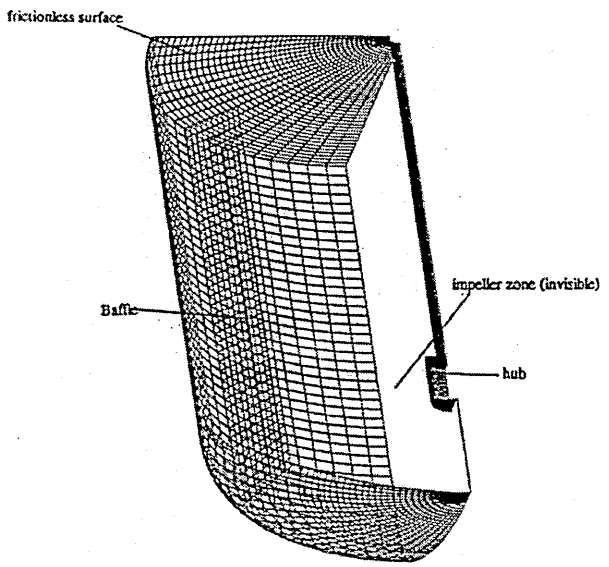

Figure 7.53. Computational domain and grid.

The solution algorithm is described below:

1. The flow was simulated with a very low particle concentration (0.1% vol/vol) to build up the initial flow field.
2. The flow with the true solids concentration (6.3% vol/vol) was then simulated with the initial flow field that was generated in (1) for the starting values.
3. Convergence was checked for both phases.
4. If converged, go to (5) otherwise, go back to (2) with the new flow field.
5. If too many solids remain on the base then redistribute them over the volume and repeat (2).

The test cases for the validated CFD models are:

Tank diameter:	T=0.61m and 1.83m
Impeller type:	4PBT45
Impeller diameter:	T/3 for T_{61} and T/2 for T_{183}
Impeller speed:	315rpm in T_{61}
	130 rpm in T_{183}
Particle size:	590 μm (Experimental)
	655 μm (CFD model)

The particle size was estimated for the CFD model since it had not been measured. The value of 590 μm was found after the simulation had been performed. The small difference in particle sizes will not cause a large error when compared to the errors associated with the CFD model itself.

The value of Pr_T was set to a range of values (0.2 – 10) and it was found that a value of 0.9 produced the best comparison between the experimental data and the results obtained numerically and it was this value that was used in the simulations. Comparisons between the CFD predictions and the experimental results are shown in Figure 7.54 to Figure 7.56.

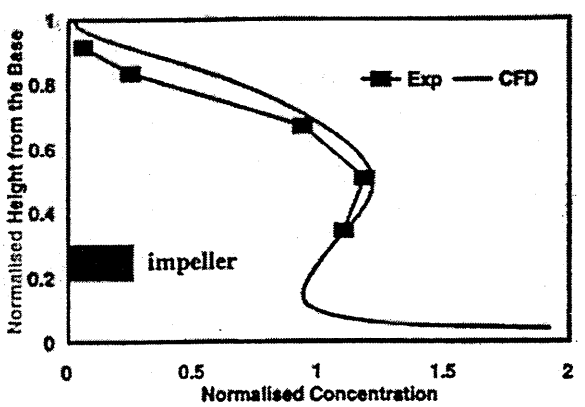

Figure 7.54. Axial solids concentration profile with 4PBT45 (D=T/3, C=T/4) in T_{61} (r/R=0.5).

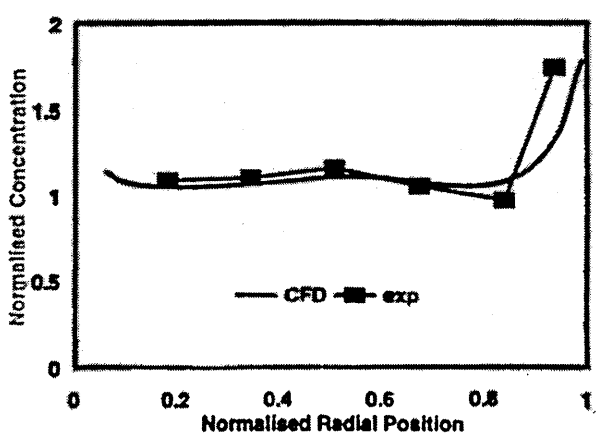

Figure 7.55. Radial solids concentration profile with 4PBT45 (D=T/3, C=T/4) in T_{61} (h/H=0.27).

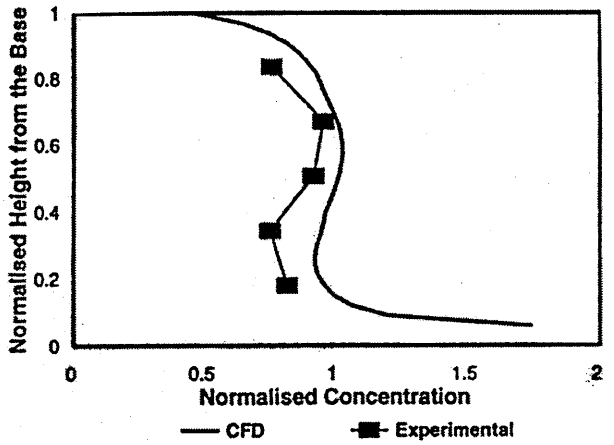

Figure 7.56. Axial solids concentration profile with 4PBT45 (D=T/3, C=T/4) in T_{183} (r/R=0.5).

The comparisons were found to be very good. Both radial and axial solids concentration profiles were modelled well. The position of the maximum in the axial solids concentration profile as well as its absolute values was well represented. The height to which solids were suspended was also modelled well. The worst comparisons were found in T_{183} where the model over-predicted the solids concentration.

At the vessel base, the model was found to predict a very high concentration. This was a consequence of the absence of a re-suspension mechanism in the model. Due to this, solids near the base have a tendency to settle out due to the low mean and turbulent liquid velocities in this region. This effect was alleviated by numerically re-suspending the settled particles throughout the vessel volume.

7.11 Conclusions

It has been found that in the lower half of the vessel, as the impeller speed increased up to N_{js}, the normalised solids concentration, C/C_0, increased because more solids were suspended from the vessel base. Around N_{js}, C/C_0 reached a maximum before decreasing as solids were suspended higher into the vessel. Once the solids were suspended all the way to the surface of the vessel, the value of C/C_0 remained effectively constant but not necessarily at 1.00 as the impeller speed was increased further. It may be possible to estimate the position of N_{js} by using a conductivity probe near to the vessel base since the packed bed of unsuspended solids was characterised by a much lower conductivity than the situation where all of the solids were suspended.

A poor mass balance was originally calculated using only 5 measurement points. As more points were included, it was found that the mass balance improved significantly. More measurement points would have resulted in a better mass balance. This effect was due to the strong gradients in concentration that existed within the vessel.

When comparisons were made between two vessels of diameters 0.61 m and 1.83 m, it was found that C/C_0 scaled better with constant power per unit volume than impeller tip speed for a variety of impeller types and diameters. Constant power per unit volume was the better scale-up rule when a standard vessel was stirred using a single 45PBT4(D=T/2, C=T/4), a 45PBT4(D=T/3, C=T/4) or an A310(D=T/3, C=T/4).

A hydrofoil impeller, A310 (D=T/3, C=T/4) and a mixed flow impeller, 4PBT-45 (D=T/3, C=T/4) were found to produce similar concentration profiles when operated at the same power per unit volume. Since an A310 operates at a lower torque than a PBT of the same diameter when P/V is held constant, industrial use of this impeller would be advantageous since a smaller gearbox could be used. This can result in a lower capital cost for the mixer.

Constant P/V was found to be better than V_{tip} when the concentration profiles generated by two PBTs of different diameter were compared. However, a 4PBT-45 (D=T/2, C=T/4) produced qualitatively different concentration profiles in T_{61} when compared with a 4PBT-45 (D=T/3, C=T/4) due to the differences in the flow patterns generated by these impellers. The 4PBT-45 (D=T/2, C=T/4) was found to produce a large main circulation loop. This was found to suspend solids high in the vessel. At the centre of this loop C/C_0 was found to be lower than the surrounding region. When the 4PBT-45 (D=T/2, C=T/4) was operated in T_{61} it was observed that large packets of suspension were transported high into the clear layer by large intermittent turbulent bursts. These packets resulted in a region of high concentration in the measurement plane. Both PBTs generated a region of high concentration underneath them due to the up-flow of slurry that occurs due to the mixed-flow characteristics of this type of impeller.

Comparisons were made between the solids distribution produced by different particle diameters. It was found that larger particles required higher impeller speeds for a given C/C_0 than the smaller particles due to their higher settling velocity. The data obtained at different particle sizes and vessel scales was correlated using the form shown in Equation 7.5:

$$N_{mod} = N(C)d^{a}\left(VPo^{-1}D^{-5}\right)^{b} \tag{7.5}$$

Power per unit volume was found to correlate well for the effect of scale when the data from all of the 4PBT-45 (D=T/3, C=T/4) results were correlated. The exponent on the effect of particle size was found to change from -0.25 to -0.40, when power per unit volume was used as the scale-up rule, at successively higher points in the vessel. This was due to particle settling through the quiescent liquid higher up in the vessel.

The best correlations for the variation of solids concentration are based on Equations 7.12 to 7.16.

$$N(C)d^{-0.38}\left(VPo^{-1}D^{-5}\right)^{-0.36} \tag{7.12}$$

$$N(C)d^{-0.36}\left(VPo^{-1}D^{-5}\right)^{-0.37} \tag{7.13}$$

$$N(C)d^{-0.32}\left(VPo^{-1}D^{-5}\right)^{-0.41} \tag{7.14}$$

$$N(C)d^{-0.28}\left(VPo^{-1}D^{-5}\right)^{-0.37} \quad (7.15)$$

$$N(C)d^{-0.23}\left(VPo^{-1}D^{-5}\right)^{-0.37} \quad (7.16)$$

When the data was correlated on the basis of Equation 7.17 for each measurement point in the vessel the spread of the data was much larger than when Equations 7.12 to 7.16 were used.

$$N(C)d^{-0.32}\left(VPo^{-1}D^{-5}\right)^{-0.39} \quad (7.17)$$

Qualitative comparisons of the particle concentration across a whole plane situated midway between the baffles has shown that the effect of particle size is best compensated for by assuming that $N(C) \propto d^{0.4}$ rather than $N(C) \propto d^{0.25}$. This is because the eye reacts more to strong gradients than absolute values. It was found, therefore, that the effect of particle size that resulted from the measurements higher up in the vessel was dominant.

The solids in a stirred vessel were modelled as an array of vibrating spheres. This model predicted the variation of C/C_0 with N very well. The empirical constant that allowed for any deviation from the ideal close-packed structure, α, was found to be equal to 0.84. The empirical constant that allowed for local variations in the energy dissipation rate, β, was found to be equal to 91 which was much higher than was expected ($\beta \approx 1$). The deviation from ideality was probably due to the implementation of the vessel's characteristic shear rate.

The stirred vessel was modelled using a 1-d sedimentation-dispersion model. This was very unsuccessful probably due to the solids dispersion coefficient varying significantly throughout the vessel volume.

A design procedure for the calculation of solids concentration profiles has been outlined. This allows an engineer to specify a minimum concentration at a given point; specify the maximum concentration at a given point; or calculate the likely range of concentration that could occur at a particular impeller speed.

Experimental data has been used to optimise the empirical parameters in CFD models of two mechanically stirred vessel. Comparisons between the experimental data and the CFD predictions were found to be generally very good. CFD predicted well the position of the maximum in the axial solids concentration profiles and the height to which solids were suspended. However, an over-prediction in the solids concentration profile in T_{183} was found from the CFD model.

7.12 General Concluding Remarks

Most workers who have examined the solids concentration profiles in stirred vessels have operated at scales smaller than about 0.6m. Of the large-scale work available, only that of Mak (1992) covered industrially relevant scales with a range of concentrations and that work was specific to one particle size and impeller type. This has meant that industrial design has been based on laboratory data that is much smaller than the final plant. It is desirable that scale-up is performed within the valid range of the correlations. Unfortunately, it is inevitable that scale-up will occasionally occur outside of the experimental range of the correlations due to the wide range of processes and products that exist. To minimise the degree of extrapolation from the limits of the correlations, it is best that the pilot scale work be performed at scales as close as possible to those found within the process industry which are of the order of metres. The correlations presented in this thesis satisfy this need for data from industrially relevant scales.

The data presented in this work covers a range of impeller types and particle sizes all obtained at a scale that is industrially relevant. Consequently, it is possible to extrapolate the results from this work to industrial practice with greater confidence than before. As with all correlations, the design correlations presented here should still be used with caution, especially outside of their experimental range, because delays in the start-up of a chemical plant can be very expensive due to the loss of production capacity or time required for trouble shooting. In the pharmaceutical industry the lost profit can easily enter into the millions of pounds since a finite amount of time is available to market the pharmaceutical product exclusively due to the period of the patent. The greater confidence in the scale-up data presented here could result in increases in

profitability within the process industry.

As new approaches to modelling stirred vessels become possible with increasing computing power the results from these models will inevitably become more reliable. Designers will then be able to rely on CFD to optimise the design for industrial equipment and also to identify problems with existing equipment. Optimal designs mean that the correct product is produced from the outset and expensive periods of down-time are reduced to fix problems that were not realised from the outset. To enable such models to be tested a wide range of experimental data is needed to help validate them. Models need to be tested and the results scrutinised before they are implemented for design otherwise inappropriate designs may result.

A good CFD model will inevitably result in some approximations being used to supplement the physics that form the model. It is the understanding of how these approximations influence the results of the model that is important. The model's results will have limitations on their range of validity. For instance, it may be found that the model predicts the energy dissipation rate very well in the bulk of the vessel but underestimates it in the impeller region. Energy dissipation rate is very important for reactions that are micromixing sensitive and it is the engineer's responsibility to recognise this fact and act accordingly by adjusting the geometry or flow conditions to suit. The actual modifications will depend on a mixture of experience and process specifications. It is this aspect of the design process that will always be most important: assimilation of the information available and implementing it in a sensible way using a knowledge of the information's limitations. As CFD models improve and their range of validity increases the design engineer will be able to rely more confidently upon the results that it provides which will result in increased profitability for the process industry.

CHAPTER 8.RECOMMENDATIONS FOR FURTHER WORK

The effect of particle size distributions on the spatial variation of concentration still has many outstanding issues. There remains a question about how particles of different sizes would interact. They may have a tendency to segregate as they do in air-solid systems through shear-induced migration. Mono-modal, bi-modal and tri-modal distributions of particles should be examined so as to give a broad base for comparison of the data. Comparative studies on the spatial distribution, diffusivities and mean particle and liquid velocities could be obtained through the application of positron emission particle tracking.

Many solid-liquid processing facilities are continuous processes. The effect of moving from batch to continuous would make an interesting study since it is known that the technique of sampling to measure solids concentration is strongly dependant on the ability to sample iso-kinetically and this has been shown by Nasr-el-din *et al.* (1996) to be a strong function of sampling velocity and the geometry of the sampling tube. Measuring the characteristics of continuous flow systems would encounter these difficulties. Design strategies for vessel internals would be developed from this work which could be used in large scale vessels.

This work has shown that the interface between the suspension and clear liquid layer above it is clear-cut. The interface has been observed to fluctuate significantly which could have serious consequences in a vessel with a slurry overflow because the outlet of the vessel may undergo periods of removing solid-free liquid followed by slurry with a higher than average concentration. This is likely to have an impact downstream such as in continuous centrifuges where unsteady feed rates can cause problems with product quality due to segregation of the solids and inefficient de-watering. The extent to which this problem occurs would be an important study. The fluctuations of this interface could be measured and modelled using a Large Eddy Simulation (LES) or Direct Numerical Simulation (DNS) in CFD. LES models dynamically the eddies in the bulk flow down to the grid scale. Below the grid scale a sub-grid model is implemented so that the smallest eddies are also represented within the model. With DNS the grid is

made sufficiently fine such that even the smallest eddies are resolved. No sub-grid model is necessary when DNS is used although this means that the number of cells must be very large. LES would be the preferred modelling method and can be considered to be a truncated DNS model. Since the large flow instabilities are modelled directly, rather than by Reynolds averaging and the implementation of a turbulence model, the fluctuations at the interface could be modelled numerically. Unfortunately, since the eddies down to the grid size are modelled dynamically, this type of model is immensely computationally intensive but not as intensive as with a DNS model. DNS models (Bartels *et al.*, 2000) and LES models (Bakker *et al.*, 2000) of stirred tanks have been performed already but these have been limited to single phase systems. Cate *et al.* (2000) modelled a crystalliser using LES but they also treated it as a single phase problem, multiphase interactions were not included. Given the rate of increase in computing power LES simulations of multiphase systems will become practicable and modelling the slurry-clear layer interface will be possible.

REFERENCES

Aeschbach, S. and Bourne, J. R. (1972). 'The attainment of homogeneous suspension in a continuous stirred tank'. The Chemical Engineering Journal, vol. 4, 234-242.

Bagnold, R.A. (1954). 'Experiments on a gravity-free dispersion of large solid spheres in a Newtonian fluid under shear'. Proceedings of the Royal Society of London: Series A. Mathematical and Physical Sciences, vol. 225, 49-63.

Bakker, A., Oshinowo, L.M., Marshall, E.M. (2000). The use of large eddy simulation to study stirred vessel hydrodynamics. In: *10th European Conference on Mixing*, 2-5 July 2000, Delft, The Netherlands, 247-254.

Barresi, A. and Baldi, G. (1987a). 'Solid dispersion in an agitated vessel'. Chemical Engineering Science, vol. 42, no. 12, 2949-2956.

Barresi, A. and Baldi, G. (1987b). 'Solid dispersion in an agitated vessel: effect of particle shape and density'. Chemical Engineering Science, vol. 42, no. 12, 2969-2972.

Bartels, C., Breuer, M. and Durst, F. (2000). Comparison between Direct Numerical Simulation and k-ε prediction of the flow in a vessel stirred by a Rushton turbine. In: *10th European Conference on Mixing*, 2-5 July 2000, Delft, The Netherlands, 239-246.

Bittorf, K. and Kresta, S. (1999). The prediction of solids cloud height within a stirred tank. Presented as a poster in: *17th Biennial North American Mixing Conference*, 15th-20th August 1999, Alberta, Canada, session 7.18.

Bittorf, K. (2000). Private communication.

Bohnet, M. and Niesmak, G. (1980). 'Distribution of solids in stirred suspensions'. German Chemical Engineering, vol. 3, 57-65.

Bujalski, W., Takenaka, K., Paolini, S., Jahoda, M., Paglianti, A., Takahashi, K., Nienow, A. W., and Etchells, A.W. (1999). 'Suspension and liquid homogenisation in high solids concentration stirred chemical reactors'. Transactions of the Institute of Chemical Engineers, vol. 77, Part A, 241-247.

Buurman, C., Resoort, G. and Plaschkes, A. (1985). Scaling-up rules for solids suspension in stirred vessels. In: *5th European Conference on Mixing*, 10th-12th June 1985, Würzburg, Germany, 15-26.

Buurman, C., Resoort, G. and Plaschkes, A. (1986). 'Scaling-up rules for solids suspension in stirred vessels'. Chemical Engineering Science, vol. 41, no. 11, 2865-2871.

ten Cate, A., Bermingham, S.K., Derksen, J.J. and Kramer, H.M.J. (2000). Compartmental modeling of an 11001 DTB crystallizer based on large eddy flow simulation. In: *10th European Conference on Mixing*, 2-5 July 2000, Delft, The Netherlands, 255-264.

Chatfield, C. (1997). *Statistics for technology*. Chapman & Hall, p. 126.

Corpstein, R. R., Fasano, J. B. and Myers, K. J. (1994). 'The high efficiency road to liquid - solid agitation'. Chemical Engineering, vol. 101, No. 10, 138-144.

Einenkel, Wolf-Dieter. (1980). 'Influence of physical properties and equipment design on the homogeneity of suspensions in agitated vessels'. German Chemical Engineering, vol. 3, 118-124.

Fajner, D., Magelli, F., Nocentini, M. and Pasquali, G. (1985). 'Solids concentration profiles in a mechanically stirred and staged column slurry reactor'. Chemical Engineering Research and Design, vol. 63, 235- 240.

Harnby, N., Edwards, M.F. and Nienow, A.W. (1997). *Mixing in the Process Industries.* Butterworth Heinemann, p. 400.

Heywood, N. I., Rehman, S. and Whittemore, R. G. (1991). A comparison of the efficiency of five agitator designs for solids suspension duties at high solids concentrations. In: *7th European Mixing Congress*, 18-20 September 1991, Bruges, Belgium, 469-482.

Hetsroni, G. (1989). 'Particles-turbulence interaction'. International Journal of Multiphase Flow, vol. 15, no. 5, 735-746.

Hicks, M.T., Myers, K.J., Bakker, A. (1997). 'Cloud height in solids suspension agitation'. Chemical Engineering Communications, vol. 160, 137-155.

Hixson, A. W. and Tenney, A.H. (1935). 'Quantitative evaluation of mixing as the result of agitation in liquid-solid systems'. Transactions of the American Institute of Chemical Engineers, vol. 31, 113-127.

Kolář, V. (1961). 'Suspending solid particles in liquids by means of mechanical means'. Collection of Czechoslovak Chemical Communications, vol. 26, 613-627.

Kudrna, Vladimír, Sýsová, Marie and Fořt, Ivan. (1986). 'A probability form of the diffusion equation and its use to describe the distribution of the solid phase particle concentrations in a mechanically agitated charge'. Collection of Czechoslovak Chemical Communications, vol. 51, 1910-1924.

Levins, D. M. and Glastonbury, J. R. (1972). 'Particle-liquid hydrodynamics and mass transfer in a stirred vessel'. Transactions of the Institute of Chemical Engineers, vol. 50, 32-41.

Liu, S. and Masliyah, J.H. (1996). *Suspensions: Fundamentals and applications in the petroleum industry*. American Chemical Society, p. 126.

Magelli, F., Fajner, D., Nocentini, M., and Pasquali, G. (1990). 'Solid distribution in vessels stirred with multiple impellers'. Chemical Engineering Science, vol. 45, 615-625.

Magelli, F., Fajner, D., Nocentini, M., Pasquali, G., Marisko, V. and Ditl, P. (1991). 'Solids concentration distribution in slurry reactors stirred with multiple axial impellers'. Chemical Engineering Processing, vol. 29, 27-32.

Mak, A.T.C. (1988). Research review; The measurement of power, solids suspension and distribution in a 0.61 m diameter vessel. BHR Group, Cranfield FMP report 032.

Mak, A. T. C. (1992), *Solid-liquid mixing in mechanically agitated vessels*. Ph.D. Thesis, University of London.

Mak, A.T.C. and Ruszkowski, S. (1992), Scale-up of just suspension speed and solids distribution for pitched blade turbines in dish base vessels. BHR Group, Cranfield FMP report 1069.

McCabe, W.L., Smith, J.C. and Harriott, P. (1985). *Unit operations of chemical engineering*. McGraw-Hill, p. 143.

McDonough, R.J. (1992). *Mixing for the process industries*. Van Nostrand Reinhold, p.141.

Musgrove, M.E. (1998). Further LDA Measurements at 0.292m and 1.82m scales. BHR Group, Cranfield internal confidential report CR 6822.

Musgrove, M.E. and Ruszkowski, S. (1993). The mean flow in the discharge of some novel hydrofoil impellers and its effect on mixing processes, BHR Group, Cranfield FMP report 1071.

Musil, L. and Vlk, J. (1978). 'Suspending solid particles in an agitated conical-bottom tank'. Chemical Engineering Science, vol. 33, 1123-1131.

Nasr-el-din, H. (1987). 'Comments on scaling-up rules for solids suspension in stirred vessels'. Chemical Engineering Science, vol. 42, 2986.

Nasr-el-din, H. A., Mac Taggart, R. S. and Masliyah, J. H. (1996). 'Local solids concentration measurement in a slurry mixing tank'. Chemical Engineering Science, vol. 51, no. 8, 1209-1220.

Nienow, A. W. (1968). 'Suspension of solid particles in turbine agitated baffled vessels'. Chemical Engineering Science, vol. 23, 1453-1459.

Oldshue, J. Y. (1969). 'Suspending solids and dispersing gases in mixing vessel'. Industrial and Engineering Chemistry, vol. 61, no. 9, 79-87.

Pavlushenko, I. S., Kostin, N. M. and Matveev, S. F. (1957) 'Stirrer speeds in the stirring of suspensions'. Journal of Applied Chemistry of the USSR, vol. 30, 1235-1243.

Peňáz, F., Rod, V. and Řeháková, M. (1978). 'Concentration distribution of suspension in a mixed vessel'. Collection of Czechoslovak Chemical Communications, vol. 43, 848-861.

Pinelli, D., Nocentini, M., and Magelli, F., 1996, Modelling of the solid distribution in slurry reactors stirred with multiple impellers: influence of suspension characteristics. In: *12th International Congress of Chemical and Process Engineering*, 25th-30th August 1996, Praha, Czech Republic, paper D1.2.

Raghavendra Rao, S. and Mukherji, B. K., (1953). 'Studies on solid-liquid agitation'. Transactions of the Indian Institute of Chemical Engineers, vol. 7, 63-77.

Rieger, F., Ditl, P. and Havelková, O., 1988, Suspension of solid particles – concentration profiles and particle layer on the vessel bottom. In: *6th European Conference on Mixing*, 24th-26th May 1988, Pavia, Italy, 251-258.

Schempp, A. and Bohnet, M. (1995). 'Untersuchungen zur verteilung der dispersen phase in fest/flüssig-rührreaktoren'. Chemie-Ingenieur-Technik, vol. 67, no. 5, 608-612.

Schwartzberg, H. G. and Treybal, R. E. (1968). 'Fluid and particle motion in turbulent stirred tanks'. Industrial and Engineering Chemistry Fundamentals, vol. 7, no. 1, 1-11.

Sessiecq, P., Mier, P., Gruy, F. and Cournil, M. (1999). 'Solid particles concentration profiles in an agitated vessel'. Transactions of the Institute of Chemical Engineers, vol. 77, 741-746.

Shamlou, P. A. and Koutsakos, E. (1989). 'Solids suspension and distribution in liquids under turbulent actions'. Chemical Engineering Science, vol. 44, 529-542.

Shamlou, P. A. (1993). *Processing of Solid-Liquid Suspensions*. Oxford Butterworth Heinemann, p. 311.

Sýsová, M., 1984, Flow of Solid-Liquid Suspension in Agitated System. In: *8th International Congress of Chemical Engineering, Chemical Equipment Design and Automation*, 3rd-8th September 1984, Praha, Czechoslovakia, paper V3.49.

Taylor, D.J. (1999). The effect of impeller type, size and scale on the distribution of solids in stirred tanks, BHR Group, Cranfield FMP report 1114.

Tojo, K. and Miyanami, K. (1982). 'Solids suspension in mixing tanks'. Industrial and Engineering Chemistry Fundamentals, vol. 21, no. 3, 214-220.

Weisman, J. and Efferding, L. E. (1960). 'Suspension of Slurries by Mechanical Mixers'. A.I.Ch.E. Journal. (American Institute of Chemical Engineering.), vol. 6, 419-426.

White, A. M., Sumerford, S. D., Bryant, E. O. and Lukens, B. E. (1932). 'Studies in Agitation. Suspension of sand in water'. Industrial and Engineering Chemistry, vol. 24, 1160-1162.

White, A. M. and Sumerford, S. D. (1933). 'Studies in Agitation. II. Sand Concentration as Function of Sand Size and Agitator Speed'. Industrial and Engineering Chemistry, vol. 25, 1025-1027.

Yamazaki, H., Tojo, K. and Miyanami, K. (1991). 'Effect of power consumption on solids concentration profiles in a slurry mixing tank'. Powder Technology, vol. 64, 199-206.

Yang, X. and Taylor, D.J., 1998, CFD Simulation for Solid Liquid Mixing in Stirred Tanks. In: *World Fluid Dynamics Days 1998. 4th World Conference and Exhibition in Applied Fluid Dynamics*, 7th-11th June 1998, Freiburg i. Br., Germany, paper 9.

Yung, B. (1995). FMP report 1091, "The effect of particle size and solid density on solid suspension and solid distribution". BHR Group, Cranfield.

Zwietering, T.N. (1958) 'Suspending of solid particles in liquid by agitators'. Chemical Engineering Science, vol. 8, 244-253.

APPENDICES

A1. Summary of findings in the literature

A1.1. Effect of impeller design, impeller diameter and scale

Table A1.1. Experimental conditions in the literature examining the effect of impeller design, D/T and T.

Paper	T(m)	D/T	C/T	H/T	n	Impeller type	Materials	ρ_S(kgm^{-3})	μ (mPas)	C_0 (%vol/vol)	D(μm)
Buurman *et al.* (1985)	0.24-4.26	0.40	0.37	1	4	45PBT4	Sand Coal Polystyrene Glass	Not stated	1-?	3-40	157-2200
Magelli *et al.* (1991)	0.236	0.41-0.53	0.18-3.5	2.31-44	4	2-blade turbine 4-blade turbine A310	Glass	2450	0.9-19	0.05-0.14	140-980
Bohnet and Niesmak (1980)	0.290	0.34	0.17	1.05	4	Propeller	Styropor Glass Bronze	1050-8850	1	0.2-2.0	100-1150
Yung (1995)	0.61	0.33-0.50	0.25	1	4	45PBT4	Polystyrene Polyplus Sand Alumina Zirconia	1050-5550	1	2.3-14.4	180-900
Shamlou and Koutsakos (1989)	0.225	0.29-0.44	0.50-0.67	3	4	45PBT6	Glass	2900	1	0.35-2.15	175-1100
Rieger *et al.* (1988)	0.3	0.33	0.17	1	4	45PBT6	Glass	?	1	2.5-10	185-1360
Heywood *et al.* (1991)	0.900	0.33-0.67	0.17-0.72	1	4	45PBT4 Ekato Intermig Marine propeller Denver MIL Propeller Scaba SHP	Sand	2650	1	25.6-39.0	100-380
Barresi and Baldi (1987)	0.390	0.33	0.40	1.19	4	A310 45PBT-4 45PBT-6	Glass beads	2600-2670	1	0.19-1.9	139-459

Paper	T(m)	D/T	C/T	H/T	n	Impeller type	Materials	ρ_S(kgm^{-3})	μ(mPas)	C_0(%vol/vol)	D(μm)
Magelli *et al.* (1990)	0.13-0.24	0.33	0.5, 1.5, 2.5, 3.5	4	4	4 x RDT6	Glass beads PMMA Bronze	1020-8410	0.9-21	0.041-0.61	140-980
Mak (1988)	0.61	0.33-0.59	0.17-0.25	1	4/2	A310 PBT RCI	Sand	2600-2650	1	2.0-20	180-605
Mak and Ruszkowski (1992)	0.31-2.7	0.5	0.25	1	4	PBT	Sand	2630	1	6.3-14	180
Mak (1992)	0.61-2.67	0.3-0.6	0.25	1	4	45PBT-4	Sand	2630	1	2.0-14	180

A1.2. Effect of liquid and particle properties

Table A1.2. Experimental conditions in the literature examining the effect liquid and particle properties.

Paper	T(m)	D/T	C/T	H/T	n	Impeller type	Materials	ρ_s(kgm^{-3})	μ(mPas)	C_0(%vol/vol)	D(μm)
Buurman *et al.* (1985)	0.24-4.26	0.40	0.37	1	4	45PBT4	Sand Coal Polystyrene Glass	Not stated	0.5-3.0	3-40	157-2200
Barresi and Baldi (1987b)	0.390	0.33	0.40	1.19	4	A310, 45PBT4	Crushed silica Crushed barytes Glass beads	2600-4280	1	0.12-0.66	100-500
Magelli *et al.* (1991)	0.236	0.41-0.53	0.18-3.5	2.31-4	4	2-blade turbine 4-blade turbine A310	Glass	2450	0.9-19	0.05-0.14	140-980
Bohnet and Niesmak. (1980)	0.290	0.34	0.17	1.05	4	Propeller	Styropor Glass Bronze	1050-8850	1	0.2-2.0	100-1150
Yung (1995)	0.61	0.33-0.50	0.25	1	4	45PBT4	Polystyrene Polyplus Sand Alumina Zirconia	1050-5550	1	2.3-14.4	180-900
Shamlou and Koutsakos (1989)	0.225	0.29-0.44	0.50-0.67	3	4	45PBT6	Glass	2900	1	0.35-2.15	175-1100
Rieger *et al.* (1988)	0.3	0.33	0.17	1	4	45PBT6	Glass	?	1	2.5-10	185-1360
Heywood *et al.* (1991)	0.900	0.33-0.67	0.17-0.72	1	4	45PBT4 Ekato Intermig Marine propeller Denver MIL Propeller Scaba SHP	Sand	2650	1	25.6-39.0	100-380
Einenkel (1980)	0.365-0.790	0.315	0.30	1	4	Propeller	Glass	2870	1-96	5-25	90-1500

Paper	T(m)	D/T	C/T	H/T	n	Impeller type	Materials	ρ_S(kgm^{-3})	μ(mPas)	C_0(%vol/vol)	d(μm)
White and Sumerford (1933)	1.32	0.48	0.10	0.46	4	Simple paddle stirrer	Sand	2600?	1	0.09-0.42	137-416
White and Sumerford (1932)	1.32	0.48	0.10	0.46	4	Simple paddle stirrer	Sand	2600?	1	0.41-1.4	200
Peňáz *et al.* (1978)	0.447	0.20-0.33	C/D=0.25	1	4	45PBT-3	Glass ballotini	2600?	1	3	? (Settling velocity = 0.0383 ms^{-1}
Nasr-el-din *et al.* (1996)	0.292	0.33	0.3	1	4	RDT	Sand	2650	1	10-30	82-410
Schempp and Bohnet (1995)	0.3	0.33-0.5	?	3	4	Propeller, RDT	Sand	2600?	0.38-70	0-15	200-900
Buurman *et al.* (1986)	0.24-4.26	0.4	0.37	1	4	45PBT-4	Sand Coal Polystyrene Glass	2590 1500? 1050? 2600?	0.5-3.0	3-40	157-2200
Yamazaki *et al.* (1991)	0.3	0.23-0.33	0.1-0.5	1	4	6-blade disc turbine 4-blade marine impeller	Glass Sand	2370-2620	1	5-20	87-230
Pavlushenko *et al.* (1957)	0.3	0.25-0.5	0.1	1	0	45PBT-3	Sand Iron ore	2630-4750	1.12-120.6	1.9-16	35-825

Paper	T(m)	D/T	C/T	H/T	n	Impeller type	Materials	ρ_S(kgm^{-3})	μ(mPas)	C_0(%vol/vol)	D(μm)
Kolář (1961)	0.165-0.345	0.159-0.319	0.33-0.11	1	4	45PBT-4 Propeller	MMA Glass Sand	1500 2900 2648	1-7	0.12-10	131-1641
Barresi and Baldi (1987a)	0.390	0.33	0.40	1.19	4	A310 45PBT-4 45PBT-6	Glass beads	2600-2670	1	0.19-1.9	139-459
Weisman and Efferding (1960)	0.14-0.29	0.18-0.35	0.09-0.17	1-2	4	6-bladed paddle	Glass beads Thorium Oxide	2250 4850	1-25	0.0047-0.039	45-140
Sýsová *et al.* (1984)	?	0.4	?	?	4	45PBT-6?	?	?	1-4	4-8	450-925
Fajner *et al.* (1985)	0.132	0.33	0.5, 1.5, 2.5, 3.5	4	7 (3 ring 4 radial)	4 x RDT6	Glass beads	2450	0.9-21	0.041-0.61	137-327
Kudrna *et al.* (1986)	0.29	0.33-0.40	0.29	1	4	45PBT-6	Glass ballotini	2640	4	4-8	450-925
Nienow (1968)	0.14	0.26-0.52	0.14-0.33	1	4	RDT6	Glass ballotini Potassium sulphate Sodium chloride Ammonium alum Ammonium chloride Potassium chloride	1527-2662	1	0.038-4.3	324-2230
Magelli *et al.* (1990)	0.13-0.24	0.33	0.5, 1.5, 2.5, 3.5	4	4	4 x RDT6	Glass beads PMMA Bronze Polystyrene	1020-8410	0.9-21	0.041-0.61	140-980
Mak (1992)	0.61-2.67	0.3-0.6	0.25	1	4	45PBT-4	Sand	2630	1	2.0-14	180

Paper	T(m)	D/T	C/T	H/T	n	Impeller type	Materials	ρ_S(kgm^{-3})	μ(mPas)	C_0(%vol/vol)	d(μm)
Bujalski *et al.* (1999)	0.290-0.720	0.42-0.52	0.24	1-1.3	4	A310 Intermig A315	Glass ballotini Sand Ion exchange resin Zircon sand	2500 2500 1350 4450	1	0-13.8	115-678
Raghavendra Rao, and Mukherji (1953)	0.15	0.5	0.40	0.88	0	Twisted sheet	Marble Barytes Pyrolusite	2620 4300 5500	1	1.2-2.5	81
Hixson and Tenney (1935)	0.457	0.22	0.15	1	0	4PBT45	Sand	2630?	0.89-43.9	2.0	800
Tojo and Miyanami (1982)	0.10	0.42	0.16	1	4	4PBT45 Vibrating disc	Sand PVC Glass Carborundum	2690 1500 2500 3300	1	1	74-250
Hicks *et al.* (1997)	0.289	0.15-0.53	0.10-0.40	1-1.75	4?	4PBT45 HE-3	Acrylic plastic Ion exchange resin Sand	1179 1053 2590	1	0-49	600-2950
Sessiecq *et al.* (1999)	0.15	0.33	0.38	1	4	4PBT45	Alumina powder Glass beads	3980 2680	1	0.070-0.56	44-234

A2. An ideal close packed structure

Variation of inter-particle distances for a close-packed structure.

Consider the well-defined slurry structure in Figure A2.1.

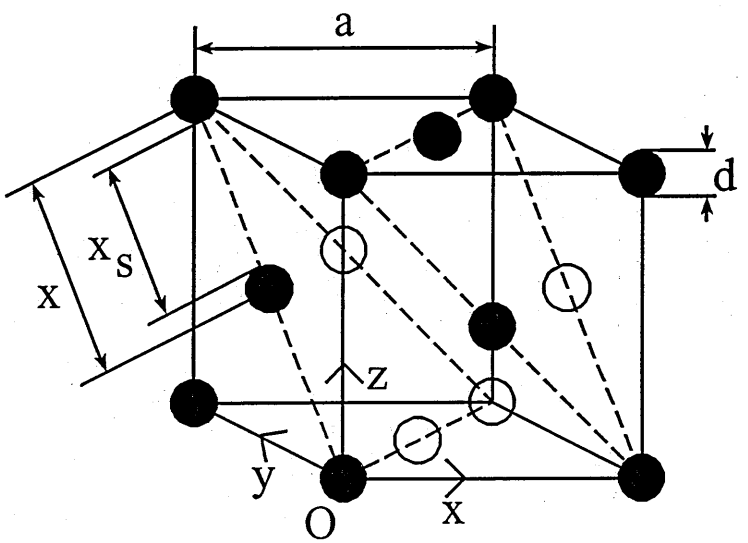

Figure A2.1. A close-packed structure of spheres.

In one cell there are 6 x 1/2 + 8 x 1/8 =4 particles

$$\text{Volume of particles} = V_S = 4 \text{ x } \frac{\pi d^3}{6} = \frac{2\pi d^3}{3} \tag{A2.1}$$

Volume of one cell $=V_T= a^3$

$$C = \frac{V_S}{V_T} = \frac{2\pi d^3}{3a^3} \tag{A2.2}$$

$$a = \alpha\left(\frac{2\pi d^3}{3C}\right)^{1/3} \tag{A2.3}$$

Here, the parameter α has been included to account for the likely differences between the slurry structure and the close-packed arrangement. Distance between particle centres, x, is given by Eq. A2.4.

$$x = \frac{\alpha}{\sqrt{2}}\left(\frac{2\pi d^3}{3C}\right)^{1/3} \tag{A2.4}$$

Distance between particle surfaces, x_S, is given by Eq. A2.5.

$$x_S = \left(\frac{\alpha}{\sqrt{2}} \left(\frac{2\pi}{3C} \right)^{1/3} - 1 \right) d \tag{A2.5}$$

The dimensionless distance L is given by Equation A2.6.

$$L = \frac{x_S}{d} \tag{A2.6}$$

Rearranging Equation A2.6 gives Equation A2.7:

$$L = \frac{\alpha}{\sqrt{2}} \left(\frac{2\pi}{3C} \right)^{1/3} - 1 \tag{A2.7}$$

One close-packed plane has been shown in Figure A2.2, the vector coordinates are respect to the bottom left partice in Figure A2.1.

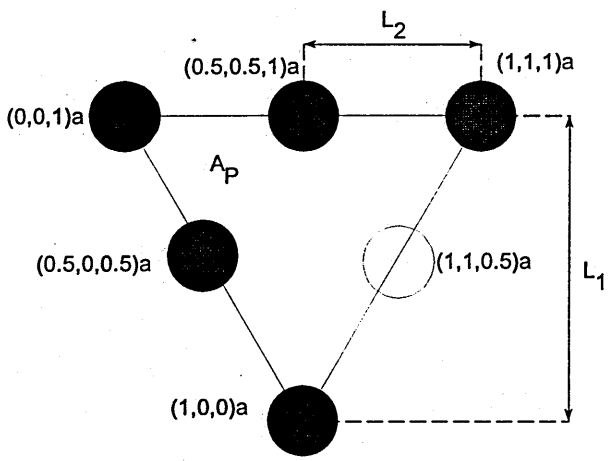

Figure A2.2. Schematic of one close-packed plane.

The distance between point (1,0,0)a and (0.5,0.5,1)a, L_1 is given by Equation A2.8:

$$L_1 = \left[(1-0.5)^2 + (0-0.5)^2 + (0-1)^2 \right]^{0.5} a = \sqrt{\frac{3}{2}} a \tag{A2.8}$$

The distance between (0.5,0.5,1)a and (1,1,1)a, L_2, is given by Equation A2.9:

$$L_2 = \left[(0.5-1)^2 + (0.5-1)^2 + (1-1)^2 \right]^{0.5} a = \sqrt{\frac{1}{2}} a \tag{A2.9}$$

The area of the plane is therefore given by Equation A2.10:

$$A_P = \left(\sqrt{\frac{3}{2}} \right) \left(\sqrt{\frac{1}{2}} \right) a^2 = \frac{\sqrt{3}}{2} a^2 \tag{A2.10}$$

Substituting Equation A2.3 into Equation A2.10 produced a relation between A_P and the particle concentration (Equation A2.11).

$$A_P = \frac{\sqrt{3}\alpha^2}{2}\left(\frac{2\pi d^3}{3C}\right)^{2/3} = \sqrt{3}\left(\frac{\pi^2}{18C^2}\right)^{1/3}\alpha^2 d^2 \qquad \text{(A2.11)}$$

On this plane there are 2 particles (3 x 1/2 + 3 x 1/6) the area per particle, A, is therefore shown in Equation A2.12:

$$A = \frac{\sqrt{3}}{2}\left(\frac{\pi^2}{18C^2}\right)^{1/3}\alpha^2 d^2 \qquad \text{(A2.12)}$$

A3. Calculation of settling velocity

The settling velocity of a particle can be correlated from Equation A3.1 (McCabe *et al.* (1985)).

$$u_t = \left[\frac{4gd^{1+n_{McC}} \Delta\rho}{3b\mu^{n_{McC}} \rho_L^{1-n_{McC}}} \right]^{\frac{1}{(2-n_{McC})}} \tag{A3.1}$$

The values of b and n_{McC} depend upon the flow regime that the particle is in which can be characterised by a dimensionless group, K (Equation A3.2) and are defined in Table A3.1.

$$K = d\left[\frac{g\rho_L \Delta\rho}{\mu^2} \right]^{\frac{1}{3}} \tag{A3.2}$$

Table A3.1 Values of the parameters to calculate settling velocity

Regime	Range	b	n_{McC}
Stokes	$K < 2.6$	24.6	1.0
Intermediate	$2.6 \leq K \leq 68.9$	18.5	0.6
Turbulent	$68.9 \leq K \leq 2360$	0.44	0

A4. Experimental results

Table A4.1. Results from T=0.61 m, 45°PBT4 (D=T/3), d=590 μm.

r/R	h/H	N(rpm)	V_{tip} (ms^{-1})	P/V (W/m^3)	C/C_0	95%C/C_0
0.67	0.51	360	3.83	740	1.63	0.01
0.67	0.51	380	4.05	902	1.40	0.01
0.67	0.51	390	4.15		1.28	0.01
0.67	0.51	400	4.26	1097	1.26	0.02
0.67	0.51	420	4.47	1292	1.14	0.01
0.67	0.51	445	4.74	1536	1.05	0.01
0.67	0.67	360	3.83	739	0.90	0.02
0.67	0.67	380	4.05		1.02	0.01
0.67	0.67	390	4.15	1012	1.06	0.01
0.67	0.67	400	4.26	1087	1.18	0.01
0.67	0.67	420	4.47	1275	1.16	0.01
0.67	0.67	445	4.74	1535	1.14	0.01
0.67	0.34	360	3.83	746	1.23	0.01
0.67	0.34	380	4.05		1.05	0.01
0.67	0.34	390	4.15	996	0.99	0.01
0.67	0.34	400	4.26		0.95	0.01
0.67	0.34	420	4.47	1281	0.95	0.01
0.67	0.34	445	4.74		0.89	0.01
0.67	0.18	360	3.83	742	1.35	0.01
0.67	0.18	380	4.05	896	1.19	0.01,
0.67	0.18	390	4.15	1002	1.11	0.01
0.67	0.18	400	4.26	1113	1.03	0.03
0.67	0.18	420	4.47	1270	1.03	0.01
0.67	0.18	445	4.74	1538	1.00	0.04
0.67	0.84	360	3.83	729	0.01	0.01
0.67	0.84	380	4.05		0.26	0.01
0.67	0.84	390	4.15	988	0.35	0.01
0.67	0.84	400	4.26	1106	0.59	0.01
0.67	0.84	420	4.47	1280	0.64	0.01
0.67	0.84	445	4.74	1534	0.75	0.01
0.34	0.67	360	3.83		0.27	0.01
0.34	0.67	380	4.05	886	0.69	0.01
0.34	0.67	390	4.15	1000	0.93	0.01
0.34	0.67	400	4.26	1093	0.94	0.02
0.34	0.67	420	4.47	1275	0.98	0.01
0.34	0.67	445	4.74	1541	1.03	0.01
0.34	0.34	360	3.83	740	1.37	0.01
0.34	0.34	380	4.05	887	1.28	0.00
0.34	0.34	390	4.15	1009	1.17	0.00
0.34	0.34	400	4.26	1094	1.10	0.01
0.34	0.34	420	4.47	1273	1.04	0.00
0.34	0.34	445	4.74	1508	1.03	0.01
0.34	0.51	360	3.83		1.00	0.02
0.34	0.51	380	4.05		1.14	0.01
0.34	0.51	390	4.15	1007	1.09	0.01
0.34	0.51	400	4.26	1091	1.18	0.01
0.34	0.51	420	4.47	1295	1.08	0.01
0.34	0.51	445	4.74	1542	1.03	0.01

r/R	h/H	N(rpm)	V_{tip} (ms^{-1})	P/V (W/m^3)	C/C_0	$95\%C/C_0$
0.34	0.18	360	3.83	728	1.22	0.01
0.34	0.18	380	4.05	866	1.01	0.01
0.34	0.18	390	4.15	959	0.90	0.01
0.34	0.18	400	4.26	1075	0.99	0.01
0.34	0.18	420	4.47	1248	0.94	0.00
0.34	0.18	445	4.74	1482	0.92	0.01
0.34	0.84	360	3.83	731	0.03	0.04
0.34	0.84	380	4.05	906	0.15	0.02
0.34	0.84	390	4.15	995	0.22	0.02
0.34	0.84	400	4.26	1100	0.39	0.02
0.34	0.84	420	4.47		0.53	0.02
0.34	0.84	445	4.74	1531	0.69	0.01
0.11	0.34	360	3.83		0.77	0.01
0.11	0.34	380	4.05	882	1.04	0.01
0.11	0.34	390	4.15		1.06	0.01
0.11	0.34	400	4.26	1080	1.00	0.01
0.11	0.34	420	4.47	1270	1.04	0.02
0.11	0.34	445	4.74	1539	1.03	0.02
0.11	0.51	360	3.83	741	0.61	0.02
0.11	0.51	380	4.05	865	0.65	0.02
0.11	0.51	390	4.15	991	0.97	0.01
0.11	0.51	400	4.26	1096	1.02	0.01
0.11	0.51	420	4.47	1269	1.02	0.01
0.11	0.51	445	4.74	1524	1.00	0.01
0.11	0.18	360	3.83	732	1.46	0.02
0.11	0.18	380	4.05	860	1.41	0.01
0.11	0.18	390	4.15	955	1.33	0.01
0.11	0.18	400	4.26	1046	1.35	0.01
0.11	0.18	420	4.47	1235	1.30	0.01
0.11	0.18	445	4.74	1466	1.22	0.01
0.11	0.84	360	3.83	738	0.00	0.02
0.11	0.84	380	4.05	872	0.01	0.00
0.11	0.84	390	4.15	953	0.10	0.01
0.11	0.84	400	4.26	1043	0.14	0.01
0.11	0.84	420	4.47	1258	0.45	0.01
0.11	0.84	445	4.74	1524	0.58	0.02
0.11	0.67	360	3.83	732	0.03	0.01
0.11	0.67	380	4.05	914	0.29	0.01
0.11	0.67	390	4.15	988	0.54	0.01
0.11	0.67	400	4.26	1095	0.89	0.01
0.11	0.67	420	4.47	1271	0.82	0.02
0.11	0.67	445	4.74	1548	1.03	0.01
0.97	0.51	360	3.83		1.84	0.02
0.97	0.51	380	4.05	896	1.85	0.02
0.97	0.51	390	4.15	1051	1.78	0.01
0.97	0.51	400	4.26	1104	1.87	0.01
0.97	0.51	420	4.47		1.80	0.01
0.97	0.51	445	4.74	1538	1.64	0.01
0.97	0.84	360	3.83	731	0.04	0.01
0.97	0.84	380	4.05		0.08	0.01
0.97	0.84	390	4.15	987	0.16	0.02
0.97	0.84	400	4.26	1083	0.24	0.01
0.97	0.84	420	4.47	1277	0.23	0.01

r/R	h/H	N(rpm)	V_{tip} (ms^{-1})	P/V (W/m^3)	C/C_0	95%C/C_0
0.97	0.84	445	4.74	1538	0.29	0.01
0.97	0.18	360	3.83	737	1.38	0.01
0.97	0.18	380	4.05	894	1.26	0.02
0.97	0.18	390	4.15	979	1.20	0.02
0.97	0.18	400	4.26	1074	1.11	0.00
0.97	0.18	420	4.47	1303	0.94	0.00
0.97	0.18	445	4.74	1543	1.02	0.01
0.97	0.34	360	3.83	739	1.69	0.01
0.97	0.34	380	4.05	909	1.43	0.01
0.97	0.34	390	4.15	1021	1.41	0.01
0.97	0.34	400	4.26	1089	1.28	0.01
0.97	0.34	420	4.47	1281	1.19	0.01
0.97	0.34	445	4.74	1507	1.10	0.01
0.97	0.67	360	3.83	735	0.39	0.01
0.97	0.67	380	4.05	899	0.82	0.02
0.97	0.67	390	4.15	991	0.89	0.02
0.97	0.67	400	4.26	1107	0.93	0.02
0.97	0.67	420	4.47	1295	0.96	0.02
0.97	0.67	445	4.74	1516	1.05	0.02
-0.00	0.18	360	3.83	746	1.49	0.01
-0.00	0.18	380	4.05	889	1.50	0.07
-0.00	0.18	390	4.15	966	1.40	0.01
-0.00	0.18	400	4.26	1061	1.28	0.01
-0.00	0.18	420	4.47	1256	1.21	0.01
-0.00	0.18	445	4.74	1502	1.18	0.01
-0.00	0.13	360	3.83	733	1.75	0.02
-0.00	0.13	380	4.05	870	1.66	0.01
-0.00	0.13	390	4.15	957	1.56	0.01
-0.00	0.13	400	4.26	1046	1.55	0.01
-0.00	0.13	420	4.47	1237	1.44	0.00
-0.00	0.13	445	4.74	1504	1.37	0.01
-0.00	0.08	360	3.83	731	1.86	0.01
-0.00	0.08	380	4.05	889	1.85	0.01
-0.00	0.08	390	4.15	968	1.82	0.01
-0.00	0.08	400	4.26	1076	1.61	0.01
-0.00	0.08	420	4.47	1296	1.68	0.16
-0.00	0.08	445	4.74	1548	1.60	0.01

Table A4.2. Results from T=0.61 m, 45°PBT4 (D=T/2) , d=590 μm.

r/R	h/H	N(rpm)	V_{tip} (ms^{-1})	P/V (W/m^3)	C/C_0	95%C/C_0
0.67	0.84	200	3.19	623	0.18	0.01
0.67	0.67	200	3.19	623	0.95	0.01
0.67	0.51	200	3.19	623	1.17	0.04
0.67	0.34	200	3.19	623	0.93	0.02
0.67	0.18	200	3.19	626	0.94	0.01
0.51	0.20	200	3.19	623	0.80	0.02
0.41	0.11	200	3.19	634	1.09	0.01
0.34	0.84	200	3.19	647	0.12	0.01
0.34	0.67	200	3.19	653	0.86	0.03

r/R	h/H	N(rpm)	V_{tip} (ms^{-1})	P/V (W/m^3)	C/C_o	95%C/C_o
0.34	0.51	200	3.19	653	1.10	0.01
0.34	0.34	200	3.19	667	1.09	0.00
0.28	0.11	200	3.19	634	1.31	0.02
0.26	0.20	200	3.19	623	1.12	0.07
0.10	0.84	200	3.19	638	0.11	0.03
0.10	0.67	200	3.19	646	0.81	0.01
0.10	0.51	200	3.19	637	1.11	0.01
0.10	0.34	200	3.19	644	1.05	0.05
0.08	0.20	200	3.19	623	1.49	0.02
0.02	0.11	200	3.19	631	1.75	0.01
0.67	0.84	220	3.51	830	0.36	0.01
0.67	0.67	220	3.51	850	1.07	0.02
0.67	0.51	220	3.51	850	1.19	0.02
0.67	0.34	220	3.51	850	0.80	0.02
0.67	0.18	220	3.51	854	0.91	0.01
0.51	0.20	220	3.51	850	0.72	0.03
0.41	0.11	220	3.51	855	0.89	0.01
0.34	0.84	220	3.51	874	0.52	0.02
0.34	0.67	220	3.51	887	0.89	0.04
0.34	0.51	220	3.51	894	1.07	0.00
0.34	0.34	220	3.51	886	1.04	0.01
0.28	0.11	220	3.51	855	1.29	0.05
0.26	0.20	220	3.51	850	1.12	0.04
0.10	0.84	220	3.51	861	0.48	0.02
0.10	0.67	220	3.51	909	0.89	0.01
0.10	0.51	220	3.51	874	1.06	0.01
0.10	0.34	220	3.51	881	1.05	0.01
0.08	0.20	220	3.51	850	1.51	0.02
0.02	0.11	220	3.51	855	1.78	0.01
0.67	0.84	240	3.83	1123	0.51	0.01
0.67	0.67	240	3.83	1129	1.10	0.01
0.67	0.51	240	3.83	1129	1.04	0.06
0.67	0.34	240	3.83	1129	0.79	0.01
0.67	0.18	240	3.83	1123	0.82	0.01
0.51	0.20	240	3.83	1129	0.71	0.01
0.41	0.11	240	3.83	1132	0.96	0.01
0.34	0.84	240	3.83	1159	0.70	0.02
0.34	0.67	240	3.83	1160	1.03	0.02
0.34	0.51	240	3.83	1173	1.07	0.01
0.34	0.34	240	3.83	1173	0.95	0.01
0.28	0.11	240	3.83	1132	1.26	0.01
0.26	0.20	240	3.83	1129	1.06	0.01
0.10	0.84	240	3.83	1185	0.74	0.05
0.10	0.67	240	3.83	1156	1.05	0.01
0.10	0.51	240	3.83	1136	1.06	0.02
0.10	0.34	240	3.83	1153	1.02	0.03
0.08	0.20	240	3.83	1129	1.62	0.01
0.02	0.11	240	3.83	1114	1.68	0.04
0.67	0.84	260	4.15	1435	0.66	0.01
0.67	0.67	260	4.15	1447	1.08	0.02
0.67	0.51	260	4.15	1447	1.05	0.01
0.67	0.34	260	4.15	1447	0.81	0.00
0.67	0.18	260	4.15	1435	0.81	0.00

r/R	h/H	N(rpm)	V_{tip} (ms^{-1})	P/V (W/m^3)	C/C_o	95%C/C_o
0.51	0.20	260	4.15	1447	0.68	0.01
0.41	0.11	260	4.15	1448	1.01	0.01
0.34	0.84	260	4.15	1481	0.85	0.02
0.34	0.67	260	4.15	1504	1.06	0.00
0.34	0.51	260	4.15	1498	1.02	0.00
0.34	0.34	260	4.15	1493	0.97	0.02
0.28	0.11	260	4.15	1448	1.22	0.01
0.26	0.20	260	4.15	1447	1.07	0.01
0.10	0.84	260	4.15	1496	0.74	0.01
0.10	0.67	260	4.15	1471	1.13	0.03
0.10	0.51	260	4.15	1477	0.99	0.00
0.10	0.34	260	4.15	1470	0.96	0.02
0.08	0.20	260	4.15	1447	1.50	0.02
0.02	0.11	260	4.15	1421	1.61	0.02
0.67	0.84	280	4.47	1827	0.78	0.01
0.67	0.67	280	4.47	1814	1.08	0.01
0.67	0.51	280	4.47	1814	0.96	0.02
0.67	0.34	280	4.47	1814	0.81	0.02
0.67	0.18	280	4.47	1814	0.76	0.03
0.51	0.20	280	4.47	1814	0.64	0.01
0.41	0.11	280	4.47	1834	1.05	0.03
0.34	0.84	280	4.47	1858	0.85	0.01
0.34	0.67	280	4.47	1866	1.08	0.02
0.34	0.51	280	4.47	1866	1.04	0.02
0.34	0.34	280	4.47	1870	0.91	0.01
0.28	0.11	280	4.47	1834	1.26	0.02
0.26	0.20	280	4.47	1814	1.09	0.05
0.10	0.84	280	4.47	1872	0.99	0.03
0.10	0.67	280	4.47	1860	1.09	0.02
0.10	0.51	280	4.47	1857	1.02	0.01
0.10	0.34	280	4.47	1845	1.01	0.02
0.08	0.20	280	4.47	1814	1.45	0.01
0.02	0.11	280	4.47	1745	1.51	0.03
0.67	0.84	300	4.79	2241	0.83	0.01
0.67	0.67	300	4.79	2241	1.03	0.04
0.67	0.51	300	4.79	2241	0.94	0.03
0.67	0.34	300	4.79	2241	0.82	0.01
0.67	0.18	300	4.79	2241	0.76	0.01
0.51	0.20	300	4.79	2241	0.62	0.02
0.41	0.11	300	4.79	2241	1.02	0.01
0.34	0.84	300	4.79	2297	0.90	0.02
0.34	0.67	300	4.79	2304	1.02	0.02
0.34	0.51	300	4.79	2334	1.03	0.03
0.34	0.34	300	4.79	2319	0.91	0.04
0.28	0.11	300	4.79	2241	1.23	0.03
0.26	0.20	300	4.79	2241	1.07	0.03
0.10	0.84	300	4.79	2300	0.97	0.02
0.10	0.67	300	4.79	2311	1.03	0.01
0.10	0.51	300	4.79	2291	0.99	0.02
0.10	0.34	300	4.79	2304	0.97	0.02
0.08	0.20	300	4.79	2241	1.41	0.01
0.02	0.11	300	4.79	2241	1.43	0.02

Table A4.3. Results from T=0.61 m, A310 (D=T/3), d=605 μm.

(After Mak 1988)

			C/C_0				
N(rpm)	V_{tip} (ms^{-1})	P/V(W/m^3)	h/H=0.18	h/H=0.34	h/H=0.51	h/H=0.67	h/H=0.84
200	2.02	21	0.16	0.09	0.00	0.00	0.00
230	2.32	30	0.26	0.00	0.00	0.00	0.00
260	2.63	38	0.39	0.29	0.00	0.00	0.00
290	2.93	57	0.62	0.40	0.00	0.00	0.00
320	3.23	75	0.82	0.60	0.00	0.00	0.00
350	3.54	98	1.05	0.76	0.00	0.00	0.00
380	3.84	128	1.31	0.97	0.00	0.00	0.00
410	4.14	158	1.54	1.21	0.00	0.00	0.00
440	4.45	195	1.62	1.44	0.00	0.00	0.00
470	4.75	243	1.58	1.79	0.00	0.00	0.00
500	5.05	298	1.53	1.99	0.03	0.00	0.00
530	5.36	369	1.49	2.32	0.00	0.00	0.00
560	5.66	488	2.16	2.09	0.11	0.00	0.00
590	5.96	555	1.63	2.09	1.15	0.00	0.00
620	6.27	648	1.31	1.44	1.40	0.44	0.00
650	6.57	730	1.22	1.19	1.47	0.80	0.02
680	6.87	854	1.15	1.11	1.31	0.93	0.26

Table A4.4. Results from T=1.83 m, 45°PBT4 (D=T/3) , d=590 μm.

			C/C_0					$95\%C/C_0$				
N(rpm)	V_{tip} (ms^{-1})	P/V (W/m^3)	h/H=0.18	h/H=0.34	h/H=0.51	h/H=0.67	h/H=0.84	h/H=0.18	h/H=0.34	h/H=0.51	h/H=0.67	h/H=0.84
60	1.90	40	0.06	0.12	0.08	0.00	0.00	0.00	0.00	0.04	0.00	0.00
80	2.53	97	0.27	0.37	0.19	0.00	0.00	0.02	0.02	0.02	0.00	0.00
100	3.17	204	0.88	1.12	0.17	0.00	0.00	0.04	0.02	0.01	0.00	0.00
110	3.48	282	1.27	1.51	0.16	0.00	0.00	0.01	0.01	0.02	0.00	0.00
120	3.80	381	1.89	1.98	0.30	0.01	0.00	0.04	0.02	0.01	0.03	0.00
130	4.12	478	1.77	1.81	1.43	0.00	0.00	0.02	0.01	0.03	0.01	0.00
140	4.43	575	1.52	1.39	1.37	0.53	0.00	0.03	0.01	0.03	0.01	0.00
150	4.75	695	1.33	1.21	1.29	0.91	0.06	0.02	0.01	0.01	0.01	0.02
160	5.07	831	1.05	1.03	1.13	1.03	0.52	0.03	0.01	0.03	0.01	0.04
170	5.39	990	1.04	0.96	1.01	0.99	0.74	0.03	0.01	0.04	0.05	0.01
180	5.70	1171	0.97	0.92	0.97	0.96	0.75	0.03	0.02	0.02	0.04	0.03
190	6.02	1362	0.93	0.80	0.92	0.95	0.82	0.03	0.19	0.05	0.03	0.02
200	6.34	1600	0.93	0.88	0.91	0.94	0.87	0.07	0.03	0.00	0.03	0.06

Table A4.5. Results from T=1.83 m, 45°PBT4 (D=T/2), d=590 μm.

			C/C_0					$95\%C/C_0$				
N (rpm)	V_{tip} (ms^{-1})	P/V (W/m^3)	h/H=0.18	h/H=0.34	h/H=0.51	h/H=0.67	h/H=0.84	h/H=0.18	h/H=0.34	h/H=0.51	h/H=0.67	h/H=0.84
10	0.48	0	-0.00	0.00	0.00	0.00	0.00	0.04	0.00	0.00	0.00	0.00
20	0.96	7	0.01	-0.00	0.00	0.00	0.00	0.04	0.01	0.00	0.00	0.00
30	1.44	25	0.02	0.02	0.03	0.02	0.00	0.03	0.01	0.01	0.00	0.00
40	1.92	61	0.06	0.08	0.08	0.07	0.00	0.04	0.00	0.01	0.00	0.00
50	2.40	120	0.15	0.21	0.20	0.18	0.00	0.05	0.00	0.01	0.00	0.00
60	2.87	216	0.39	0.51	0.38	0.24	0.00	0.13	0.02	0.01	0.00	0.00
70	3.35	354	0.73	0.87	0.72	0.45	0.00	0.19	0.01	0.02	0.01	0.00
80	3.83	528	0.99	0.95	1.06	0.57	-0.00	0.17	0.02	0.01	0.01	0.01
90	4.31	749	0.89	0.85	1.03	0.82	0.14	0.14	0.01	0.01	0.01	0.01
100	4.79	1016	0.87	0.78	0.95	0.85	0.44	0.15	0.01	0.01	0.06	0.01
110	5.27	1356	0.84	0.76	0.91	0.90	0.56	0.13	0.01	0.03	0.01	0.02
120	5.75	1762	0.82	0.74	0.89	0.91	0.69	0.13	0.01	0.02	0.01	0.01
130	6.23	2229	0.82	0.75	0.92	0.95	0.76	0.12	0.01	0.01	0.02	0.04

Table A4.6. Results from T=1.83 m, A310 (D=T/3) , d=590 μm.

			C/C_0					$95\%C/C_0$				
N(rpm)	V_{tip} (ms^{-1})	P/V (W/m^3)	h/H=0.18	h/H=0.34	h/H=0.51	h/H=0.67	h/H=0.84	h/H=0.18	h/H=0.34	h/H=0.51	h/H=0.67	h/H=0.84
60	1.90	6	-0.01	0.01	0.01	0.00	0.00	0.02	0.00	0.00	0.00	0.00
80	2.53	14	0.03	0.03	0.01	0.00	0.00	0.01	0.02	0.00	0.00	0.00
100	3.17	26	0.11	0.08	0.03	0.00	0.00	0.02	0.01	0.00	0.00	0.00
120	3.80	47	0.30	0.25	0.04	0.00	0.00	0.04	0.01	0.00	0.00	0.00
140	4.43	76	0.61	0.47	0.01	0.00	0.00	0.02	0.01	0.00	0.00	0.00
160	5.07	117	1.19	0.79	0.02	0.00	0.00	0.03	0.02	0.00	0.00	0.00
180	5.70	175	1.59	1.29	0.01	0.00	0.00	0.01	0.02	0.00	0.00	0.00
200	6.34	252	1.74	1.85	0.01	0.00	0.00	0.01	0.01	0.00	0.00	0.00
220	6.97	348	2.38	2.28	0.01	0.00	0.00	0.01	0.02	0.00	0.00	0.00
240	7.60	432	1.73	1.75	1.09	0.01	0.02	0.01	0.03	0.00	0.00	0.00
200	6.34	252	1.50	1.82	0.02	0.01	0.02	0.01	0.02	0.02	0.03	0.03
220	6.97	348	1.91	2.21	0.78	0.01	0.05	0.02	0.04	0.04	0.04	0.09
240	7.60	432	1.51	1.63	1.63	0.22	0.02	0.02	0.02	0.03	0.03	0.04
260	8.24	522	1.22	1.19	1.29	1.11	0.25	0.01	0.07	0.04	0.02	0.04
280	8.87	641	1.03	0.99	1.04	1.03	0.79	0.03	0.03	0.03	0.02	0.02
300	9.50	787	0.94	0.97	0.97	1.00	0.80	0.00	0.06	0.01	0.04	0.04

Table A4.6. Results from T=0.61 m, 45°PBT4 (D=T/3), d=150 μm.

r/R	h/H	N (rpm)	V_{tip} (ms^{-1})	P/V (W/m^3)	C/C_0	95%C/C_0
-0.00	0.08	190	2.02	82	2.03	0.02
-0.00	0.11	190	2.02	86	2.05	0.01
0.11	0.18	190	2.02	85	1.91	0.00
0.11	0.34	190	2.02	87	1.37	0.01
0.11	0.51	190	2.02	84	0.96	0.02
0.11	0.67	190	2.02	86	0.01	0.00
0.11	0.84	190	2.02		0.00	0.00
0.34	0.18	190	2.02	85	1.70	0.02
0.34	0.34	190	2.02	89	1.72	1.58
0.34	0.51	190	2.02	85	1.52	0.03
0.34	0.67	190	2.02	85	0.24	0.01
0.34	0.84	190	2.02	84	-0.01	0.00
0.67	0.18	190	2.02	85	1.73	0.01
0.67	0.34	190	2.02	89	1.83	0.00
0.67	0.51	190	2.02	85	1.95	0.01
0.67	0.67	190	2.02	84	0.03	0.00
0.67	0.84	190	2.02		0.00	0.00
0.90	0.18	190	2.02	87	1.53	0.02
0.90	0.34	190	2.02	85	1.61	0.02
0.90	0.51	190	2.02	84	1.69	0.01
0.90	0.67	190	2.02	88	0.68	0.03
0.90	0.84	190	2.02		0.00	0.00
-0.00	0.08	200	2.13	98	1.89	0.01
-0.00	0.11	200	2.13	100	1.75	0.01
0.11	0.18	200	2.13	97	1.73	0.00
0.11	0.34	200	2.13	101	1.23	0.00
0.11	0.51	200	2.13	99	1.16	0.01
0.11	0.67	200	2.13	105	0.68	0.01
0.11	0.84	200	2.13	100	-0.01	0.00
0.34	0.18	200	2.13	99	1.48	0.01
0.34	0.34	200	2.13	101	1.50	1.38
0.34	0.51	200	2.13	102	1.41	0.06
0.34	0.67	200	2.13	101	1.09	0.01
0.34	0.84	200	2.13	101	0.00	0.02
0.67	0.18	200	2.13		1.56	0.01
0.67	0.34	200	2.13	99	1.59	0.01
0.67	0.51	200	2.13	101	1.70	0.01
0.67	0.67	200	2.13	100	0.52	0.01
0.67	0.84	200	2.13		0.00	0.00
0.90	0.18	200	2.13	103	1.33	0.02
0.90	0.34	200	2.13	100	1.39	0.01
0.90	0.51	200	2.13	103	1.37	0.01
0.90	0.67	200	2.13	105	1.48	0.02
0.90	0.84	200	2.13	101	0.03	0.05
-0.00	0.08	220	2.34	136	1.57	0.01
-0.00	0.11	220	2.34	142	1.51	0.01

r/R	h/H	N (rpm)	V_{tip} (ms^{-1})	P/V (W/m^3)	C/C_0	$95\%C/C_0$
0.11	0.18	220	2.34	139	1.35	0.01
0.11	0.34	220	2.34	140	1.09	0.01
0.11	0.51	220	2.34	138	1.10	0.00
0.11	0.67	220	2.34	141	0.96	0.00
0.11	0.84	220	2.34	140	0.16	0.02
0.34	0.18	220	2.34	139	1.23	0.02
0.34	0.34	220	2.34	140	1.21	1.12
0.34	0.51	220	2.34	141	1.23	0.01
0.34	0.67	220	2.34	144	1.18	0.02
0.34	0.84	220	2.34	139	0.22	0.03
0.67	0.18	220	2.34	144	1.33	0.01
0.67	0.34	220	2.34	144	1.36	0.00
0.67	0.51	220	2.34	142	1.41	0.10
0.67	0.67	220	2.34	141	1.32	0.01
0.67	0.84	220	2.34	137	0.09	0.01
0.90	0.18	220	2.34	140	1.14	0.01
0.90	0.34	220	2.34	137	1.20	0.01
0.90	0.51	220	2.34	142	1.18	0.02
0.90	0.67	220	2.34	152	1.29	0.01
0.90	0.84	220	2.34	140	0.66	0.04
-0.00	0.08	240	2.56	194	1.42	0.01
-0.00	0.11	240	2.56	201	1.34	0.00
0.11	0.18	240	2.56	186	1.37	0.01
0.11	0.34	240	2.56	196	0.98	0.01
0.11	0.51	240	2.56	201	1.04	0.01
0.11	0.67	240	2.56	201	1.07	0.02
0.11	0.84	240	2.56	201	0.83	0.01
0.34	0.18	240	2.56	189	1.05	0.00
0.34	0.34	240	2.56	199	1.09	1.00
0.34	0.51	240	2.56	198	1.09	0.03
0.34	0.67	240	2.56	198	1.15	0.02
0.34	0.84	240	2.56	200	0.86	0.03
0.67	0.18	240	2.56	201	1.21	0.01
0.67	0.34	240	2.56	199	1.21	0.01
0.67	0.51	240	2.56	199	1.28	0.01
0.67	0.67	240	2.56	200	1.19	0.01
0.67	0.84	240	2.56	204	0.79	0.02
0.90	0.18	240	2.56	202	0.99	0.01
0.90	0.34	240	2.56	197	1.08	0.00
0.90	0.51	240	2.56	196	1.17	0.01
0.90	0.67	240	2.56		1.22	0.01
0.90	0.84	240	2.56	200	0.77	0.01
-0.00	0.08	260	2.77	246	1.36	0.02
-0.00	0.11	260	2.77	254	1.32	0.01
0.11	0.18	260	2.77	249	1.28	0.00
0.11	0.34	260	2.77	246	0.93	0.01
0.11	0.51	260	2.77	250	0.99	0.01
0.11	0.67	260	2.77	258	1.09	0.01
0.11	0.84	260	2.77	252	0.92	0.01

r/R	h/H	N (rpm)	V_{tip} (ms^{-1})	P/V (W/m^3)	C/C_0	$95\%C/C_0$
0.34	0.18	260	2.77	251	0.98	0.00
0.34	0.34	260	2.77	255	1.03	0.93
0.34	0.51	260	2.77	253	1.03	0.04
0.34	0.67	260	2.77	253	1.10	0.01
0.34	0.84	260	2.77	253	0.93	0.01
0.67	0.18	260	2.77	255	1.15	0.00
0.67	0.34	260	2.77	253	1.16	0.01
0.67	0.51	260	2.77	254	1.16	0.00
0.67	0.67	260	2.77	258	1.18	0.01
0.67	0.84	260	2.77	255	0.88	0.01
0.90	0.18	260	2.77	251	0.99	0.02
0.90	0.34	260	2.77	254	1.06	0.01
0.90	0.51	260	2.77	234	1.03	0.02
0.90	0.67	260	2.77	253	1.19	0.03
0.90	0.84	260	2.77	252	1.02	0.01
-0.00	0.08	280	2.98	317	1.30	0.01
-0.00	0.11	280	2.98	316	1.28	0.01
0.11	0.18	280	2.98	303	1.21	0.01
0.11	0.34	280	2.98	311	0.92	0.01
0.11	0.51	280	2.98	314	0.95	0.01
0.11	0.67	280	2.98	322	1.02	0.01
0.11	0.84	280	2.98	317	0.98	0.01
0.34	0.18	280	2.98	314	1.03	0.01
0.34	0.34	280	2.98	312	0.98	0.90
0.34	0.51	280	2.98	310	1.02	0.01
0.34	0.67	280	2.98	314	1.07	0.03
0.34	0.84	280	2.98	316	1.01	0.00
0.67	0.18	280	2.98	319	1.10	0.02
0.67	0.34	280	2.98	314	1.09	0.00
0.67	0.51	280	2.98	313	1.13	0.00
0.67	0.67	280	2.98	320	1.18	0.01
0.67	0.84	280	2.98	316	0.93	0.02
0.90	0.18	280	2.98		0.94	0.01
0.90	0.34	280	2.98	310	0.95	0.01
0.90	0.51	280	2.98	315	1.08	0.01
0.90	0.67	280	2.98	307	1.16	0.01
0.90	0.84	280	2.98	316	1.01	0.03
-0.00	0.08	300	3.19	379	1.26	0.01
-0.00	0.11	300	3.19	392	1.23	0.04
0.11	0.18	300	3.19	383	1.24	0.01
0.11	0.34	300	3.19	380	1.16	0.49
0.11	0.51	300	3.19	384	0.94	0.01
0.11	0.67	300	3.19	390	0.98	0.02
0.11	0.84	300	3.19	386	1.02	0.03
0.34	0.18	300	3.19	382	0.90	0.01
0.34	0.34	300	3.19	386	0.97	0.90
0.34	0.51	300	3.19	384	0.99	0.03
0.34	0.67	300	3.19	389	1.07	0.01
0.34	0.84	300	3.19	390	1.06	0.02

r/R	h/H	N (rpm)	V_{tip} (ms^{-1})	P/V (W/m^3)	C/C_0	$95\%C/C_0$
0.67	0.18	300	3.19	392	1.09	0.02
0.67	0.34	300	3.19	376	1.08	0.01
0.67	0.51	300	3.19	390	1.13	0.01
0.67	0.67	300	3.19	388	1.14	0.01
0.67	0.84	300	3.19	384	1.04	0.01
0.90	0.18	300	3.19	393	0.91	0.02
0.90	0.34	300	3.19	381	0.97	0.00
0.90	0.51	300	3.19	390	1.02	0.01
0.90	0.67	300	3.19	389	1.13	0.01
0.90	0.84	300	3.19	390	0.98	0.03

Table A4.7. Results from T=1.83 m, 45°PBT4 (D=T/3), d=150 μm.

			C/C_0					$95\%C/C_0$				
N(rpm)	V_{tip} (ms^{-1})	P/V (W/m^3)	h/H=0.18	h/H=0.34	h/H=0.51	h/H=0.67	h/H=0.84	h/H=0.18	h/H=0.34	h/H=0.51	h/H=0.67	h/H=0.84
75	2.43	77	1.98	2.17	-0.04	-0.03	-0.00	0.02	0.02	0.01	0.00	0.00
80	2.60	94	1.95	1.76	1.87	-0.06	-0.00	0.00	0.03	0.02	0.00	0.00
85	2.76	113	1.57	1.56	1.55	0.13	-0.00	0.01	0.01	0.03	0.01	0.01
90	2.92	134	1.26	1.38	1.38	1.23	0.01	0.02	0.01	0.02	0.01	0.01
100	3.25	184	1.16	1.14	1.14	1.11	0.78	0.01	0.04	0.02	0.03	0.02
110	3.57	244	1.03	1.02	1.03	0.99	0.95	0.03	0.02	0.02	0.01	0.01
120	3.90	317	0.97	0.97	0.97	0.94	0.96	0.00	0.01	0.02	0.02	0.01
130	4.22	403	0.97	0.96	0.94	0.95	0.95	0.01	0.01	0.00	0.00	0.01

Table A4.8. Results from T=1.83 m, 45°PBT4 (D=T/3), d=320 μm.

			C/C_0					$95\%C/C_0$				
N(rpm)	V_{tip}	P/V (W/m^3)	h/H=0.18	h/H=0.34	h/H=0.51	h/H=0.67	h/H=0.84	h/H=0.18	h/H=0.34	h/H=0.51	h/H=0.67	h/H=0.84
40	1.30	12	0.00	-0.04		-0.01		0.03	0.01		0.02	
60	1.95	40	0.23	0.18	0.08	-0.04		0.01	0.07	0.03	0.00	
80	2.60	94	0.65	0.63	0.01	-0.04		0.03	0.07	0.03	0.02	
100	3.25	184	1.65	1.70	-0.04	-0.04		0.02	0.03	0.00	0.00	
105	3.41	212	2.00	1.95				0.04	0.05			
110	3.57	244	1.91	1.82	0.56	-0.03	-0.04	0.04	0.04	0.02	0.02	0.01
115	3.73	279	1.82	1.65				0.02	0.01			
120	3.90	317	1.66	1.38	1.43	0.04	-0.02	0.02	0.02	0.03	0.02	0.02
125	4.06	358	1.54	1.34				0.03	0.02			
130	4.22	403	1.40	1.24	1.28	0.91	-0.03	0.03	0.01	0.02	0.02	0.03
135	4.38	452	1.23	1.18				0.01	0.04			
140	4.54	504	1.13	1.04	1.02	1.01	0.45	0.02	0.02	0.01	0.02	0.04
145	4.71	560	1.08	1.02				0.02	0.01			
150	4.87	619	1.01	0.88	0.96	0.98	0.67	0.02	0.05	0.03	0.01	0.01
160	5.19	752	0.97	0.88	0.88	0.96	0.74	0.03	0.02	0.06	0.02	0.02
170	5.52	902	0.96	0.89	0.85	0.89	0.81	0.01	0.01	0.05	0.01	0.03

180	5.84	1070	0.93	0.83	0.82	0.91	0.82	0.01	0.03	0.01	0.01	0.02
190	6.17	1259	0.92	0.78	0.80	0.87	0.85	0.02	0.04	0.04	0.03	0.01
200	6.49	1468	0.93	0.83	0.80	0.91	0.85	0.01	0.02	0.03	0.02	0.02

Table A4.9. Results from T=1.83 m, 45°PBT4 (D=T/3), d=1050 μm.

			C/C_0					$95\%C/C_0$				
N(rpm)	V_{tip}	P/V (W/m³)	h/H=0.18	h/H=0.34	h/H=0.51	h/H=0.67	h/H=0.84	h/H=0.18	h/H=0.34	h/H=0.51	h/H=0.67	h/H=0.84
80	2.60	94	1.01	0.18	0.04			0.03	0.01	0.01		
100	3.25	184	0.50	0.49	0.12			0.02	0.01	0.03		
110	3.57	244	0.61	0.69	0.17			0.01	0.02	0.01		
120	3.90	317	0.62	0.98	0.12			0.01	0.02	0.01		
130	4.22	403	0.87	1.22	0.13			0.02	0.02	0.01		
135	4.38	452	0.95	1.30	0.14			0.02	0.01	0.02		
140	4.54	504	1.07	1.40	0.33	-0.03		0.02	0.01	0.02	0.02	
145	4.71	560	1.22	1.45	0.45	-0.04		0.02	0.01	0.02	0.01	
150	4.87	619	1.29	1.75	0.55	-0.06		0.01	0.01	0.02	0.01	
155	5.03	683	1.30	1.78	0.76	-0.01		0.02	0.02	0.03	0.02	
160	5.19	752	1.24	1.60	1.06	-0.02		0.02	0.02	0.04	0.02	
165	5.36	824	1.26	1.49	1.18	0.04	-0.02	0.01	0.01	0.02	0.02	
170	5.52	902	1.11	1.34	1.23	0.17		0.01	0.02	0.02	0.06	
175	5.68	984	1.11	1.28	1.22	0.29	-0.04	0.02	0.03	0.03	0.05	
180	5.84	1070	0.99	1.08	1.23	0.39	-0.04	0.03	0.03	0.02	0.04	
185	6.01	1162	0.96	0.99	1.23	0.51		0.02	0.03	0.04	0.02	
190	6.17	1259	0.93	0.88	1.15	0.68	0.09	0.02	0.02	0.03	0.02	0.01
200	6.49	1468	0.83	0.82	1.04	0.78	0.24	0.02	0.02	0.03	0.02	0.02

Appendix 5.

Publication by author.

WUA-CFD

World User Association
in Applied
Computational Fluid Dynamics

4th World Conference and Exhibition in Applied Fluid Dynamics

World Fluid Dynamics Days '98

Computational and Experimental Methods:
Validation, Quality and Reliability

Conference Proceedings

June 7 to 11, 1998

Freiburg i. Br., Germany

9

CFD Simulation for Solid Liquid Mixing Flow in Stirred Tanks

CFD SIMULATION FOR SOLID LIQUID MIXING FLOW IN STIRRED TANKS

YANG X. and TAYLOR D. J.

BHR Group Limited, Cranfield, Bedfordshire MK43 0AJ, UK

ABSTRACT

Solid-liquid mixing flow in stirred tanks with a pitched blade impeller (45°) has been simulated by CFD, using the momentum source model for the impeller and an Eulerian approach for the particle phase, at impeller speeds above N_{JS} (Just Suspension Speed). The simulation was carried out in two different scales of stirred tanks with a commercial CFD code, CFX4.

By simulating particle transportation caused by mean liquid flow and turbulent diffusion, there is good agreement for the solids volume fraction with experimental data on a longitudinal plane between two baffles. The characteristic 'belly plot' curve of the vertical solid volume fraction profile has also been successfully replicated by the CFD simulation.

It has also been found that the liquid flow pattern in single phase flow is slightly different from that in solid-liquid multiphase flow.

1. INTRODUCTION

Mixing in stirred tanks is a very important and widely used operation in the chemical industry. It is well known that better understanding of the mixing flow in stirred tanks can lead to a huge saving in cost for industrial operations. Mixing processes are often classified by the type of process materials such as solid-liquid, gas-liquid and liquid-liquid etc., of which solid-liquid is one of the most important processes.

When studying the performance of stirred tanks used for solid suspension, two aspects should normally be considered: 'complete suspension', which is minimum impeller speed to keep all particle off the tank base, and the way the solid particles are distributed in stirred tanks. The first subject has received extensive investigation to estimate 'Just Suspended Speed' (N_{JS}) as defined by Ref.1. However the knowledge about the particle distribution, which can lead to better design for the apparatus, is very limited.

There are two ways to investigate the particle distribution: experimental study (Ref.2) and numerical simulation by Computational Fluid Dynamics (CFD). Reliable results can usually be obtained by experimental measurements. However these measurements usually involve a large amount of investment and labour and due to limitations of measuring instrumentation it is normally difficult to obtain all details of solid-liquid mixing flow in stirred tanks.

CFD is a rapidly developing technique which features low cost numerical simulation, and enables a more comprehensive understanding of flow details. CFD models used for simulations of such a multiphase flow normally need to be validated because there is only limited knowledge about mixing flow. However there is little work found in the literatures about the validation.

In this paper, validation of a CFD model for solid-liquid mixing flow in stirred tanks, using a commercial CFD code and momentum source model for impeller modelling, is presented by comparing CFD prediction with experimental measurements on a longitudinal plane in two different scale tanks.

2. PHYSICAL FEATURES OF SOLID LIQUID MIXING FLOW IN STIRRED TANKS

Before discussing CFD model for the simulation, it is necessary to summarise the flow features of solid liquid mixing flow in stirred tanks.

2.1 States of Solid Liquid Mixing Flow in Stirred Tanks

The states of the mixing flow can be classified as follows (Ref.3)

i. *Just complete suspension*: No particles remain on tank base for more than 2 seconds

ii. *Homogeneous suspension*: Constant solid concentration through the tank is achieved

iii. *Bottom or corner fillets:* Some particles remain on part of the base.

It will be seen in this paper that the mixing flow with bottom or corner fillets cannot be simulated by the CFD model presented.

2.2 Particle Transportation

In any state of solid-liquid mixing flow in stirred tanks, all particles, or some of particles if they are not fully suspended, are moved by liquid through the tank. This movement is related to the mean velocity, the turbulence diffusion around the particle and gravitational force.

2.3 Particles Near the Base

If the impeller speed is above the **Just Suspension Speed (N_{JS})**, it can be assumed that no particle remains stationary on the base for more than 1-2 sec. Particles near the base can be transported by a boundary layer mechanism.

Unfortunately, at impeller speeds lower than N_{JS}, particle movement near the base, largely due to settling and re-suspension, is not well understood.

2.4 Typical Particle Concentration Distribution in Stirred Tanks

At impeller speeds just above N_{JS}, the solid concentration in stirred tanks is usually a function of the height which reaches a maximum just above the impeller. Above this point, the concentration gradually decreases. Below the impeller, the concentration remains almost constant. In the region very close to the base, the particle distribution is still unknown due to difficulties in the measurements. More details can be found in Ref.3.

Above N_{JS}, the concentration generally becomes more uniform with increasing impeller speed.

Compared with the vertical concentration profile, the radial concentration profile is generally believed to be more uniform.

3. CFD MODEL FOR SOLID LIQUID MIXING FLOW IN STIRRED TANKS

Due to lack of knowledge about particle suspension near the base, only particle transportation by mean flow and turbulence diffusion is simulated in this investigation. Therefore the impeller speed simulated must be higher than N_{JS}.

3.1 Multi fluid model for both phases

Each phase is considered as a continuum. For each phase, conservation equations of mass and momentum can be derived separately. The multi fluid model solves the full set of the conservation equations simultaneously together with constitutive equations describing the interphase momentum exchanges which is determined by an empirical particle drag coefficient.

3.2 Turbulence Modelling

For most of the working conditions for solid-liquid mixing flow in stirred tanks, both phases are turbulent therefore a turbulence model has to be used for the simulation.

Little is known about turbulence modelling in multi phase flow. In this simulation the standard k-ϵ model for single phase flow is directly adopted for solid-liquid mixing flow. The turbulent diffusion for the particulate phase is determined by the eddy diffusivity hypothesis which states that the particle diffusion is proportional to eddy viscosity:

$$\Gamma_T = \frac{\mu_T}{\sigma_T} \qquad (1)$$

where σ_T is the turbulent Prandtl Number or the turbulent Schmidt Number which should be determined using experimental data, μ_T is the eddy viscosity and Γ_T is the turbulence diffusivity for the particle phase.

3.3 Impeller modelling

A momentum source model, developed by the authors, is used to model the impeller. Therefore the transient effects of interaction between impeller blades and the baffles are omitted and steady state flow assumed. The averaged body force produced by the impeller is determined by empirical drag coefficients correction based upon experimental data. Details about the momentum source model can be found in Ref.4.

3.4 Particle drag coefficient

The particles are assumed to be spherical and the particle Reynolds number varies from 0 to 1000 approximately (in the Allen regime) for the cases studied. Therefore the standard drag curve can be used (Ref.5):

$$C_D = \frac{24}{Re} + \frac{5.48}{Re^{0.573}} + 0.36 \qquad (2)$$

where Re is the Reynolds Number based on particle diameter and C_D is the drag coefficient.

3.5 Other assumptions

- There is no particle-particle interaction such as through particle collisions. Therefore the mean solid concentration has to be relatively low.
- The flow is fully three dimensional
- The flow is at steady state.
- The liquid surface is considered as a frictionless surface.

3.4 Limitations of the CFD Model

- Possible large errors in regions of high particle concentration
- Only applicable for spherical particles or particles with a similar shape
- Not applicable for any impeller speeds lower than N_{JS}.

3.5 CFD Solver and the Simulation

The simulations were carried out using CFX4.1 and its multiphase flow solver *SINCE* (Ref.6).

Due to the symmetry of the geometry, a quadrant of the tank was used as the computational domain. About 70,000 cells were used for 0.61m tank and 90,000 cells for 1.83m tank. Grid independence tests were carried out for both tanks, showing that grid independence could be obtained with the grids as above. Fig.1 shows the grids and flow domain used for the simulation.

6 Solution Algorithm

i. Simulate the flow with very low particle concentration (0.1% v/v for example) to build up an initial flow field

ii. Simulate the flow with actual particle concentration by the initial flow field obtained in the previous step

iii. Check the convergence for both phases

iv. Go to next step if converged, otherwise go back to step ii with the new initial flow field

v. If too many particles remain on the base, redistribute the particles and repeat step ii.

4. TESTING CASES

Two vessels have been chosen to validate the model in small and large scales.

Geometry

Tank diameter: T=0.61m & 1.83m

Impeller type: Four bladed pitched blade (45°) impeller

Impeller diameter: T/3 for 0.61m tank and T/2 for 1.83m tank

N_{JS}: 315 rpm in 0.61m tank (measured)

96 rpm in 1.83m tank (estimated by correlation from Ref.1)

Impeller speed: 360 rpm for 0.61m tank; 130 rpm for 1.83m tank

Particle parameters

Particle type	density(kg/m^3)	mean diameter (μm)	volumetric solid fraction (%)
Sand	2630	655	6.3

The solid concentration was measured along several vertical traverses using a conductivity probe. Details about the measurements can be found in Ref.7.

5. RESULTS AND DISCUSSION

5.1 Determination of the turbulent Schmidt Number

To investigate its effect and to optimise the value used for the simulation, results for a range of values (σ_T=0.2 - 10.0) were produced and predicted solid concentrations were compared with experimental data around N_{JS}. This showed that a value of 0.9 produced the best comparison for all cases tested. This value was therefore used in all of the simulations for the solid-liquid mixing flow in stirred tanks.

5.2 Flow pattern in 0.61m tank

The liquid flow patterns and the solid concentration contours are plotted in Fig.2 and 3. As seen in the figures, there is a circulation loop of high particle concentration around the impeller. This is similar to the circulation loop of the liquid phase, showing the mean convective flow transportation to the particles. In the centre of this high concentration loop, the concentration is lower due to the effect of the centrifugal force. When the concentration is plotted vertically such that it traverses this high concentration loop and lower concentration centre of the loop, the characteristic 'belly plot' curve of the solid concentration profile can be obtained.

5.3 Comparison of solid concentration profiles in 0.61m tank

The solid concentration profiles along three vertical lines at radial position of 0.15m, 0.25m and 0.05m are shown in Fig.4,5 & 6. The predicted results show very good agreement with the experimental data. Both results show the typical belly plot curves and the peak positions of the predicted curves are close to those measured.

Near the shaft the belly-plot profile gradually disappears and solid distribution becomes almost homogeneous up to the solid suspension height. It can also be noticed that near the shaft the particle suspension height predicted by CFD is higher than the measured results. This may be caused by inaccurate modelling of the liquid surface and local turbulence behaviour near the top.

From the horizontal profile comparison shown in Fig.7 - 9, it can be seen that when the height is well below the particle suspension height (less than 2/3T from the base) the predicted profile shows very good agreement with measured results. At a height of T/3 (40cm below the liquid top) solid distribution is almost homogeneous except for the region close to the wall where the solid concentration is significantly increased.

At a height of T/2 (30cm below the liquid surface) the solid concentration gradually increaseds from the shaft to the wall which means that the solid distribution is not homogeneous at this height.

When the height is above 2/3T, larger CFD errors have been shown because of less accurate modelling of the mixing flow near the top as mentioned above.

5.4 Comparison between multiphase and single phase flow patterns

Fig.10 shows a single phase flow pattern predicted in under the same conditions. By comparison with Fig.2, it can be seen that the mean velocity loop in single phase flow is larger than that in multiphase flow. This means that flow pattern in solid-liquid multiphase flow can be different from that in pure single phase flow. Therefore, simulation of solid transportation by liquid flow based on single phase flow pattern prediction may lead to a large error.

5.5 Solid-Liquid Mixing Flow Prediction in a 1.83m tank

This testing case was chosen to validate the capability of the 3-D CFD model for large scale vessels.

The measurement was carried out for this tank and the results have shown that there is a characteristic belly plot curve in a vertical concentration profile. The flow pattern and solid distribution have been predicted by the simulation in this tank. In Fig.11 the comparison between CFD prediction and measured results is shown along a vertical line at a radial position of 30 cm from the side wall. It can be seen that the prediction shows a belly plot curve and the predicted peak position is close to the measured position.

However, there is a difference between averaged solid concentrations along this line by CFD prediction and by the measurement. The possible reason for this difference can be the high solid concentration region in the tank such as the region below the impeller. If there is a high solid fraction region, it may not be predicted correctly by this CFD model since the particle-particle interaction is not considered.

6. CONCLUSIONS

Solid distribution in stirred tanks has been successfully predicted by CFD simulation using commercial CFD code, with momentum source modelling for the impeller. The predicted results indicate that theve is a high solid concentration loop mainly following the mean flow recirculation loop, showing the particle transportation caused by the liquid phase. This explains why the characteristic belly plot in particle concentration profile along a vertical line occurs.

By comparing prediction with measured vertical profiles of particle concentration, agreement is satisfactory in most regions of the tanks, which has validated the CFD model for further prediction of solid distribution in stirred tanks. However, prediction in the region near the liquid surface is less satisfactory because of difficulties in turbulence modelling and boundary conditions used for the free surface in this region.

The results have also shown that the liquid flow pattern when mixed with solid can be different from that in single phase flow, indicating that modelling particle transportation based on the single phase flow pattern may lead to large errors.

For a large scale of tank, the model can still produce reasonable predictions when the impeller speed is well above N_{JS}.

7. REFERENCES

1. Zweitering, T. N., *'Suspending of solid particles in liquid by agitators'*, Chem. Eng. Sci., Vol. 8, pp 244 - 253, 1958

2. Magelli, F., Fajner, D., Nocentini, M. & Pasquali, G., *'Solid concentration distribution in slurry reactors stirred with multiple axial impellers'*, Chem. Eng. Process. 29, p27, 1991

3. Nienow, A. W., in N.Harnby, M.F.Edwards & A.W.Nienow (eds), 'Mixing in the process industries', 2nd edition, Butterworth Heinemann, 1992

4. Pericieous, K. A., & Patel, M. K., *'The source sink approach in the modelling of stirred reactors'*, PCH Physico-Chemical Hydrodynamics, V.9, No.1(2), pp 279 - 297, 1987

5. Ihme, F., Schmidt-Throb, H. & Brauer, H., Chemier-Ing.- Tech., 44(5) p306, 1972.

6. Lo, S. M., 'Mathematical basis of a multi-phase flow model, AERE R 13432, 1989.

7. Mak, A., Yang, X. & Ozcan-Taskin, N. G. *'The effect of scale on the suspension and distribution of solids in stirred vessels'*, Récents en Génie és, Vol.11, No.52, pp97 - 104, ISBN 2-910239-26-8, ed. Lavoisier, Paris, France, 1997

8. ACKNOWLEDGEMENTS

The authors gratefully acknowledge the support of the member companies of the Fluid Mixing Process (FMP) consortium at BHR Group Limited.

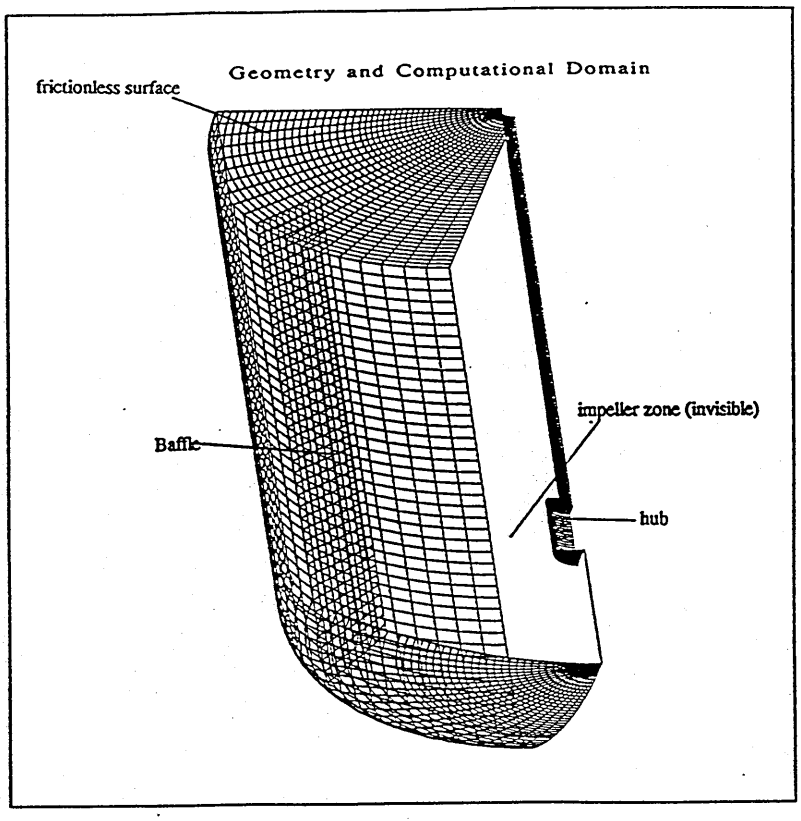

Fig.1 Computational domain and grids

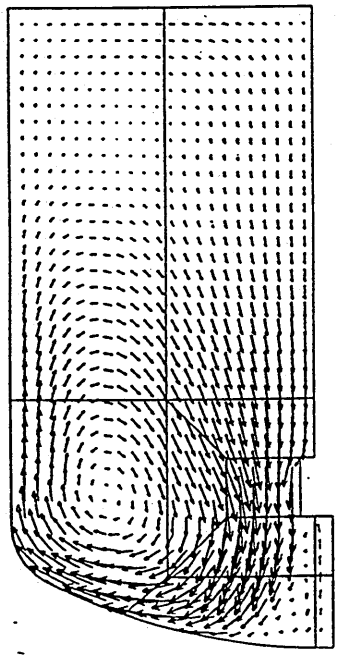

Fig.2 Liquid flow pattern in solid liquid mixing flow (0.61m tank)

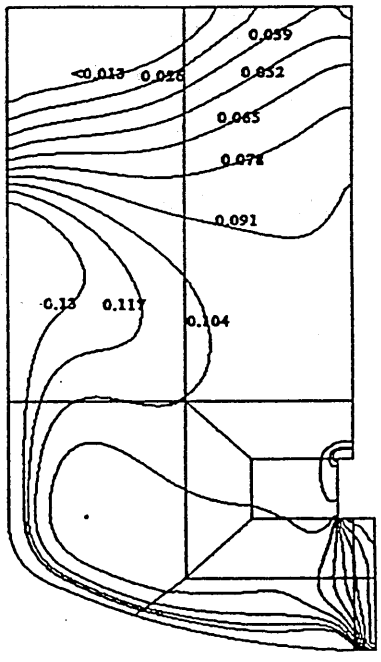

Fig.3 Distribution of solid concentration in 0.61m tank

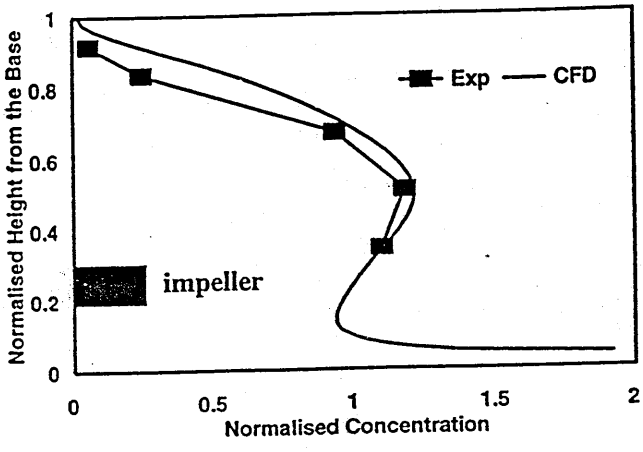

Fig.4 Solid concentration profile along a vertical line at radial position of 0.15m in 0.61m tank

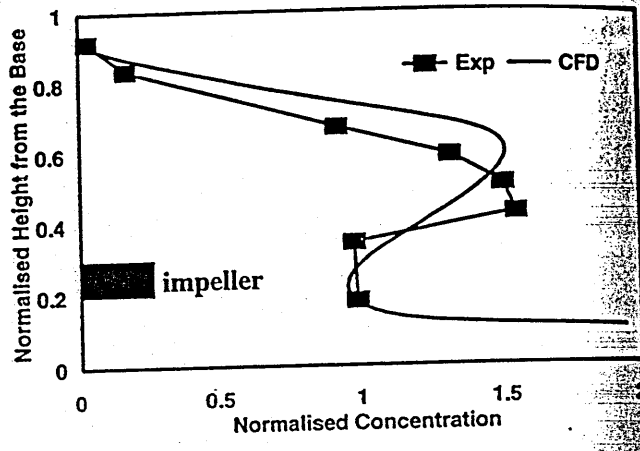

Fig.5 Solid concentration profile along a vertical line at radial position of 0.25m in 0.61m tank

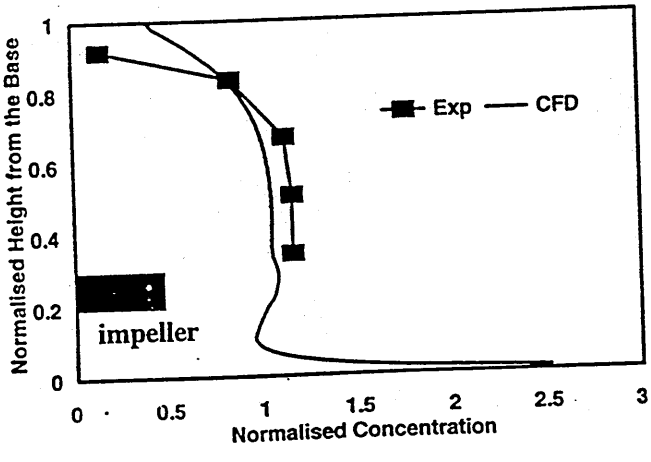

Fig.6 Solid concentration profile along a vertical line at radial position of 0.05m in 0.61m tank

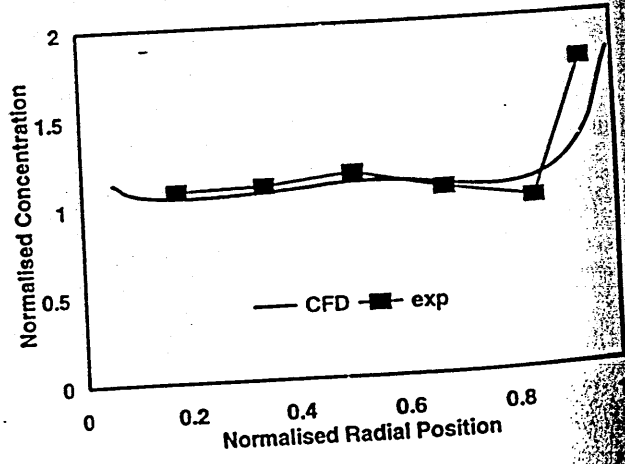

Fig.7 Horizontal solid concentration profile at height of 0.2m from the base

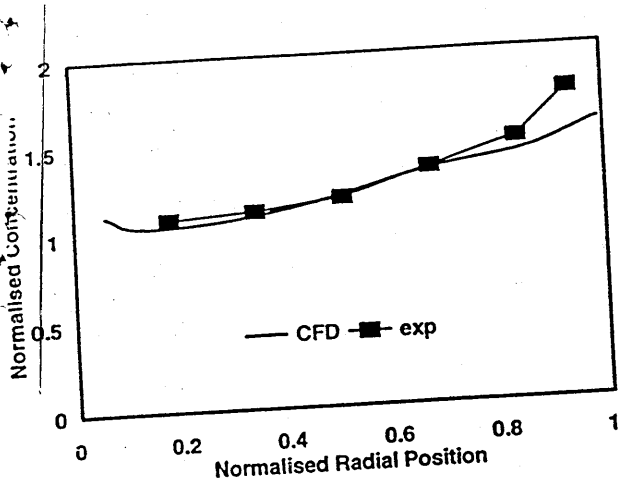

Fig.8 Horizontal solid concentration profile at height of 0.3m from the base

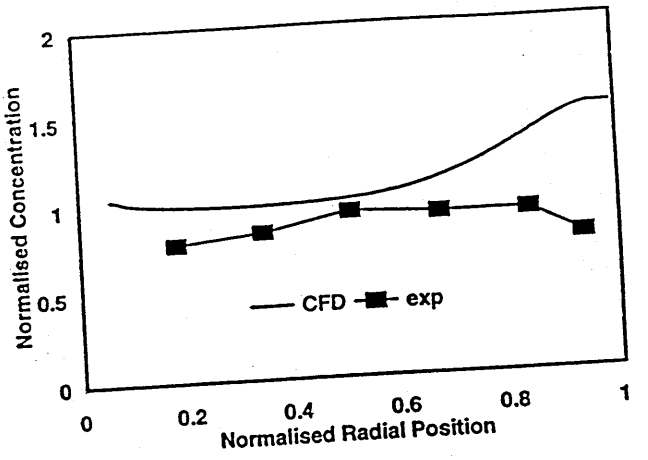

Fig.9 Horizontal solid concentration profile at height of 0.4m from the base

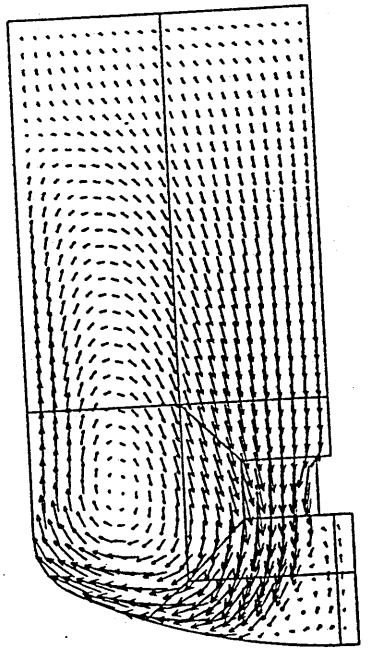

Fig.10 Flow patter in single phase flow (0.61m tank)

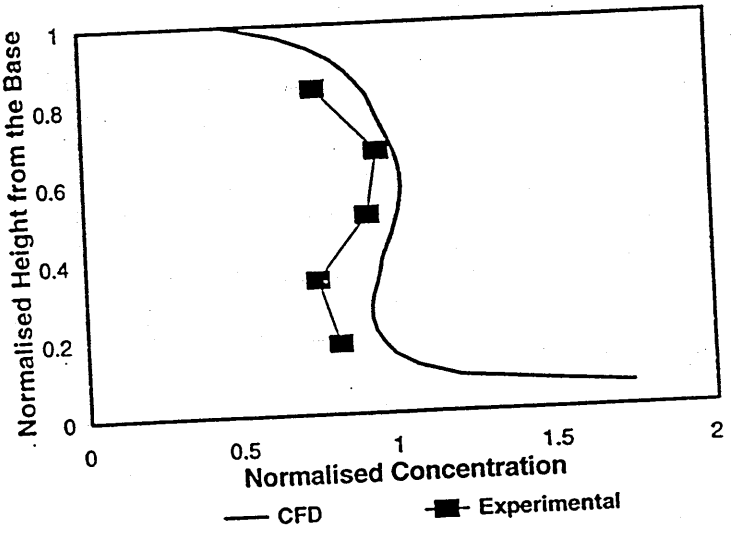

Fig.11 Vertical solid concentration profile at radial position of 0.3m in 1.83m tank